ABANT IZZET BAYSAL UNIVERSITY

THE GRADUATE SCHOOL OF NATURAL AND APPLIED SCIENCES

CERIA SUPPORTED COPPER(0) AND TITANIA SUPPORTED RHODIUM(0) NANOPARTICLES AS CATALYSTS IN DEHYDROGENATION OF DIMETHYLAMINE BORANE

DOCTOR OF PHILOSOPHY

SEDA KARABOĞA

BOLU, NOVEMBER 2017

ABANT IZZET BAYSAL UNIVERSITY

THE GRADUATE SCHOOL OF NATURAL AND APPLIED SCIENCES

DEPARTMENT OF CHEMISTRY

CERIA SUPPORTED COPPER(0) AND TITANIA SUPPORTED RHODIUM(0) NANOPARTICLES AS CATALYSTS IN DEHYDROGENATION OF DIMETHYLAMINE BORANE

DOCTOR OF PHILOSOPHY

SEDA KARABOĞA

BOLU, NOVEMBER 2017

APPROVAL OF THE THESIS

CERIA SUPPORTED COPPER(0) AND TITANIA SUPPORTED RHODIUM(0) NANOPARTICLES AS CATALYSTS IN DEHYDROGENATION OF DIMETHYLAMINE BORANE submitted by **Seda KARABOĞA** in partial fulfillment of the requirements for the degree of **Doctor of Philosophy** in **Department of Chemistry, The Graduate School of Natural and Applied Sciences of ABANT IZZET BAYSAL UNIVERSITY in 17/11/2017** by

Examining Committee Members	**Signature**
Supervisor Prof. Dr. İzzet MORKAN Abant İzzet Baysal University	.....
Member Prof. Dr. Yalçın TONBUL Dicle University	.....
Member Prof. Dr. Özdemir ÖZARSLAN Abant İzzet Baysal University	.....
Member Assoc. Prof. Dr. Önder METİN Atatürk University	.....
Member Assist. Prof. Dr. Sevim DEMİRÖZÜ ŞENOL Abant İzzet Baysal University	.....

Graduation date: ...../...../20....

Prof. Dr. Duran KARAKAS .....

Director of Graduate School of Natural and Applied Sciences

TO MY FAMILY

DECLARATION

I hereby declare that all information in this document has been obtained and presented in accordance with academic rules and ethical conduct. I also declare that, as required by these rules and conduct, I have fully cited and referenced all material and results that are not original to this work.

SEDA KARABOĞA

_____

ABSTRACT

CERIA SUPPORTED COPPER(0) AND TITANIA SUPPORTED RHODIUM(0) NANOPARTICLES AS CATALYSTS IN DEHYDROGENATION OF DIMETHYLAMINE BORANE
PHD THESIS
SEDA KARABOĞA
ABANT IZZET BAYSAL UNIVERSITY GRADUATE SCHOOL OF NATURAL AND APPLIED SCIENCES
DEPARTMENT OF CHEMISTRY
(SUPERVISOR: PROF. DR. İZZET MORKAN)

BOLU, NOVEMBER 2017

In recent years, hydrogen is accepted as clean and important energy carrier in the most applications such as heating, electrical generation, transportation and mechanical power. The lack of safe, effective and cost-effective hydrogen storage sources for transportable and stationary applications is one of the main obstacles to overcome for the application of the hydrogen economy. Chemical storage materials consist of high percent of hydrogen by weight are hopeful as hydrogen sources using in fuel cells. The hydrogen sources such as ammonia borane and its derivatives have the high gravimetric storage density, high stability and non-toxicity, so interest in them is increasing day by day. One of them, dimethylamine borane $(Me)_2NH.BH_3$, DMAB) could release hydrogen by means of proper catalyst in mild conditions. Transition metal nanoparticles can be utilized as active catalysts for the dehydrogenation of amine borane adducts due to the unique properties of them. The tendency of metal nanoparticles to agglomerate with the formation of bulk metal causes a significant decrement of activity with increasing particle size in their catalytic applications. Metal oxides used as a support are one of the way to avoid from agglomeration of metal nanoparticles. The usage of metal oxides as a stabilizer in the synthesis of transition metal nanoparticles supply advantegous in terms of long lifetime, thermal stability, and reusability for catalysts. In this dissertation, we reveal the in-situ preparation, characterization and catalytic activity of ceria supported copper(0) and titania supported rhodium(0) nanoparticles in dehydrogenation of DMAB. Copper(0) nanoparticles supported on ceria were in situ generated from the reduction of Cu^{2+}/CeO_2 during the catalytic dehydrogenation of DMAB in toluene. Rodium(II) hexanoate was used as a precursor to be formed rhodium(0) nanoparticles, $Rh(0)/nanoTiO_2$ throughout the dehydrogenation of DMAB at temperature of 60.0 ± 0.5 ^oC. The characterization of metal oxides supported transition metal(0) nanoparticles were performed by means of UV-Visible electronic absorption spectroscopy (UV-Vis), Scanning electron microscopy (SEM), Transmission electron microscopy (TEM), Energy dispersive X-ray (EDX), Brunauer-Emmett-Teller (BET), X-ray photoelectron

spectroscopy (XPS), X-ray diffraction (XRD), inductively coupled plasma optical emission spectrometry (ICP-OES and FT-IR techniques. The catalytic activity of ceria supported copper(0) and titania supported rhodium(0) nanoparticles was performed in the dehydrogenation of DMAB. The catalytic activity of ceria supported copper(0) and titania supported rhodim(0) nanoparticles and kinetics of hydrogen generation from the dehydrogenation of DMAB were tested depending on catalyst concentration and temperature. The obtained kinetic data was used for the calculation of rate laws and activation parameters such as Arrhenius activation energy, Ea; activation enthalpy, ΔH#; and activation entropy, ΔS# for both catalytic dehydrogenation reactions.

KEYWORDS: Dehydrogenation, Dimethylamine borane, Heterogeneous catalyst, Copper(0) Nanoparticles, Cerium(IV) oxide, Rhodium(0) Nanoparticles , Titanium(IV) oxide.

ÖZET

DİMETİLAMİN BORANIN DEHİDROJENLENMESİNDE KATALİZÖR OLAN SERYUM OKSİT DESTEKLİ BAKIR(0) VE TİTANYUM OKSİT DESTEKLİ RODYUM(0) NANOPARÇACIKLAR
DOKTORA TEZİ
SEDA KARABOĞA
ABANT İZZET BAYSAL ÜNİVERSİTESİ FEN BİLİMLERİ ENSTİTÜSÜ
KIMYA ANABILIM DALI
(TEZ DANIŞMANI: PROF. DR. İZZET MORKAN)

BOLU, KASIM - 2017

Son yıllarda, hidrojen, ısınma, elektrik enerjisi, ulaşım ve mekanik güç gibi birçok uygulama için dünyaca temiz ve önemli bir enerji taşıyıcısı olarak kabul edilmektedir. Taşınabilir ve sabit uygulamalarda güvenli, etkili ve düşük maliyetli hidrojen depolama malzemelerinin olmaması, hidrojen ekonomisinin uygulanması için üstesinden gelinmesi gereken en büyük engellerden biridir. Yakıt hücrelerinde kullanılan ağırlıkça hidrojen yüzdesi yüksek olan kimyasal depolama malzemeleri, hidrojen kaynakları olarak umut vericidir. Kütlece yüksek hidrojen depolama kapasitesi, yüksek kararlılık ve zehirli olmayışı nedeniyle amonyak boran ve türevleri gibi hidrojen depolama kaynaklarına ilgi artmaktadır. Bunlardan biri olan dimetilamin boran $(Me)_2NH.BH_3$, DMAB) uygun koşullar altında uygun katalizör varlığında hidrojen salabilir. Geçiş metali nanoparçacıkları, eşsiz özelliklerinden dolayı amin boran türevlerinin dehidrojenlenmesinde aktif katalizörler olarak kullanılabilir. Metal nanoparçacıkların aglomerasyon ile külçe metal oluşumuna olan eğilimleri, artan parçacık boyutu ile katalitik uygulamalardaki etkinliğin düşmesine sebep olmaktadır. Kararlaştırıcı bir destek olarak kullanılan metal oksitler, metal nanoparçacıklarının aglomerasyonunu önlemenin yollarından biridir. Geçiş metali nanoparçacıklarının sentezi için kararlaştırıcı olarak metal oksitlerin kullanılması tekrar kullanılabilirlik, termal kararlılık ve uzun ömür açısından avantajlı olmaktadır. Bu tezde, seryum oksit destekli bakır(0) nanoparçacıklar ve titanyum oksit destekli rodyum(0) nanoparçacıklarının hazırlanması, karakterizasyonu ve dimetil amin boranın dehidrojenlenmesindeki katalitik etkinliklerini sunuyoruz. Seryum oksit üzerine tutturulan bakır(0) nanoparçacıklar, dimetilamin boranın katalitik dehidrojenlenmesi boyunca Cu^{2+} / CeO_2'nin indirgenmesinden elde edildi. Dimetilamin boranın dehidrojenlenmesi boyunca oluşan Rh(0) nanoparçacıklar (Rh(0)/nanoTiO_2) için rodyum(II) hekzanoat öncü olarak kullanıldı. Metal oksitler üzerine tutturulan geçiş metali(0) nanoparçacıkları UV-görünür bölge elektronik soğurma spektroskopisi (UV-Vis), taramalı elektron mikroskopisi (SEM), geçirgenli electron mikroskopisi (TEM), enerji dağıtımı X ışını spektroskopisi (EDX), Brunauer-Emmett-Teller (BET), X-ışını fotoelektron spektroskopisi (XPS), X- ışınları kırınımı (XRD) indüktif olarak çiftlesmis plazma-optik emisyon spektroskopisi (ICP-OES) ve infared spektroskopisi (FT-IR) ile tanımlandı. Seria destekli bakır (0) ve titanya destekli rodyum (0) nanoparçacıklarının katalitik etkinliği dimetilamin boranın dehidrojenlenmesinde test edildi. Seryum(IV) oksit destekli bakır(0) ve

titanyum(IV) oksit destekli rodyum(0) nanoparçacıklarının katalitik etkinliği ile bu katalizörlerin varlığında dimetilamin boranın dehidrojenlenme tepkimesinin kinetiği, farklı katalizör derişimlerine ve sıcaklığa bağlı olarak çalışıldı. Elde edilen kinetik veriler kullanılarak, her iki katalitik dehidrojenlenme tepkimesine ilişkin hız kanunu ve Arrhenius aktivasyon enerjisi (Ea), aktivasyon entalpisi ($\Delta H^{\neq}$) and aktivasyon entropisi ($\Delta S^{\neq}$ gibi aktivasyon parametreleri hesaplandı.

ANAHTAR KELİMELER: Dehidrojenlenme, Dimetilamin boran, Heterojen katalizör, Bakır(0) Nanoparçacıklar, Seryum(IV) oksit, Rodyum(0) Nanoparçacıklar, Titanyum(IV) oksit.

TABLE OF CONTENTS

Page

LIST OF FIGURES

Page

LIST OF TABLES

Page

LIST OF ABBREVIATIONS AND SYMBOLS

NPs **:** Nanoparticles

DMAB **:** Dimethylamine borane

TOF **:** Turnover frequency

TON : Turnover number

$\Delta H^{\neq}$ **:** Activation enthalpy

$\Delta S^{\neq}$ **:** Activation entropy

nm **:** Nanometer

ppm **:** Parts per million

rpm **:** Revolution per minute

CS_2 **:** Carbon disulfide

MSI **:** Metal support interaction

MOF **:** Metal organic framework

MSI **:** Metal support interaction

LMCT **:** Ligand to Metal Charge Transfer

ACKNOWLEDGEMENTS

I would like to thank to my Supervisor, Prof. Dr. İzzet Amour MORKAN for his continuous contribution, friendship, patience, encouragement and support throughout this dissertation and also with my professional development.

Also, I want to thank to my Co-advisor Prof. Dr. Saim ÖZKÂR who is always accessible, guidance and is willing to assist throughout this thesis. I learnt a lot of things about Preparation and Characterization of Metal Nanoparticles. Of course, his comments, ideas, discussion and especially feedback have certainly been invaluable to interpret and improve the results obtained.

I am appreciative of the aid for their useful discussions, suggestions and valuable contributions to Assoc. Prof. Dr. Önder METİN and Assist. Prof. Dr. Sevim DEMİRÖZÜ ŞENOL.

I would like to thank my friends as Derya ÖZHAVA and Dr. Serdar AKBAYRAK, my instructor as Prof. Dr. Yalçın TONBUL from Dicle Universiy for working together in the organometallic laboratory in Middle East Technical University for all their support and help.

Last but not least, I want to thank to my husband Dr. Fırat KARABOĞA for his endless love, support and encouragement.

1. INTRODUCTION

Sustainable supply of energy and its appropriate storage is one of the global challenges for the next decades. In this respect, advances in hydrogen technology, such as the generation of hydrogen from suitable starting and renewable materials and its storage and conversion to electricity, are a central component. Unfortunately, hydrogen transportation and handling is difficult, making its widespread use in applications problematic. To solve this problem, hydrogen could be stored in chemical compounds that easily release hydrogen on demand. Lightweight and hydrogen-rich B-N species have attracted considerable interest in this regard. Amine borane adducts are considered a hopeful candidate for several applications. They have high hydrogen capacity. In addition, release of hydrogen from them as an energy carrier is easily possible by suitable catalysts (Marder, 2007; Hamilton et al., 2009). Furthermore, they are very soluble in water at room temperature and easy to process (Bluhm et al., 2006). Ammonia borane and its derivatives play a significant role in many fields as polymer industry (Clark et al., 2006), material chemistry (Jacquemin et al., 2004), transfer hydrogenation (Shi et al., 2012) and tandem dehydrogenation-hydrogenation reactions (Jaska and Manners, 2004).

It is a particular interest that hydrogen could be released from DMAB in the presence of proper catalyst under suitable conditions. (eq. 1) (Berg and Arean, 2008; Jaska et al., 2001; Jaska et al., 2003).

$$2Me_2NH.BH_3 \xrightarrow{catalyst} (Me_2N.BH_2)_2 + 2H_2 \qquad (1)$$

Until now, various kinds of transition metal catalysts have been used for dehydrogenation of dimethylamine borane such as ruthenium and iridium. (Jiang and Berke, 2007). The hydrogenation of homogenous Re-catalyzed alkenes by means of DMAB as a hydrogen source have been recorded by Berke and colleagues (Jiang and Berke, 2007). Titanium precursor complex $[(\eta5\text{-}C_5H_3\text{-}1,3\text{-}(SiMe_3)_2)_2Ti]_2(\mu2,\eta1,\eta1\text{-}N_2)$ was explored for homogeneous system in dehydrogenation of DMAB by Chirik (Pun et al., 2007). Moreover, Willams and co-workers have used ruthenium and copper complexes as homogenous catalysts for in situ reduction of organic moities and

dehydrogenation of DMAB (Van der Waals et al., 2014; Nixon, 2011). Despite of potential benefits of homogenous catalysts, these protocol have limited for usage due to the long reaction time, severe reaction conditions and difficulty in separating the catalyst.

The present investigation has been shifted to the development of heterogeneous catalysts having high activity due to the advantages of heteregenous systems as easy product isolation, catalyst recovery and reusability. In hydrogen evolution reaction, nanocatalysts are very important due to the having smaller size and high surface volume ratio, following then better catalytic performance and a great number of active atoms lying on the surface. (Lee et al., 2007; Amendola et al., 2000; Stephens et al., 2007; Mohajeri et al., 2007; Ramachandran and Gagare, 2007; Fernandes et al., 2009; Yan et al., 2009; Patel et al., 2010). However, transition metal nanoparticles incline into bulk metals with aggregation causing a decrease in catalytic activity (Ozkar and Finke, 2002a; Ozkar and Finke, 2002). The usage of proper supports as polymers, metal oxides, meso-structured and carbon materials can also afford unique catalytic functions that include site isolation of active metal NPs from agglomeration and the synergistic effects due to strong metal-support interactions (SMSI). Several ways have been tried to ascend the surface area of the catalysts using various support to prevent the agglomeration. In this context, different material candidates such as zeolites (Tosheva and Valtchev, 2005; Kato et al., 2004), carbonaceous materials (Castillejos et al., 2009), metal oxides (Sayle et al., 2003; Haruta, 1997), polymers (Shi et al., 2005; Graeser et al., 2007), metal-organic-frameworks (El-Shall et al., 2009) may be used as an alternative way to inhibit further growing of NPs. Also, TiO_2 and CeO_2 based catalyst supporting materials are known to have unique properties (Bamwenda et al., 1997) due to TiO_2/ CeO_2 nanoparticles high chemical and thermal stability (Dai et al., 2013) and the nature of the interaction of a metal nanoparticle with TiO_2 or CeO_2 support (Bagheri et al., 2014; Sun et al., 2012). In recent publications, it has been demonstrated that using ceria or titania nanopowders as support providing long lifetime and high catalytic activity for Pd (Tonbul et al., 2016), Ru (Akbayrak et al., 2016) and Rh (Akbayrak et al., 2016) nanoparticles in the hydrolysis of ammonia borane to generate hydrogen. This result prompted us to employ ceria and titania as support for a noble (rhodium) and non-noble (copper) metal NPs catalyst in dehydrogenation of DMAB.

1.1 Hydrogen As an Energy Carrier

1.1.1 Hydrogen Economy

One of the major challenges facing modern society is to find a means of sustainable fuel generation, storage and delivery and overcome our reliance on non-renewable fossil fuels such as oil, coal and natural gases. If the negative effects of global warming, degradation of the ozone layer and consequent world's climate change is to be stopped, the development and use of a green and renewable energy vector is mandatory (Schlapbach and Züttel, 2001). Further, projections to 2040 predict an increase of 56 % in the global world energy demand (International Energy Outlook., 2015). Hydrogen, considered as an ideal energy carrier in transport and stationary applications, is an alternative to replace petroleum products. The production, storage, consumption and regeneration of H_2 fuel is known as 'hydrogen economy' and the 'sustainable hydrogen cycle' on which it is based is presented in Figure 1.1.

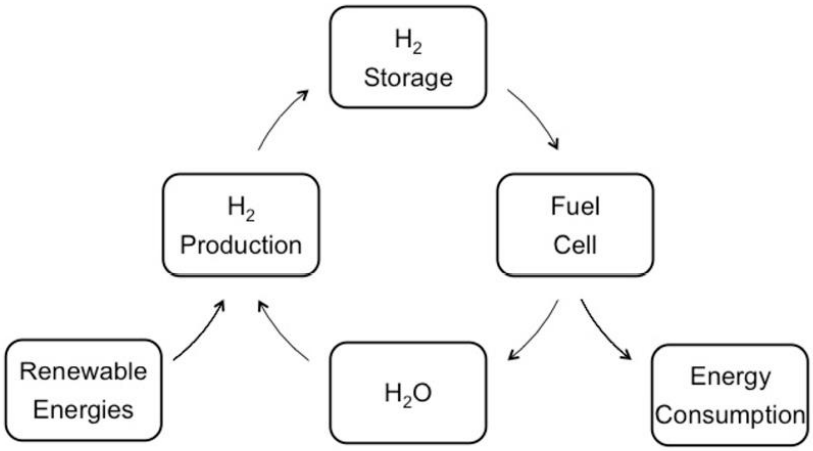

Figure 1.1. Sustainable hydrogen cycle.

Today, hydrogen can be produced from renewable sources using different methods with minimum environmental impact, although not very efficiently in many cases: for instance solar, wind, hydro, electrolysis, photolysis, water splitting, biomass gasification and fermentation can be used for hydrogen production (Alves et al., 2013; Granovskii et al., 2007; Holladay et al., 2009). The most abundant element in earth is hydrogen and can be found in universe as chemically bonded in H_2O or liquid and

gaseous hydrocarbons. It can be found less than 1% as molecular hydrogen. It is an important energy carrier and is not a primary energy source. Hydrogen can be obtained from several of resources such as water or natural gas using several processing techniques. And also, it provides great deal of energy (120 MJ/kg) compared to its peers.

1.1.2 Methods of Hydrogen storage

Before the hydrogen economy can become completely viable, the safely storage and availability of H_2 is an issue that must be overcome. The major challenge in terms of using hydrogen as a fuel is to develop influential methods for its storage that can not only store H_2 safely, but also supply it when and where it is needed.

Another key factor worth considering is that the storage systems have to be cost-competitive as well as energy efficient. H_2 can be stored in different phases as gas, liquid or solid. At present, hydrogen is stored in the form of a liquid or compressed gas in industry.

1.1.3 Physical Hydrogen Storages

Hydrogen can be stored as compressed gaseous, liquid hydrogen and cryo-compressed gaseous as well as can be stored by adsorption on high-surface-area materials under high pressure and low temperature. There is no chemical bond (covalent and ionic interactions) between hydrogen and the host compounds in physical adsorption process.

Different types of physical hydrogen storage systems are listed below;

1) CGH_2 (compressed gaseous hydrogen), 350 - 700 bar, room temperature.

2) LH_2 (liquid hydrogen), 1 – 10 bar, ~ -253 ° C.

3) CcH_2 (cryo-compressed hydrogen), 250- 350 bar, > -253 ° C.

4) Cryo-adsorption on high-surface-area materials, 2 – 5 bar, ~ -193 ° C.

5) Glass Microspheres and Glass Capillary Arrays.

Hydrogen gas could be stored in dewar that hold it at required pressure. Liquid form of hydrogen is used as a fuel for rocket applications but the storage and transport of compressed hydrogen are dangerous.

There are issues related to the safety and volume restrictions for the storage of high pressure hydrogen gas, preventing its application more widely (Sørensen, 2012). Solid state of hydrogen storage is becoming important in recent research. Physical and chemical storage are the main categories for the solid state form of hydrogen storage. The former requires H_2 to be bound or included in a host by relatively weak interactions commonly referred to as physisorption or physical absorption. Most studied materials employed for physically storing H_2 include metal-organic frameworks, porous carbon, covalent-organic frameworks, polymers and zeolites (Ren et al., 2013; Kustov et al., 2014; Yeung and Han, 2014; Furukawa and Yaghi, 2009; Feng et al., 2012). Also, the hydrogen can be found in a compound and the uptake/release process involves chemical reactions. Hydrogen could be storaged as a gas or liquid in physical hydrogen storage methods, however these methods is very hard in industrial applications due to unsafety and low density of hydrogen (Figure 1. 2).

Figure 1.2. Classification of hydrogen storage materials depending on the relationship between hydrogen and storage media (Kalidindi and Jagirdar, 2010).

In physisorption, very weak forces exist between hydrogen molecule and adsorbent such as van der Waals forces. Only at low temperatures (77 K), plausable gravimetric hydrogen storage may be obtained by using this method, while there are some

advantages of this approach as reversibility and fast kinetics (Murray et al., 2009). On the side, the greatest disadvantage of the chemisortion method, which allows hydrogen to dissociate into atoms on metal surfaces, is that high temperature is required (Grochala and Edwards, 2004).

1.1.4 Solid State Hydrogen Storage

The storage of hydrogen obtained by adsorption method on carbon materials and/or by absorption in chemical compounds has precise advantages in terms of a safety perspective, in which some form as conversion or energy input is needed to deliver the hydrogen for next use. Vast studies have been carried on modern hydrogen-storage systems as metal hydrides, metal nitrides, metal imides, doped polymers, metal organic frameworks (MOF), zeolites, clathrate hydrates, and carbon based materials. In storage of solid state, hydrogen is bonded by chemical forces such as in hydrides, imides and nitrides or physically, e.g. MOF and carbon based materials.

Physisorption has several advantages as high energy efficiency and fast adsorption/desorption cycles, while chemisorption ends up with the adsorption of greater amounts of gas but in some situations, is not reversible and needs a higher temperature to liberate the adsorbed gas. Multifarious studies have been performed to develop the alternatives for the storage of hydrogen. (Annemieke and Arean, 2008). Complex hydrides that have high gravimetric/volumetric hydrogen storage capacity (Schlapbach and Zuttel, 2001) and high energy density for H_2 storage are found as most suitable among these studies. In the complex hydrides, boron adducts have gained much attention by reason of their high hydrogen capacity, low molecular weight, and high solubility Figure 1.3. (Züttel, 2003).

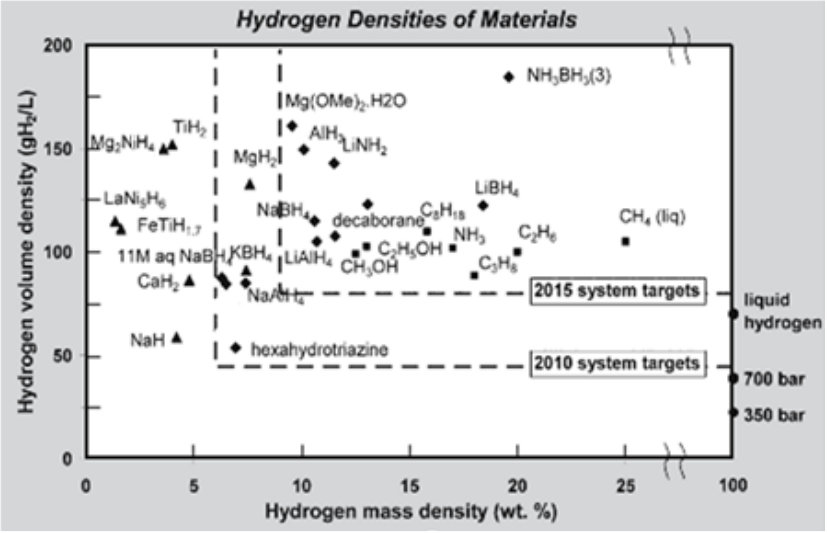

Figure 1.3. Hydrogen densities for many hydrogen storage materials (Züttel, 2003).

1.1.4.1 Amine Boranes as hydrogen storage materials

Amine borane compounds contain coordinate covalent bond between the nitrogen and boron, have been recently gained more attention. They could be used as a hydrogen storage materials because of having high hydrogen capacity. Amine boranes is a kind of lewis acid base reactions where the N is considered to provide a lone pair for B species being insufficient electron and accepts twin electrons into vacant p orbital (Figure 1. 4).

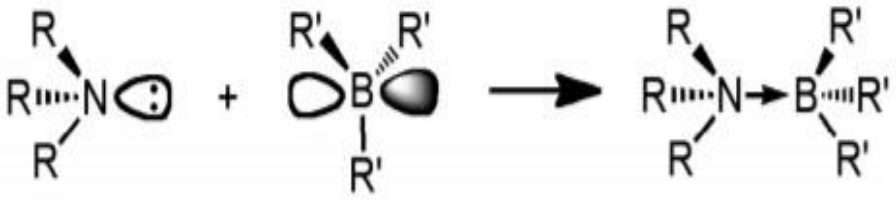

Figure 1.4. Bonding in amine-boranes

NH_3BH_3 is unique in terms of hydrogen storage and release of hydrogen through the hydrolysis or dehydrogenations when compared to other chemical hydrides due to the protic amine and the hydridic borane hydrogens. Ammonia borane has gravimetric and volumetric hydrogen contents of 19.6 wt% (Langmi and McGrady, 2007) and 0.145

kg L^{-1} respectively. And it has more hydrogen per unit mass and unit volume than liquid hydrogen (Figure 1.5).

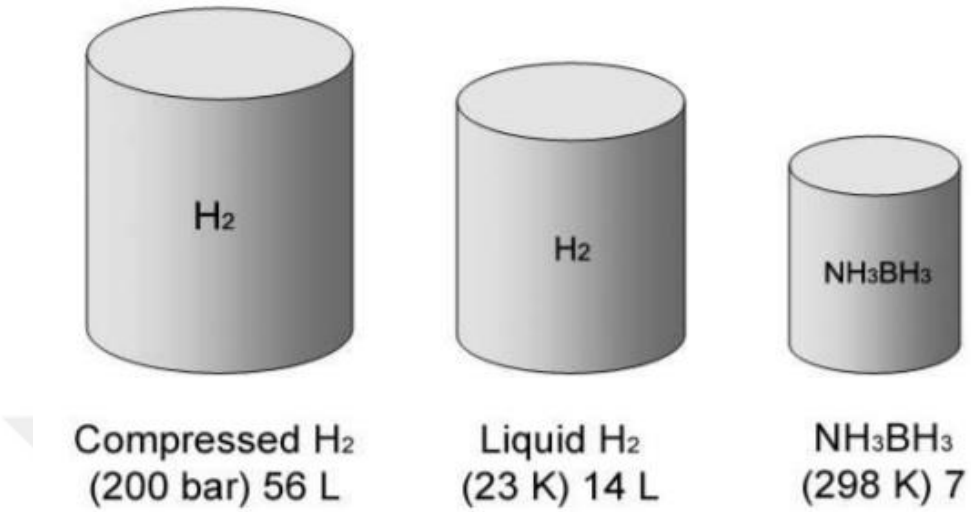

Figure 1.5. Volumes of 1 kg of hydrogen in various forms.

There is growing importance for the dehydrocoupling of amonia borane adducts in current interest in hydrogen storage. (Paul and Musgrave, 2007; Keaton et al., 2007; Denney et al., 2006). DMAB is one of the basic B-N compound with the low molecular weight (58.9 g mol-1) and high hydrogen capacity (16. 9 % wt) that has a good interest in hydrogen storage applications due to as a promising boron-based compoud (Langmi and McGrady, 2007; Hamilton, 2009; Gutowska, 2005). It is particularly important that the hydrogen can be released from the dehydrogenation of DMAB using suitable catalysts under mild conditions (Equation (1)) (Berg, and Arean, 2008; Jaska et al., 2001; Jaska et al., 2003).

1.2 Transition Metal(0) Nanoparticles As Catalyst

1.2.1 Catalysis

Catalyst is defined as chemical species that has the capability of increasing the rate of a reaction without affecting the standard Gibbs free energy, and not undergoing a net-reaction itself. Each catalyts molecule can take place in many repeated cycles without consumed in the catalytic process.

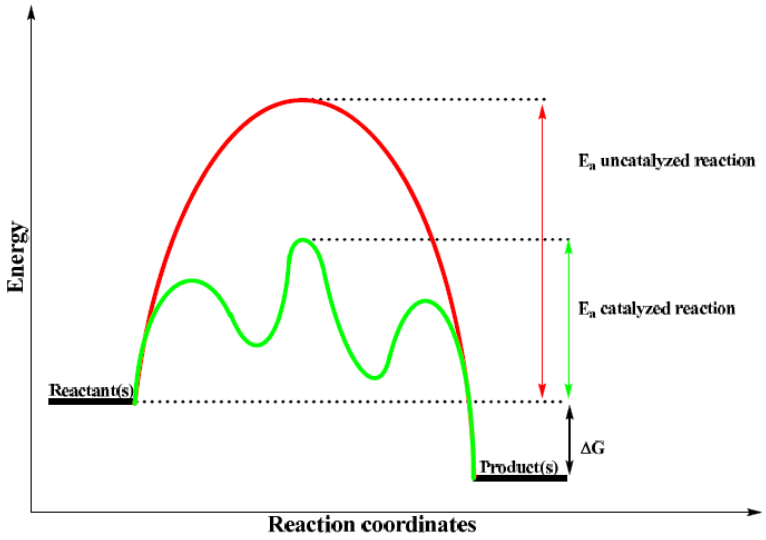

Figure 1.6. Potential energy diagram displaying the difference in activation energy and reaction pathway between a catalyzed and uncatalyzed reaction

Catalyst have altered the molecular path of the reaction that reduces the energy of activation resulting a different transition state through the reaction. Activation energy of a reaction can be defined as the minimal energy that must be accomplished to have a reaction. So, more molecular collision with the energy required to reach transition state occur with lowering energy barrier. Catalysts provide the molecular interaction between the reactants and lower the activation energy. In other words, catalyst lowers the energy of the transition state, the equilibrim state stay unaffected.

The effects of a catalyts during a chemical reaction can be analyzed considering the transition-state theory. Catalyst causes a decrement of the free energy of activation in the transition state theory. So, the activation enthalpy and entropy changes during the reaction. The entropy of the activation has lower than the corresponding uncatalyzed reaction due to the loss of translational freedom comig from the immobilization on the surface of the catalyst. One can conclude that for a catalyzed reaction, activation enthalpy must be less than uncatalyzed reaction according to the theory. Figure 1.6 shows the differences of the energy diagram of a catalyzed and uncatalyzed reaction. However, it could be noticed that the highest barrier significantly lower than the previous largest barrirer. Reaction proceed with a different pathway in catalyzed reaction having the lower activation energy. Since the rate of forward and reverse reaction is similarly affected there is no effect on the chemical equilibrium.

If the thermodynamic and the kinetic changes are favorable, chemical reaction can occur in laboratory conditions. The change of thermodyamic is measured by the change of Gibbs free energy (ΔG) and requirement of the kinetic energy is measured in terms of free energy of activation($\Delta G^{\#}$). The low free energy of the activation provides the favorable reaction in terms of thermodynamic. The conversion of diamond to graphite can be given an example. This conversion is thermodynamically favorable but it takes place very slowly at RT and pressure. Another example is the formation of ammonia from the mixture of nitrogen and hydrogen. It requires the considerable energy to overcome the activation energy barrier (Equation 2).

$$N_2(g) + 3H_2(g) \rightleftharpoons 2NH_3(g) \qquad (2)$$

The reaction can not be occured at low temperatures. The dissociation of nitrogen molecule occurs at around 3000 ^{o}C in the gas phase. While the hydrogen molecule has a weaker bond but it can be dissociated at a temperature above 1000 ^{o}C. In this case, catalyst being iron plays an important role. The hydrogen and nitrogen bond to the catalyst surface and loose their translational degree of freedom. So, the activation energy falls down and this leads to the forward reaction. The reaction take places without using hard temperature conditions. Consequently it can conclude that catalyst increase the rate of reaction with lowering the activation energy of the reaction and

does not effect on net enthalphy change and does not change the equilibrium of the reaction.

For the catalytic processes, it is more important to create both the activities and stabilities of the studied catalysts and for this assessment the quantities turnover number (TON) and turnover frequency (TOF) are utilized. TON is known as abbreviation of the number of reaction cycles that one molecule of the catalyst can perform before it is deactivated (Kozuch and Martin, 2012). TOF is desribed as catalytic cycle number per unit time (mole of product divided to per mole of catalyst per unit time) **(Equation 3-4).**

$$\text{TON} = \frac{mole\ of\ product}{mole\ of\ catalyst} \quad (3)$$

$$\text{TOF} = \frac{mole\ of\ product}{mole\ of\ catalyst\ x\ time} \quad (4)$$

1.2.2 Homogeneous *versus* Heterogeneous Catalysis

Although catalysts may be divided into several different classes, the most common classifications are heterogeneous vs. homogeneous catalysts (Figure 1.7). Homogeneous catalyts have similar phase (gas or liquid) as the reactants, while heterogeneous catalysts are not in the same state as the reactants.

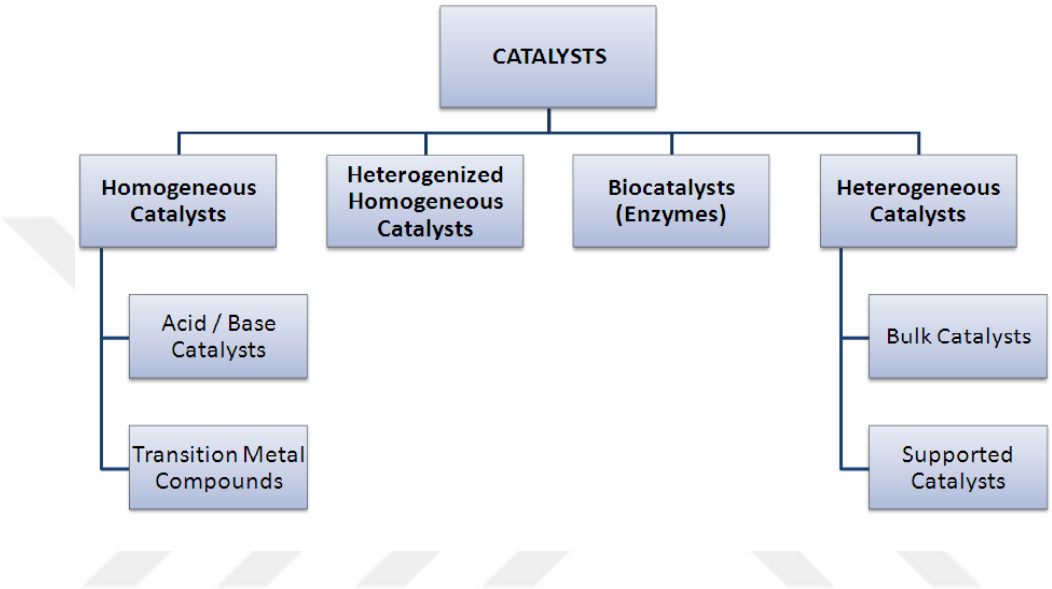

Figure 1.7. Types of Catalysts (Hagen, 2006).

Mechanism of homogeneous catalysis is usually formed by catalytic cycles. Catalyst is a part of the catalytic cycle and products and reactants are indicated outside of the cycle and attached to cycle by arrows.

For instance, catalytic reaction cycle which includes intermediates A and B is shown as below;

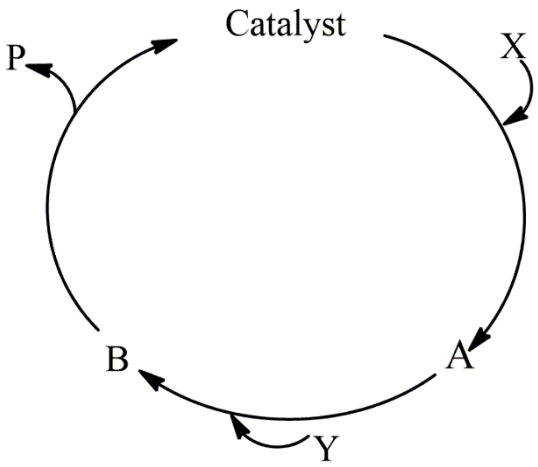

Figure 1.8. Cycle of homogeneous catalytic reaction.

Ligands surrounding metal and central atom create the catalytic centre in homogeneous catalysis. In homogeneous organometallic complex catalysts, the reaction starts with the reactant molecule bonding to a metal in the catalyst. So, vacant sites must be in metallic center. But, preserving of continuity of this situation is hard because the molecules are in the solvated conditions. Whole, the description of mechanism is transfer of ligand from the central metal and putting a reactant into the vacant sites. It seems like to substitution reaction. There is attack to vacant sites between reactant, ligand or solvent molecules. This process is suggested to comprise by associative or dissociative mechanism. In homogeneous catalysts, there is two basic roles of ligands. One of them is to stabilize metal complexes without playing a part in bond breakage and the other one is to be activated and placed in the catalytic reaction like the reactants on arrangement to a metal atom.

While the homogeneous catalysis takes place at same phases with the all reactants, in heterogeneous catalysis, reactants and catalyst exist in different phases during the reaction. In a heterogeneous catalyst mechanism, the first stage is the adsorption of the reactants onto a solid surface. Then, a surface reaction takes place and final stage is the desorption of the products from the surface of the catalyst into the liquid phase. Consequently, in a catalytic reaction, catalysts provides an alternative elementary steps to achieve the chemical reaction. The energy barrier of the catalytic path is lower than the non-catalytic path of the same reaction. So, the chemical reaction will be faster with using a catalyst. The reaction between the nitrogen and hydrogen in the presence

of iron can be given an example of heterogeneous catalysis (Eq.2). In this heterogeneous catalysis, iron acts a homogeneous catalyst and reaction carried out between the nitrogen and hydrogen on the catalyst surface. The product being ammonia released from the surface of the catalyst.

Heterogeneous catalysis is currently dominating over homogeneous catalysis by accounting for more than 85% of the area of industrial processes (Rothenberg, 2008; Gary and Handwerk, 2001; Sheldon and Van Bekkum, 2001). The use of heterogeneous catalysts has both advantages and disadvantages. The surface area affect the number of the active reaction sites of the heterogeneous catalyst, resulting detect and potentially limit the number of reaction sites. However, it can be seperated from the reaction mixture in an easy manner, such as by filtration. Hereby, expensive catalysts can be easily recovered being an important consideration for industrial manufacturing processes.

When we compare the advantages of these catalytic approaches, each of them has advantages; heterogeneous catalysts provide easy seperation and recover but requires hard reaction conditions to be fertile and the mass transport problems. However, homogeneous catalysts show high activity and selectivity however recovery of the transition metal catalysts from reaction medium is not easy as with heterogenous catalysts (Cole-Hamilton, 2003).

1.2.3 Nano-catalysis

Nanocatalysis has clearly ascended as a bridgework between heterogeneous and homogeneous catalysis with the development of nanoscience since end of the 1990s. The term nanocatalyst is defined as a material that has catalytic properties at least one nanoscale dimension. Their small size provide the excellent surface to volume ratio which is why they act as attractive catalysts. The field in which usage of nanomaterials as a catalyst in varied reactions has rapidly increased. (Thomas, 2010; Astruc, 2008). Improvement of welldefined catalyst including metal nanosized particles and nanomaterial as support is the main purpose. The nanocatalysts indicate the subsequent advantages of both heterogeneous and homogenous catalysts meaning easy recovery/recycling, high efficiency, selectivity and stability.

Even though the nano- term was used until recent times, researchers traditionally focused on very small particles of active catalytic agents in order to maximize the reaction efficiency. Nanoparticles have received remarkable attention due to the unique properties and applications in various areas such as electronics, optics, magnetism, energy technology and chemistry (Raimondi, 2005; Rao et al., 2004; Schmid, 2004; Shenhar and Rotello, 2003; Thomas and Kamat, 2003; Poizot et al., 2000). And also this interest is due to the fact that nanomaterials have more advanced catalytic properties than the bulk metal. Due to their small size the nanosized particles will have more percentage of atoms on the surface, which lead to increase catalytic activity. It was thought that gold was not catalytically active for a long time. In 1980, catalytic conversion of oxgen with carbon monoxide at low temperature was reported by Haruta (Haruta et al., 1987) and co-workers and gold catalyts was applied for the hydrochlorination of ethylene by Hutchings. (Hutchings, 1985). Since then many investigations have been made to utilize gold nanoparticles as active catalysts (Hashmi and Hutchings, 2006; Corma and Garcia, 2008; Arcad, 2008; Della Pina, 2008; Claus, 2005; McEwan et al., 2010). Then, palladium nanoparticles was used as a catalyts for some reactions such as C-C coupling (Balant et al., 2011; Fihri, 2011; Gude and Narayanan, 2011) or hydrogenations (Berhault, 2007; Piccolo, 2008) and also platinum nanoparticles (Manbeck et al., 2010; Chen et al., 2011) are discovered for hydrogenation reactions.

1.2.4 Transition metal nanoparticles as catalysts

Nanoparticles or nanowelding materials can be defined as materials within a nanometer range of length nanometers (Fahlman, 2011) Nanoparticles can be in many forms, such as powder, crystal, and cluster formulas. While nano-powder is decribed mixtre of fine powder, nanocrystals are known as ultrafine particle (Nouailhat, 2011). Nanocluster can be desribed as have a small size dispersion in the range of 1-10 nm with at least of one dimension. In the nanoscale chart, nanoparticles lies on between the molecular state and bulk materials and demonstrate significant properites. (Figure 1.9) (Pachon, 2008).

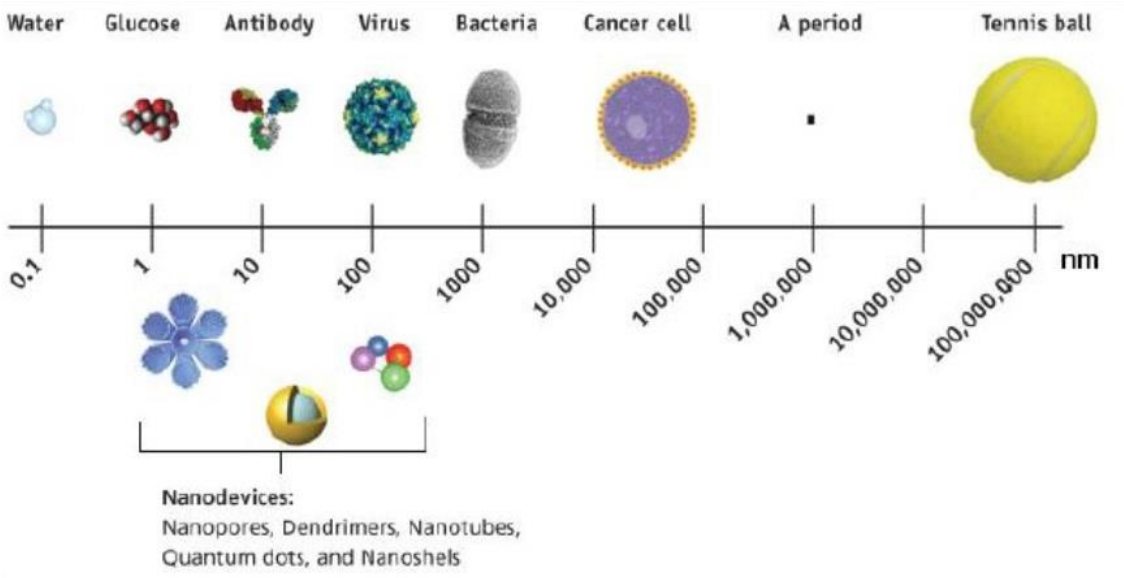

Figure 1.9. Schematic representation of the size of the particles (Flipponi and Sutherland, 2010).

The usage of nanoparticle was restricted to high-quality glass, pottery, and tile production until 18th century. In 1850s, Michael Faraday start to discover nanoparticle stability. At the end of the nineteenth century, Mie had investigations about color properties of nanoparticle. Following this research, Richard Zsigmondy won Nobel Prize in Chemistry about his study titled as colloidal suspension of gold nanoparticles using ultramicroscopic techniques in 1925.

Since metal nanoparticles have wide surface area per volume or weight unit in comparison with bulk metal they are considered to be likely candidates for catalysis, namely heterogeneous metal nanoparticles typically acts on metal surfaces. Metal nanparticles can be utilized as a catalyst due to the electrochemical properties of them. There is a grwowing interest for the metal nanoparticles. They can be utilized as catalysts due to their catalytic and electrochemical properties in a range of contexts like as a resin, vesicles, surfactant for water-soluble polymer and as well. The size of the metal nanoparticles is the driving force for the catalytic activity of them because of the fact that the MNPs are mainly defined by their size. As the particle size decreases, the surface area increases because of the surface area of the metal particle is inversely proportional to squared nanoparticle diameter. As a good example is the realationship between the percentage of surface iron atoms on spherical iron(0) nanoparticles and their size calculated by Klaube and co-workers (Figure 1. 10).

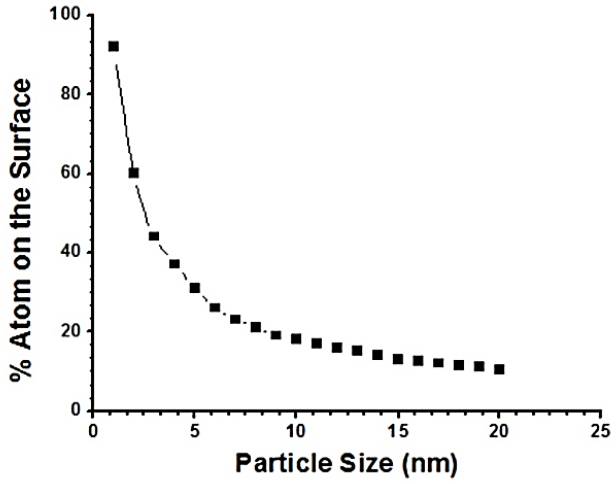

Figure 1.10. Relationship between the particle size and percentage of surface atoms.

Metal nanoparticles are more active catalysts than their bulk comppers due to the increment of surface atoms with decrement of particle size. So, higher catalytic activity is achieved with the decreasing size of the metal nanoparticles as all chemical reactions occur on the surface of catalyst (Pileni, 1997; Fu, 2002).

1.2.5 Methods of synthesizing of Metal Nanoparticles

The synthesis of transition metal nanoparticles focus on getting clean surface, smaller size particle, nice defined composition at the same time, in many applications. Two methods can be utilized for the preparation of metal NPs. First one is top-down method which is the former apporoach that bulk material has been devided into small pieces via mechanical grinding and mechanical milling (Whynano, 2016) (Figure 1. 11).

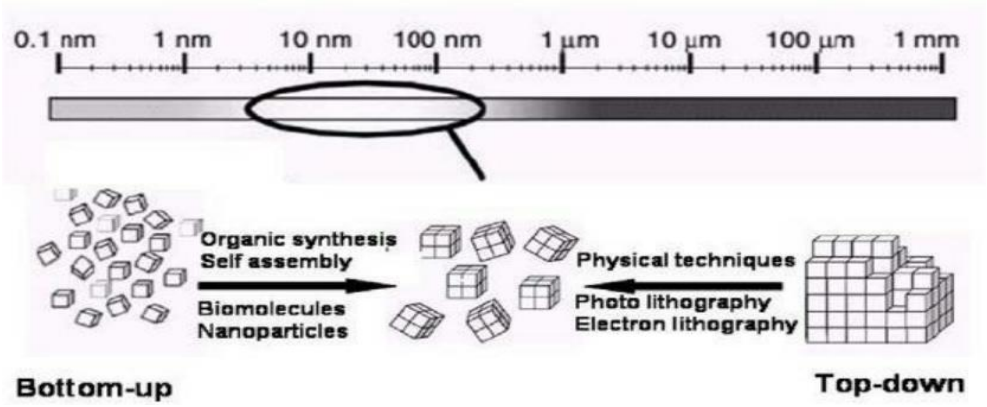

Figure 1.11. Schematic presentation of top down and bottom up approach (Yon and Lead, 2008).

In the latter approach, down-top method is consists of chemical and physical processing that is used for collecting the small pieces. Also, different types of method is existing for synthesis of metal NPs such as thermal decomposition and photochemical methods, ligand reduction, transition metal salt reduction, metal vapor synthesis, and displacement from organometallics.

1.2.6 Stabilization of metal nanoparticles

The catalytic activity of the metal nanoparticles depends on the relationship between the size of metal nanoparticles and activity, resulting in catalytic stability. Although metal nanoparticles are catalytically active, they tend to aggregate at higher temperatures and harsh reaction conditions. Aggregation or coagulation of metal nanoparticles leads to significant loss of catalyic activity of the catalysts during the catalytic reactions. The stabilization of the metallic NPs in colloidal solution and the means to preserve the catalytic activity is a major fact to be considered while synthesizing these catalysts. Several ways could be used in order to preclude agglomeration of metal NPs thus the stabilization of nanoparticles for the long terms could be achieved.

The selection of the stabilizers is important while synthesizing transition metal NPs. The chemical structure of the stabilizer used determine the shape and size of metal NPs. Many articles can be found about the types of stabilization of nanoparticles when

most of studies is examined in the literature (Pachon and Rothenberg, 2008; Schmid, 2010). Based on the nature of protective agents used, it is possible to identify five different kinds of stabilization.

1.2.7 Electrostatic Stabilization

Particles have been surrounded by an electrical double layer formed due to anions and cations from the initialing materials in electrostatic stabilization. As a result, Coulombic repulsion comes out that prevent the agglomeration. (Hunter, 1986; Hirtzel, 1985; Bard, 1986; Hunter, 1987). This electrostatic repulsion could be achieved by using ionic compounds such as halides or carboxylates. Figure 1. 12 indicates electrostatic stabilization of metal nanoparticles.

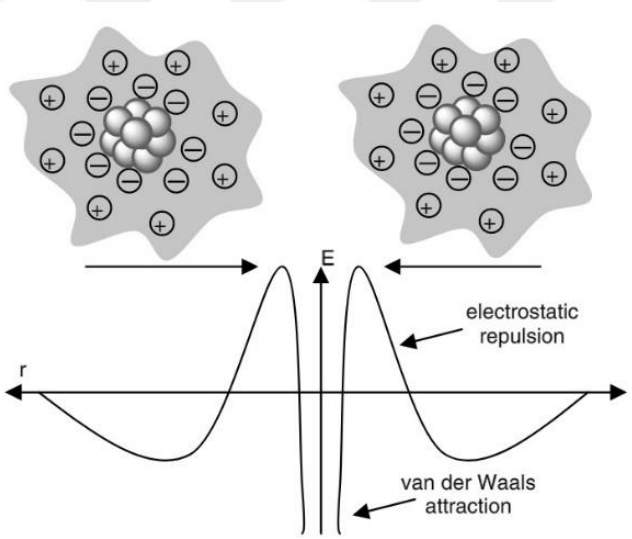

Figure 1.12. Electrostatic stabilization of metal NPs (Pachon, 2008).

1.2.8 Steric stabiliziation

In steric stabilization, metal center surrounded by sterically bulky materials such as oligomers or polymers (Erdogan et al., 2009), dendrimers (Zhao et al., 1998) or surfactants (Reetz et al., 1995, 1996) giving a layer around the metal. The bulky groups

of the materials form a protective layer on the surface of nanoparticles. So, the aggregration of nanoparticles will be prevented by bulky groups (Figure 1. 13).

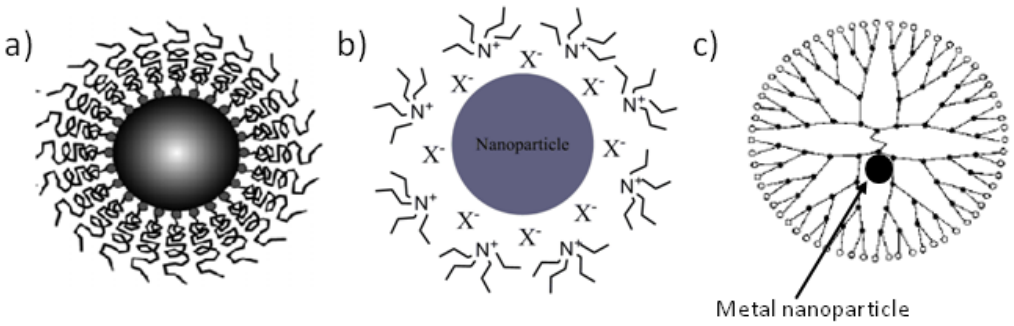

Figure 1.13. Illustration of a) polymer b) surfactant and c) dendrimer stabilized metal nanoparticles

1.2.9 Electrosteric Stabilization

Electrosteric stabilization is the combination of steric and electrostatic effects that ensure stabilization around the metal. This type of stabilization is similar to polyoxoanion-stabilized nanoclusters (Zahmakıran and Özkar, 2009; Zahmakıran et al., 2010) (Figure 1. 14).

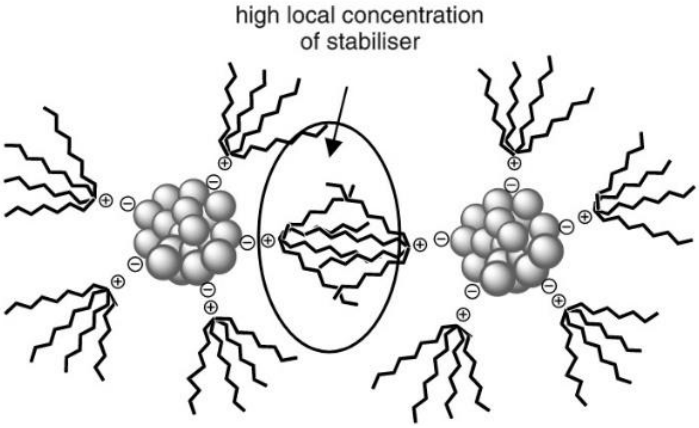

Figure1.14. Electrosteric stabilization of metal nanoparticles (Pachon, 2008).

1.2.10 Ligand Stabilization

In this type of stabilization, ligands such as phosphines, amines and S, P, N, donors of thiols are utilized as a stabilizer to prohibit the agglomeration of metal nanoparticles. Covalent interactions finds out between the metal and ligand molecule in this stabilizaton methods. Platinum, palladium and gold nanoparticles in colloidal solution have been stabilized using phosphine ligands (Duteil et al., 1995; Amiens et al., 1993). Gold nanoparticles have been stabilized with the usage of alkanethiols and functionalized thiols that were referred to as monolayer-protected clusters (MPCs) (Dasog and Scott, 2007; Hou et al., 2009). Thiol stabilized nanoparticles are often shown to be less catalytically active or inactive by reason of passivation of metal surface.

1.2.11 Stabilization on Solid Supports

Another way to avoid from the agglomeration of metal nanoparticles is confining the nanoparticles in space of the solid supports like metal oxides (Metin et al., 2010; Sayle et al., 2003), metal organic frameworks or zeolites (Zahmakıran et al., 2010).

Metal nanoparticles (< 10 nm) are thermodynamically unstable due to their wide surface areas and high surface energies. Stabilization of the metal nanoparticles is difficult to preserve the small size while retaining catalytic activity. Furthermore, the seperation of the catalyst could be difficult from the reaction solution after the catalytic reaction. It could be accomplished using the solid support for the stabilization of metal nanoparticles. Transition metal nanoparticles supported on various compounds such as silica, carbon and alumina are used as catalyst for the heterogeneous catalysis.

The supported metal nanocatalysts show advantages such as selectivity, enhanced activity, and prevention of aggregation by immobilization on solid support. There are several ways to synthesis of supported metal NPs.

The first method is impregnation method mostly used one that includes the wetting of solid support with the precursor metal solution for the synthesis of supported metal catalysts. Firstly, metal salts are dissolved in minimum amount of solvent and solid support is added to form slightly wet powder, the solvent is removed by drying and

calcination in the presence of oxidizing and reducing conditions (Choi, 2008). Polydispersed catalysts are obtained by this method (White et al., 2009; Campelo, 2008).

Another way for the synthesis of supported metal catalyst is deposition/precipitation method. In this method, precursor metal salt is dissolved in appropriate solvent and pH of the medium is adjust to get complete precipitation of precursor and then precipitate is deposited on the surface of support by using calcination method (Ertl et al., 1997).

Transition metal nanoparticles supported on metal oxides have been utilized as catalysts for a variety of organic reactions. The solid materials generally used for the synthesis of supported metal catalysts include, silica, alumina, titania due to the high surface area, high thermal stabilities and pore structures (Jong-San et al., 2003; Chen and Mou, 2004; Mingshu and Wayne, 2008; Ganapati, 2005; Sun et al., 2003).

1.3 Characterization methods for metal nanoparticles

Metal NPs can be characterized by means of several techniques however none of these are sufficient to learn information in detail about the studied materials. Therefore, combined tachniques should be used for the characterization of nanoparticles to classify each sample in size, structure, and catalytic properties. Figure 1. 15 depicts the several techniques used for the characterization of metal nanoparticles.

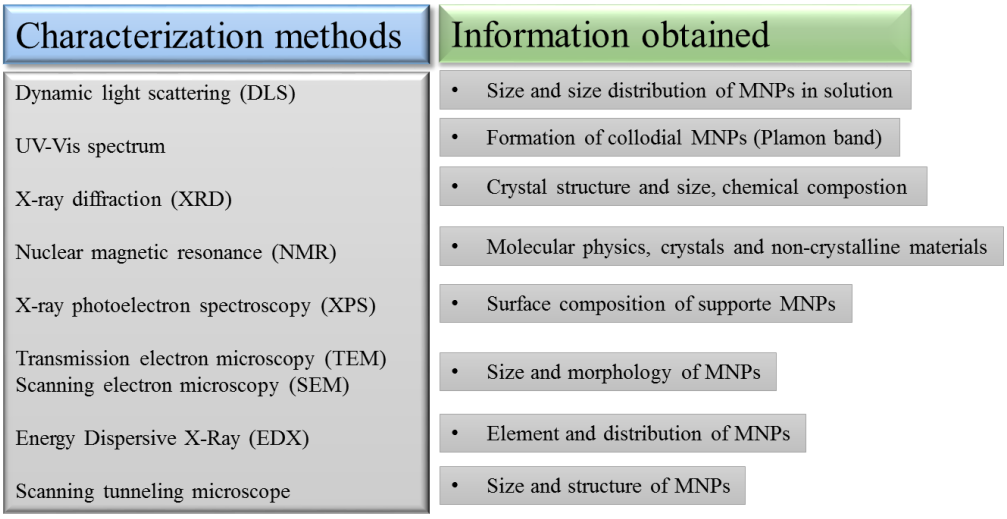

Figure 1. 15. Some characterization techniques of MNPs.

2. AIM AND SCOPE OF THIS STUDY

The goal of this dissertation is to prepare and characterize Cu(0) and Rh(0) NPs supported on ceria and titania nanopowder respectively, for the dehydrogenation of DMAB. While the copper(0) NPs stabilized on ceria nanopowder, henceforward referred to as Cu(0)/nanoCeO_2, were formed from the reduction of copper(II) 2-ethylhexanoate, rodium(II) hexanoate was used as precursor leading to the formation of Rh(0) NPs, Rh(0)/nanoTiO_2 throughout the dehydrogenation of DMAB at 60.0 ± 0.5 ^oC. After the catalytic dehydrogenation reaction of DMAB, copper(0) and rhodium(0) NPs supported on nanoceria and nanotitania, respectively were examined by means of ICP-OES, XRD, XPS, SEM, EDX, TEM, and N_2 adsorption-desorption spectroscopy. Ceria supported copper(0) nanoparticles (Cu(0)/CeO_2) are low-cost catalysts in comparison with the noble metals in dehydrogenation of DMAB. Cu(0)/CeO_2 has a remarkable catalytic activity with a turnover frequency of 40 h^{-1} in releasing 1 equivalent of pure H_2 gas per mole of $(CH_3)_2NHBH_3$ at 60.0 ± 0.5 ^oC. The results of the reusability tests and catalytic life time experiments indicate that Cu(0)/CeO_2 is an efficient catalyst in dehydrogenation of DMAB.

And also, the catalytic activity and lifetime of Rh(0)/nanoTiO_2 was tested in the dehydrogenation of DMAB, and found as with a record initial TOF value of 2900 h^{-1} in H_2 generation at 60.0 ± 0.5 °C, which is the biggest TOF value ever recorded for dehydrogenation of DMAB with the use of homogeneous or heterogeneous catalyst. Rh(0)/nanoTiO_2 is also quite reusable catalyst preserving 57% of the initial catalytic activity even after the fourth run of dehydrogenation reaction releasing 1 equivalent of pure H_2 gas per mole of $(CH_3)_2NHBH_3$ at 60.0 ± 0.5 ^oC. Kinetic study being relation with the temperature and catalyst concentration, on the catalytic dehydrogenation of $(CH_3)_2NHBH_3$ was also included in this dissertation.

3. EXPERIMENTAL PROCESSES

3.1 Materials

Copper(II) 2-ethylhexanoate ($Cu[CH_3(CH_2)_3CH(C_2H_5)CO_2]_2$), rhodium(II) octanoate ($[Rh(C_7H_{15}CO_2)_2]_2$), ceria (CeO_2, 25 nm, BET surface area 48.1 $m^2\ g^{-1}$), titania nanopowder (TiO_2, anatase, particle size $\approx$ 25 nm, BET surface area 63.3 $m^2\ g^{-1}$), dimethylamine borane ($(Me)_2NHBH_3$, DMAB, 97%) and toluene (99.7%) were bought from Aldrich. Deionized water was distilled by means of water purification system (Milli Q-pure WS). Toluene was distilled over sodium metal and stored in inert gas atmosphere before using in all dehydrogenation reactions unless otherwise specified. All glassware were cleaned with acetone and rinsed with copious distilled water and then dried in an oven at 150 ^oC.

3.2 In situ preparation of Cu(0)/nanoCeO_2 and catalytic dehydrogenation of $(CH_3)_2NHBH_3$

All experiments were performed under inert atmosphere. Schlenk tubes covering a vacuum system was used for the catalytic reactions. The schlenk tube was dried under vacuum for 30 minutes and kept under nitrogen gas to prevent moisture before all catalytic reactions. The tap on the side of the gas outlet was attached to a graduated glass tube full with water through a bubbler including 10 mL of methylcyclohexane (Figure 3.1). Cu(0) NPs supported on ceria were *in situ* generated throughout the dehydrogenation of DMAB. A stock solution of copper(II) 2-ethylhexanoate (Stock A) was prepared by dissolving 76.6 mg (0.218 mmol) copper(II) 2-ethylhexanoate in 25 mL toluene. In a typical experiment, under nitrogen purging, a 7.50 mL aliquot of the Stock A solution (8.74 mM Cu) was transferred to the flask including 100 mg ceria trough a septum by using a 10 mL syringe, which had been nitrogen-flushed three times. The resulting suspension was then stirred for 75 min to ensure a complete adherence of Cu^{2+} ions to the nanoceria support at 25.0 $\pm$ 0.5 ^oC. When a thermal equilibrium was reached, a solution of 60.1 mg (1.0 mmol) $(CH_3)_2NHBH_3$ in 2.5 mL toluene was added via a gastight syringe to the flask existing the suspension of

Cu^{2+}/nanoceria in toluene and the reaction mixture was stirred at 1000 rpm during the catalytic dehydrogenation of $(CH_3)_2NHBH_3$.

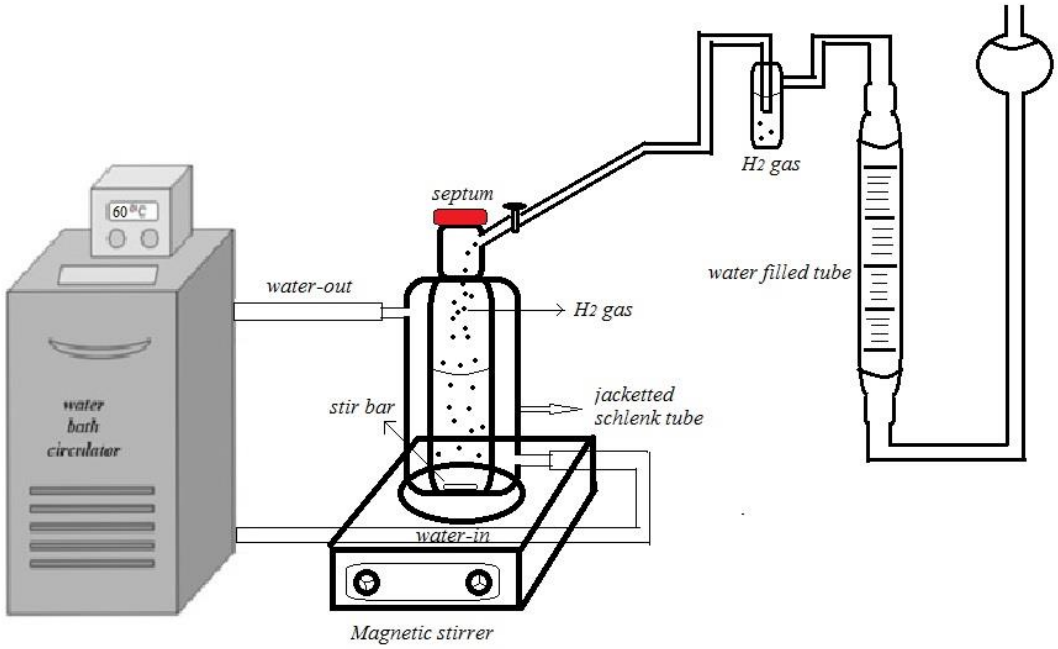

Figure 3.1. Schematic diagram of the reaction setup used for dehydrogenation of DMAB.

Reduction of copper(II) to copper(0) and the release of hydrogen gas from the dehydrogenation of DMAB was seen concomitantly after the addition of DMAB into the reaction mixture within in a short induction period. To determine the volume of hydrogen gas evolved throughout the catalytic reacton, the change of water level was measured at constant pressure, converted into the equivalent H_2 per mole DMAB. The reaction was finished as soon as hydrogen evolution was not completely observed.

3.3 Finding the most active copper loading for Cu(0)/CeO_2 in the dehydrogenation of $(CH_3)_2NHBH_3$

To find the most active copper loading for Cu(0)/CeO_2 various copper loadings in the range of 1.0-6.0 wt % were studied in hydrogen formation from dehydrogenation of DMAB starting with 6.56 mM Cu and 100 mM DMAB in 10 mL toluene solution at 60.0 ± 0.5 ^oC. The best catalytic activity was obtained by using 4.0 wt. % copper loaded

on 100 mg ceria. For all the other catalytic reactions, $Cu(0)/CeO_2$ with the loading of 4.0 wt. % Cu was utilized unless otherwise stated.

3.4 Preparation of Cu^{2+}- ion impregnated on nanoceria surface

The stock solution (Stok A) prepared in Section 4.3 was also used for the preparation of Cu^{2+}- ion impregnated on nanoceria. For each catalytic experiment an aliquot of the Stock A solution was moved into the flask including 100 mg nanoceria for obtaining samples with different additions of copper in the range of 1-6% wt. To provide a complete adherence of Cu^{2+} ions to the ceria nanopowder support, resulting mixture was then stirred for 75 min at 25.0 ± 0.5 ^{o}C.

3.5 Activation parameters for dehydrogenation of $(CH_3)_2NHBH_3$ catalyzed by $Cu(0)/CeO_2$

Catalytic dehydrogenation reaction of 100 mM DMAB was carried out starting with 6.56 mM Cu (4.0% wt.) at various temperatures (60, 55, 50, 45 ^{o}C). The data of the rate constant were found via the plots of hydrogen versus time and used for determination of the activation energy, enthalpy alteration of activation, and entropy alteration of activation by ploting Eyring-Polanyi curve.

3.6 Leaching test and kinetic competence of $Cu(0)/CeO_2$ in the hydrogen generation of $(CH_3)_2NHBH_3$

After the first run of catalytic dehydrogenation of DMAB starting with 10 mL of 100 mM DMAB (60.12 mg $(CH_3)_2NH.BH_3$) and 6.56 mM Cu(II) impregnated on 100 mg ceria (4.0 wt. % Cu) at 60.0 ± 0.5 ^{o}C, the catalyst was expected to settle down, the reaction solution was then filtered into another reaction flask under inert gas atmosphere. The isolated solid and the filtrate solution were examined for their catalytic activity under the same reaction conditions by adding a new batch of DMAB (100 mM). Furthermore, the filtrate was examined with use of ICP-OES to prove that

copper free leached into the solution from the surface of nanoceria throughout the dehydrogenation of DMAB.

3.7 Recyclability of ceria supported copper(0) nanoparticles in the catalytic dehydrogenation of $(CH_3)_2NHBH_3$

After the completed dehydrogenation of DMAB in the first run, a second batch of DMAB (60.12 mg) has been added to the solution without removing anything from the reaction medium. The catalytic activity was determined by observing the rate of hydrogen generation.

3.8 Catalytic lifetime of $Cu(0)/CeO_2$ in the dehydrogenation of $(CH_3)_2NHBH_3$

The catalytic lifetime of $Cu(0)/CeO_2$ in the dehydrogenation of DMAB was obtained by determining the total turnover number (TTO). In a lifetime experiment, 6.56 mM $Cu(0)/CeO_2$ and 250 mM DMAB was used in a 10 mL toluene solution. Once the complete conversion of DMAB was provided, extra DMAB was added into the reaction flask in N_2 purging.

3.9 Poisoning test for $Cu(0)/CeO_2$ in the dehydrogenation of $(CH_3)_2NHBH_3$

A stock solution of CS_2 in toluene (Stock B) was obtained by dissolving 120 μL CS_2 in total 25 mL toluene under inert atmosphere and used for performing the catalyst poisoning experiments,. A typical catalytic dehydrogenation reaction was started with 6.56 mM Cu (4.0% wt. Cu, $Cu(0)/CeO_2$) at 60.0 ± 0.5 ˚C. After 40% conversion of reaction was attained, 0.2 equivalent (1.31 mM, μL 160) CS_2 per copper was transferred to the reaction medium via a gastight syringe to poison the catalyst. Upon the addition of CS_2, the hydrogen generation ceased.

3.10 In situ preparation of Rh(0)/nanoTiO$_2$ and catalytic dehydrogenation of $(CH_3)_2NHBH_3$

Rhodium(0) NPs supported on titania were *in situ* generated throughout the dehydrogenation of $(CH_3)_2NHBH_3$. A stock solution of 0.49 mM Rh^{2+} was prepared by dissolving 4.77 mg Rh(II) octanoate in about 5 mL of toluene in a volumetric flask under nitrogen atmosphere and diluted to 25 mL by adding more toluene. In a typical experiment, under nitrogen purging, a 7.50 mL aliquot of stock solution (0.37 mM Rh) was transferred to the reaction flask containing 50 mg TiO_2 trough a septum by using a 10 mL syringe and the resulting mixture was stirred for an hour at 25.0 ^oC. The jacketed flask was surounded by circulating water at 60.0 ± 0.5 ^oC or at a specified temperature. A solution of 60.1 mg (1.0 mmol) $(CH_3)_2NHBH_3$ in 2.5 mL toluene was added via a gastight syringe to the flask including the suspension of rhodium(II) octanoate and titania in toluene and the reaction was began with stirring the mixture at 1000 rpm after the thermal equilibrium was reached. The changement of the water level in the glass tube was measured for the determination of the hydrogen volume evolved during the catalytic reaction. And it was transformed into the equivalent H_2 per mole of $(CH_3)_2NHBH_3$.

3.11 Influence of rhodium loading on the catalytic activity of Rh(0)/nanoTiO$_2$

A series of experiments were performed starting with 10 mL of solution containing (60.1 mg) 100 mM $(CH_3)_2NHBH_3$ in order to test the activity of the catalyst with different Rh loading and thus in various rhodium concentrations (0.1, 0.2, 0.3, 0.4, 0.5 wt. % Rh or 0.049, 0.097, 0.15, 0.20 and 0.24 mM Rh, respectively).

3.12 Recyclability of Rh(0)/nanoTiO$_2$ in the dehydrogenation of $(CH_3)_2NHBH_3$

After dehydrogenation of DMAB began with 60.1 mg (100 mM) DMAB and 0.96 mg rhodium(II) octanoate (0.50 wt.% rhodium, 2.4 μmol Rh) in 10 mL solution at 60.0 ± 0.5 ^oC was completed, the catalyst was kept in the reaction medium and a new batch

of DMAB was added to the reaction mixture. The same procedure was applied for a subsequent run of dehydrogenation of DMAB at 60.0 ± 0.5 ºC.

3.13 Catalytic lifetime of Rh(0)/nanoTiO$_2$ in the dehydrogenation of $(CH_3)_2NHBH_3$

The catalytic lifetime of Rh(0)/nanoTiO$_2$ was obtained by determining TTO number in the dehydrogenation of DMAB. For a catalytic life time experiment was carried out by starting 10 mL solution including 50 mg Rh(II)/nanoTiO$_2$ (0.50 wt.% rhodium, 2.4 μmol Rh) and 100 mM (60.1 mg) $(CH_3)_2NHBH_3$ at 60.0 ± 0.5 ºC. When dimethylamine borane in the solution was completely dehydrogenated, more DMAB was added to the raction solution and the reaction was monitored for no more hydrogen gas evolution.

3.14 CS_2 poisoning test for Rh(0)/nanoTiO$_2$ in the dehydrogenation of $(CH_3)_2NHBH_3$

For the poisoning experiment of Rh(0)/nanoTiO$_2$ in the dehydrogenation of DMAB, a 2.0 mM CS_2 stock solution has been prepared in 10 mL toluene. A typical dehydrogenation reaction of DMAB catalyzed by Rh(0)/nanoTiO$_2$ was begun with 0.24 mM Rh (0.5 wt. % Rh, Rh(0)/TiO2) at 60.0 ± 0.5 ºC. After 50% conversion of $(CH_3)_2NHBH_3$ 0.2 equivalent CS_2 (49 μM, 250 μL stock solution) was added to the reaction mixture via gastight syringe. The hydrogen gas evolution ceased immediately as soon as addition of CS_2 solution. The reaction was observed for 20 minutes to ensure no further gas evolution.

3.15 Leaching Test for Rh(0)/nanoTiO$_2$ in the dehydrogenation of $(CH_3)_2NHBH_3$

A leaching test was performed to determine the amount of rhodium transferred from the surface of nanotitania to the reaction solution for Rh(0)/nanoTiO$_2$ in dehydrogenation of DMAB. The first run of catalytic dehydrogenation of DMAB (0.5 wt. % Rh, 0.24 mM Rh) at 60.0 ± 0.5 ^oC was finished, before the reaction solution was allowed to settle down. The reacion solution was filtered under nitrogen gas atmosphere through a microfilter of 0.45 microns and transferred into another schlenk tube. A new batch of $(CH_3)_2NHBH_3$ (60.1 mg, 100 mM) was added to the solution at 60.0 ± 0.5 ^oC. The reaction was begun and hydrogen evolution was monitored. Furthermore, the solution obtained by filtration from the reaction mixure after the catalytic dehydrogenation reaction was also analyzed by ICP-OES for the rhodium content.

3.16 Characterization of ceria supported Cu(0) and titania supported Rh(0) NPs

In situ generated Cu(0) and Rh(0) NPs were characterized by using X-ray photoelectron spectra (XPS), X-ray diffraction (XRD), transmission electron microscopy (TEM), scanning electron microscopy (SEM), Nuclear magnetic resonance (NMR) and UV-vis techniques after the catalytic reaction of dimethylamine borane.

TEM analysis: A 0.2 mL of aliquot solution was taken from the reaction medium after the dehydrogenation reaction for TEM analysis and diluted in 2 mL ethanol was transferred into glass vial. Carbon coated copper grid was immersed into the colloidal solution to deposite the nanoparticles for 5 seconds and then the volatilies was evaporated from the copper grid in inert atmosphere. The analysis of the samples were done by using a JEM-2010F (JEOL) TEM instrument operating at 200 kV.

SEM analysis: A scanning electron microscope (SEM, JEOL 6390-LV) with the accelerating voltage of 20 kV was utilized to research the surface morphology of the $Cu(0)/CeO_2$ and $Rh(0)/TiO_2$ samples. The micrographs of specimen surfaces was obtained from the secondary electron image to investigate the morphological structure of samples. Samples was also coated with Au to improve resolution.

X-ray Diffraction: The samples for XRD analysis were prepared from reaction solution after dehydrogenation reaction by removing the volatiles in vacuum at room temperature. The X-ray diffraction (XRD) pattern was recorded on a Rigaku Multiflex 2kW diffractometer with Cu-Ka radition (λ= 1.5418 Å) in the range 22=10-90^o at a scan of 5^o/min and a step increment of 0.02^o at room temperature at Abant İzzet Baysal University.

(XPS)- X-Ray photoelectron spectroscopy: X-ray photelectron spectra of ceria supported Cu (0) and titania supported Rh(0) NPs were taken by using Physical 15 Electronics 5800 spectrometer. The equipment is accommodated up monochromatic Al-Kα radiation of 1486.6 eV with X-ray tube working at 15 kV, 350W.

UV-Visible Spectroscopy: Schimadzu-2540 double beam spectrometer was utilized for a 100 µL solution for the UV-vis analysis of the samples and at a spectral range of 200–800 nm. Spectrum was recorded using a 1cm quartz cuvette at room tempereture.

FT-IR Spectroscopy: ATR-IR spectra were recorded on by means of Perkin Elmer UATR Spectrum Two IR Spectrometer.

NMR Spectroscopy: Bruker Avance DPX 400 MHz spectrometer with a working frequency of 128.15 MHz was used for ^{11}B-NMR analysis of the samples. External refrence was $BF_3{\bullet}(C_2H_5)_2O$ for ^{11}B-NMR chemical shifts.

BET analysis: Nova 3000 series Quantachrome Instrument was used for the BET analysis of the samples. Degassion process was carried out for 3 h at 573 K before the N_2 adsoprtion.

4. RESULTS AND DISCUSSION

4.1 Copper(0)/Ceria nanoparticles

4.1.1 In situ formation of ceria supported copper(0) nanoparticles

Copper(II) 2-ethylhexanoate was used as a precursor for the generation of copper(0) nanoparticles catalyst in the dehydrogenation of DMAB in toluene solution. *In situ* formation of Cu(0) NPs from the reduction of copper(II) 2-ethylhexanoate and concomitant H_2 release from the catalytic dehydrogenation/dehydrocoupling of DMAB occured in the same medium. When copper(II) 2-ethylhexanoate is added to the toluene solution of DMAB at 60.0 ± 0.5 ^oC, a fast evolution of hydrogen initiates immediately without induction period (Figure 4. 1).

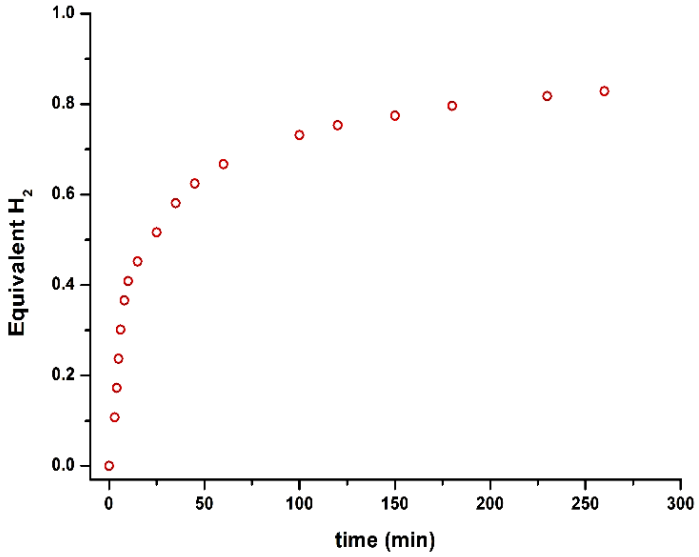

Figure 4.1. Plot of mole H_2 evolved per mole of dimethylamine borane versus time for dehydrogenation of $(CH_3)_2NHBH_3$ starting with 10.0 mL solution containing 30 mM Cu, 100 mM $(CH_3)_2NHBH_3$ at 60.0 ± 0.5 ^oC.

However, the hydrogen evolution slows down after the release of about 0.5 equivalent H_2 per mole of DMAB (ca 10 minutes) indicating deactivation of the catalyst formed. During the reduction of the precursor $Cu(C_7H_{15}CO_2)_2$, the color of reaction solution gradually changes greenish-blue to red within less than 10 minutes indicating the formation of Cu(0) NPs. This color change implies that the reaction can be followed by monitoring the changes in the UV-vis electronic absorption spectrum of solution. The starting solution containing 30 mM copper(II) 2-ethylhexanoate in toluene exhibits an intense absorption band at λ_{max} = 296 nm and a broad band at λ_{max} = 668 nm in the spectrum (Figure 4. 2).

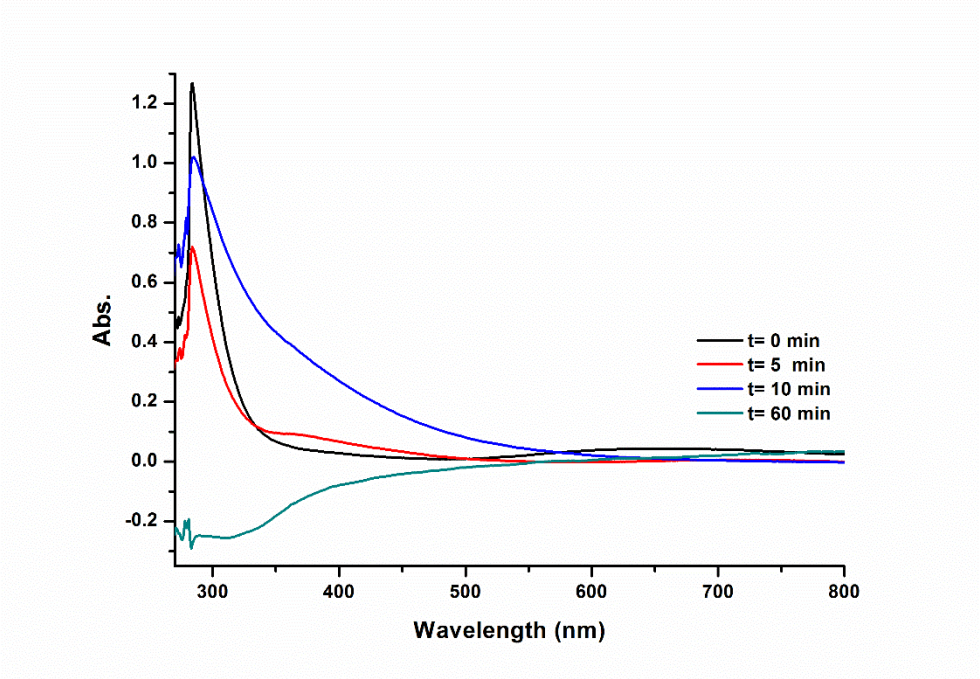

Figure 4.2. UV-vis spectra of solutions containing 30 mM of copper(II) 2-ethylhexanoate in toluene before and after addition 100 mM of $(CH_3)_2NHBH_3$ into the solution at specific time intervals.

Comparing to the literature values (Lever, 1984), the broad band at 668 nm is attributed to the *d-d* transition and the strong band at 296 nm to the LMCT transition in $Cu(C_7H_{15}CO_2)_2$. The spectral features change immediately when DMAB is added to the solution and a new band becomes clear in at 361 nm. This absorption band can be attributed to plasmon resonance band of Copper(0) Nanoparticles (Ehrenreich and Philipp, 1962, Creighton and Desmond, 1991). The latter two bands lose intensity as the reaction proceeds and ultimately disappear within 1 hour. Concomitantly, the reaction solution becomes clear with the precipitation of bulk metal. This observation

indicates that copper(0) NPs, formed from the reduction of copper(II) ions throughout dehydrogenation of DMAB, are not stable and therefore converted to the bulk metal within a short time. 2-ethylhexanoate ion is only potential stabilizer in the reaction solution which does not provide enough stabilization for the Cu(0) NPs against agglomeration. (Ozkar and Finke, 2002).

The decreasing in the catalytic activity is another evidence for the agglomeration of copper(0) nanoparticles (Figure 4.1). In order to stabilize the *in situ* generated copper(0) nanoparticles against agglomeration they were supported on the surface of ceria nanopowders. Copper(0) NPs supported on nanoceria ($Cu(0)/CeO_2$) were *in situ* formed from the reduction of copper(II) ions impregnated on nanoceria (Cu^{2+}/CeO_2) during the catalytic dehydrogenation of DMAB. When dimethylamine borane was added to a suspension of Cu^{2+}/CeO_2 in toluene, both the generation of Cu(0) nanoparticles and catalytic dehydrogenation of DMAB occur concomitantly. The formation of Cu(0) NPs and concomitant dehydrogenation of DMAB was monitored by following the volume of H_2 generated. And it was turned into the equivalent H_2 per mole of DMAB using the known 1:1 $H_2/(CH_3)_2NHBH_3$ stoichiometry. (Eq.1). Figure 4. 3 indicates the plot of equivalent H_2 per mole of DMAB versus time for the dehydrogenation of DMAB beginning with Cu^{2+}/CeO_2 precatalyst (6.56 mM Cu) and 100 mM DMAB in 10 mL toluene at 60 ± 0.5 °C.

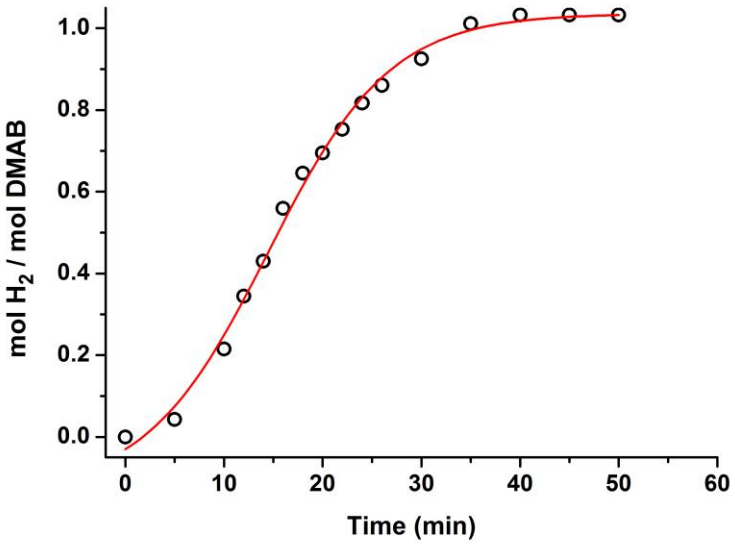

Figure 4.3. The evolution of equivalent H_2 per mole of $(CH_3)_2NHBH_3$ DMAB versus time plot for the dehydrogenation of DMAB starting with Cu(II)/Ceria precatalyst (6.56 mM Cu) and 100 mM DMAB at 60.0 ± 0.5 °C.

The generation kinetics of the Cu(0) NPs can be attained with the use of the dehydrogenation of DMAB as recorder reaction (Watzky, 1997a, Watzky, 1997b; Widegren et al., 2003) (Figure 4. 4), in which A is the added precursor $Cu(C_7H_{15}CO_2)_2$ and B is the growing copper(0) nanoparticles. The observation of a sigmodial dehydrogenation curve is very powerful demostration for the generation of metal(0) nanoparticle catalyst.

In Figure 4. 3, the determined rate constants by the nonlinear least-squares curve fit are k_1= $1.10x10^{-2} \pm 1.63x10^{-3}$ min^{-1} and k_2 = $2.80 \pm 1.31x10^{-2}$ M^{-1} min^{-1} (the mathematically required correction was made to k_2 for the stoichiometry factor of 16, as defined elsewhere (Widegren et al., 2003), but not for the 'scaling factor'; that is, any corrections have not been made for the count of Cu atoms on the growing metal surface.

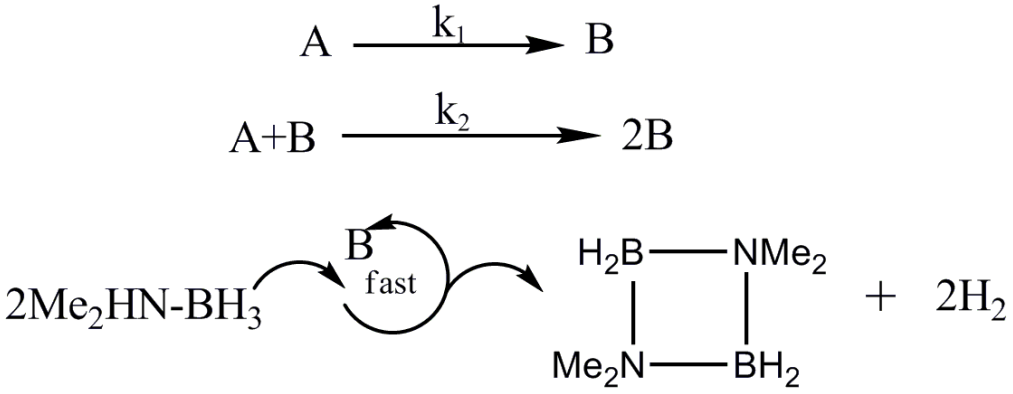

Figure 4.4. Illustration of the dehydrogenation of $(CH_3)_2NHBH_3$ as reporter reaction for the formation of copper(0) nanoparticles: A is the precursor copper(II) ion impregnated on Ceria and B is the growing $Cu(0)_n$ nanoparticles.

4.1.2 Characterization of Cu(0) NPs supported on CeO_2

The ceria supported copper(0) nanoparticles, *in situ* formed by the reduction of copper(II) precursor throughout the dehydrogenation of DMAB, were seperated from the reaction solution and characterized by means of XRD, SEM-EDS, TEM and XPS

techniques. The XRD patterns of CeO_2 and Cu(0)/CeO_2 with a copper loading of 4.0% wt. Cu, shown in Figure 4. 5 a and b, respectively, exhibits the characteristic diffraction peaks of CeO_2 at 28.5º, 33.1º, 47.5º, 56.3º, 59.1º, 69.5º, 76.8º, and 79.1º assigned to the (111), (200), (220), (311), (222), (400), (331) and (420) reflections of CeO_2 (ICDD Card 34-0394). The comparison of XRD patterns of two samples clearly show that there is no observable peak which would be attributed to copper, most likely due to low copper loading on ceria. Furthermore, no change is observed in the positions of ceria diffraction peaks. Hence, one can conclude that copper loading does not alter the structure of support. However, Debye-Scherrer equation was used to calculate the crystallite size of pure ceria and Cu(0)/CeO_2 sample and found as 24.9 nm and 13.4 nm, respectively.

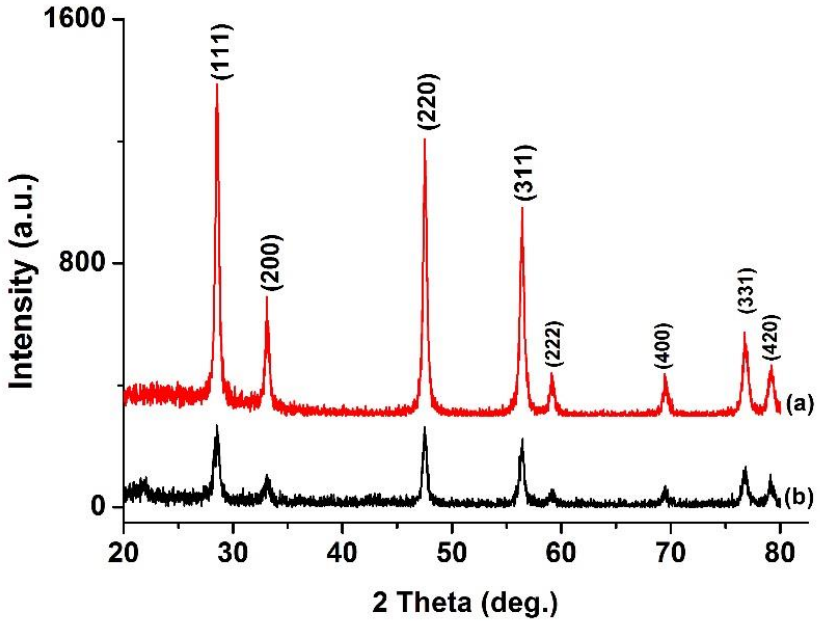

Figure 4.5. Powder XRD patterns of (a) CeO_2 and (b) Cu(0)/CeO_2 with a 4.0% wt. Cu loading.

Thus, one can conclude that copper loading during the catalytic process causes a decrement of the crystallite size and relative intensity of the main peak of CeO_2 in Figure 4. 5. The presence of copper nanoparticles in the loaded sample may cause a decrease in the crystallinity of host material.

SEM analysis was utilized to examine the morphology of the surface of ceria and Cu(0)/CeO_2. Figure 4. 6 displays the SEM image of pure ceria and ceria supported Cu(0) NPs with a metal loading of 4.0% wt.

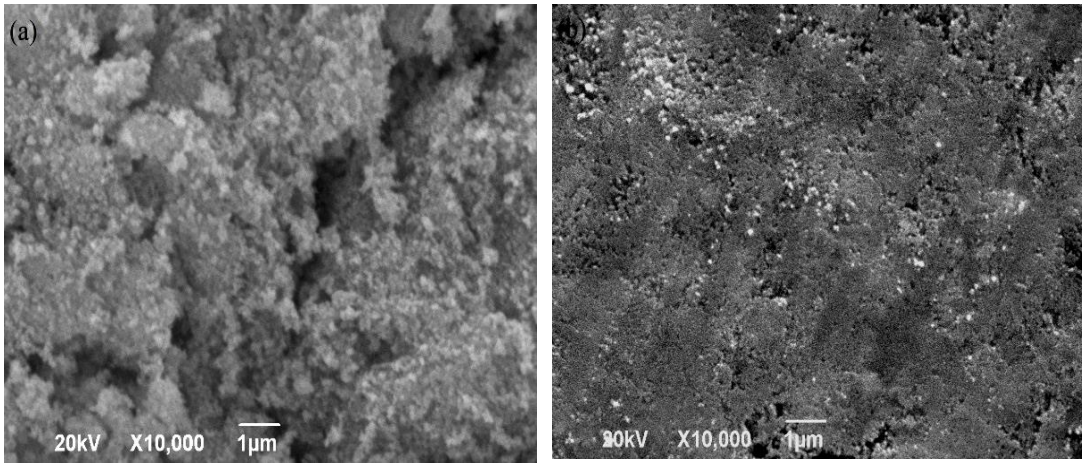

Figure 4.6. (a) SEM image of CeO_2, (b) SEM image of $Cu(0)/CeO_2$ with a 4.0% wt. Cu.

SEM-EDX spectrum and elemental mapping of $Cu(0)/CeO_2$ with a metal loading of 4.0% wt. given in Figure 4.7 indicate that copper and gold are the only elements detected in addition to the framework elements of ceria (Ce, O).

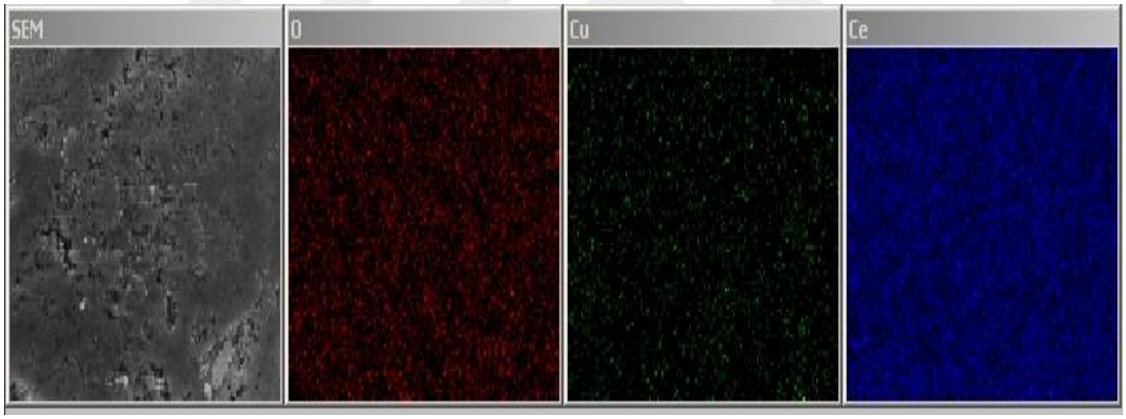

Figure 4.7. Elemental mapping of $Cu(0)/CeO_2$ with a 4.0% wt. Cu.

Moreover, SEM-EDX results show that the copper loading is 4.0 % wt. for Cu $(0)/CeO_2$ sample as seen from the Table in the inset of Figure 4.8. This indicates that all the copper are on the surface of ceria. Additionally, the mapped SEM micrograph analyses of the sample indicate good elemental distribution in the copper loaded ceria sample.

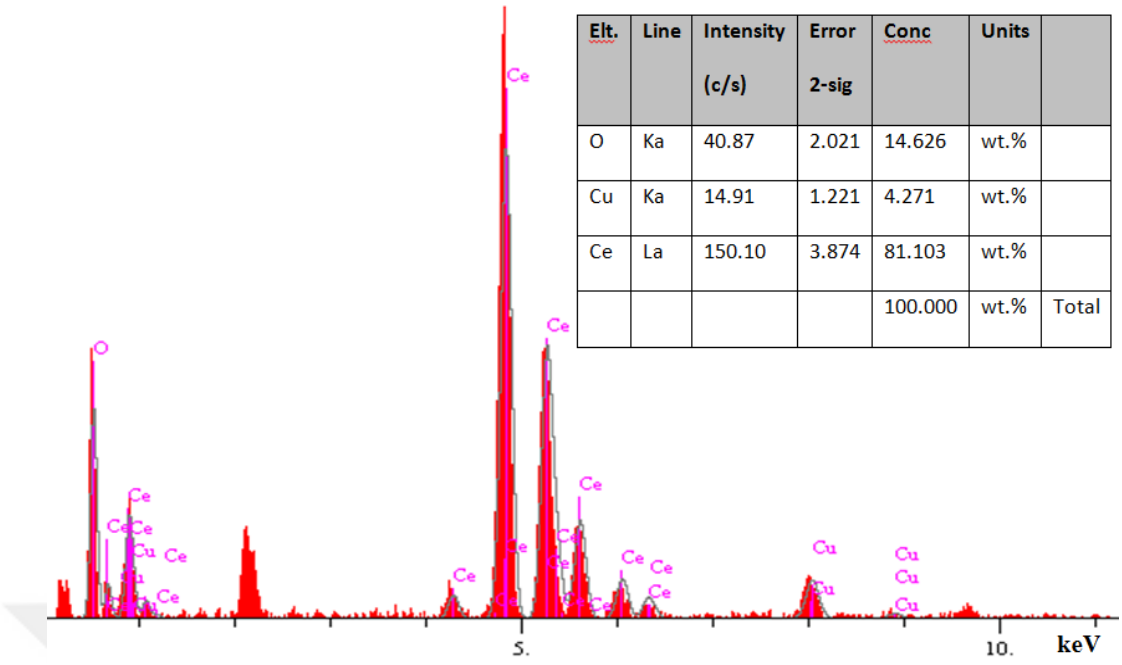

Figure 4.8. SEM-EDX spectrum of Cu(0)/CeO_2 with a 4.0% wt. Cu.

Figure 4. 9 depicts the TEM images of Cu(0)/CeO_2 with a copper loading of 4.0% wt. taken at different magnifications after catalytic reaction indicating a uniform distribution of copper(0) NPs on the surface of ceria nanopowders. The particle size histogram of copper(0) NPs was constructed measuring the size of more than 100 non-touching particles from TEM images (Figure 4.9d).

The histogram (Figure 4.9d) indicates the presence of highly dispersed copper(0) NPs on the ceria surface in the range 1.8-5.3 nm with an average particle size 3.1 ± 0.8 nm. The BET surface area was determined to be 55.1 and 48.7 m^2 g^{-1} for CeO_2 and Cu(0)/CeO_2 with a copper loading of 4.0% wt., respectively. The slight decrease in the surface area observed upon copper loading of ceria implies the presence of copper NPs on the surface of ceria.

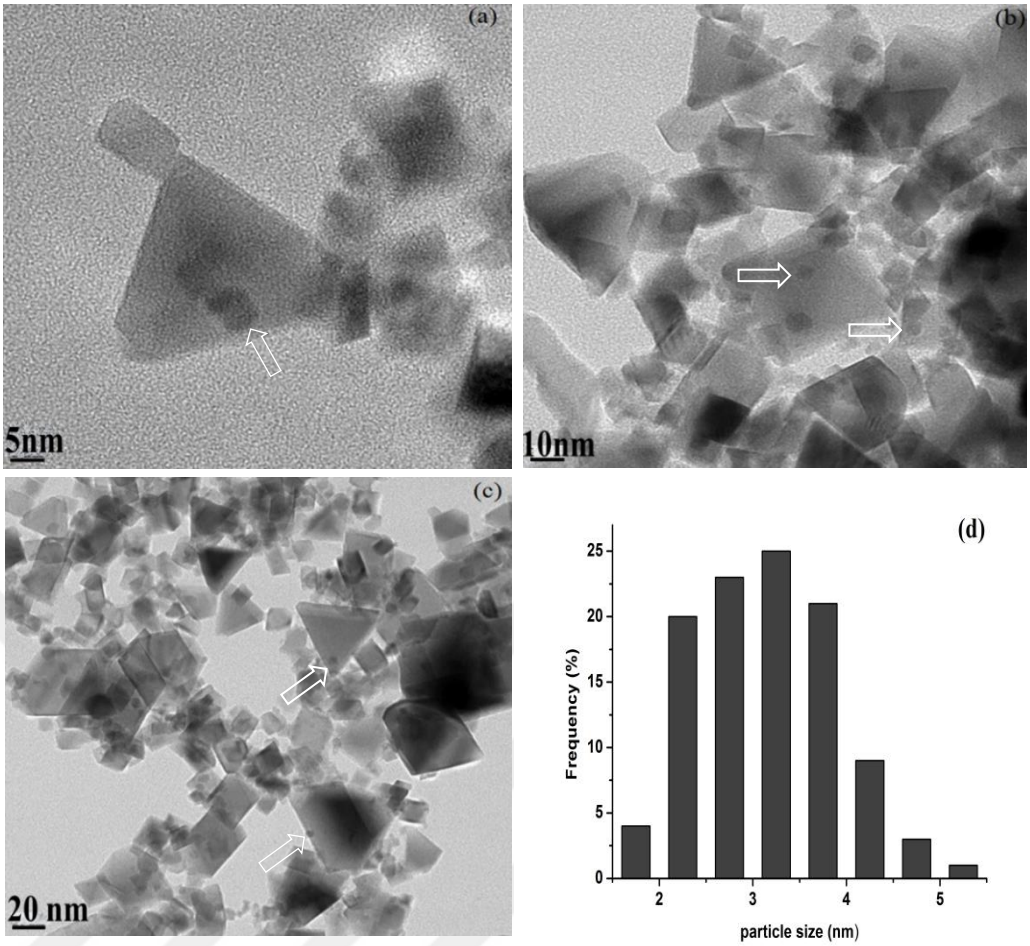

Figure 4.9. (a-c) TEM images of Cu(0)/CeO_2 with a 4.0% wt. Cu loading in different magnifications with scale bars of 5, 10, and 20 nm, respectively. (d) the histogram for the particle size distribution.

To investigate the composition of Cu(0)/CeO_2 formed in situ during the dehydrogenation reaction of DMAB and oxidation state of copper XPS technique was used (Figure 4.10). The survey-scan XPS spectrum of Cu(0)/CeO_2 with a copper loading of 4.0% wt. (Figure 4.10a) shows that copper is the only element detected in addition to the ceria framework elements (Ce, O) in agreement with SEM-EDX result. Figure 4.10b shows the high resolution scan and deconvolution for the Cu 2p core of Cu(0)/CeO_2 indicating two prominent peaks at 930.6 and 950.8 eV which are assigned to copper(0) $2p_{3/2}$ and $2p_{1/2}$, respectively (Miller and Simmons, 1993). Two relatively weak peaks observed at 933.8 and 952.2 eV are attributable to copper(II) $2p_{3/2}$ and $2p_{1/2}$, respectively (Ghijsen et al., 1988; Chawla et al., 1992). Additional weak peaks are due to shake up process. CuO is most likely formed upon air exposure of Cu(0)/CeO_2 during the XPS sampling (Chusuei et al., 1999). The high resolution XPS

spectra of Ce 3d core for the CeO_2 and $Cu(0)/CeO_2$ with a copper loading of 4.0 % wt. samples are depicted in Figure 4.10c. The two spectra in Figure 4.10c are essentially the same as given in the literature (Bêche et al., 2008). No noticeable change in the spectrum of Ce 3d is observable upon copper loading.

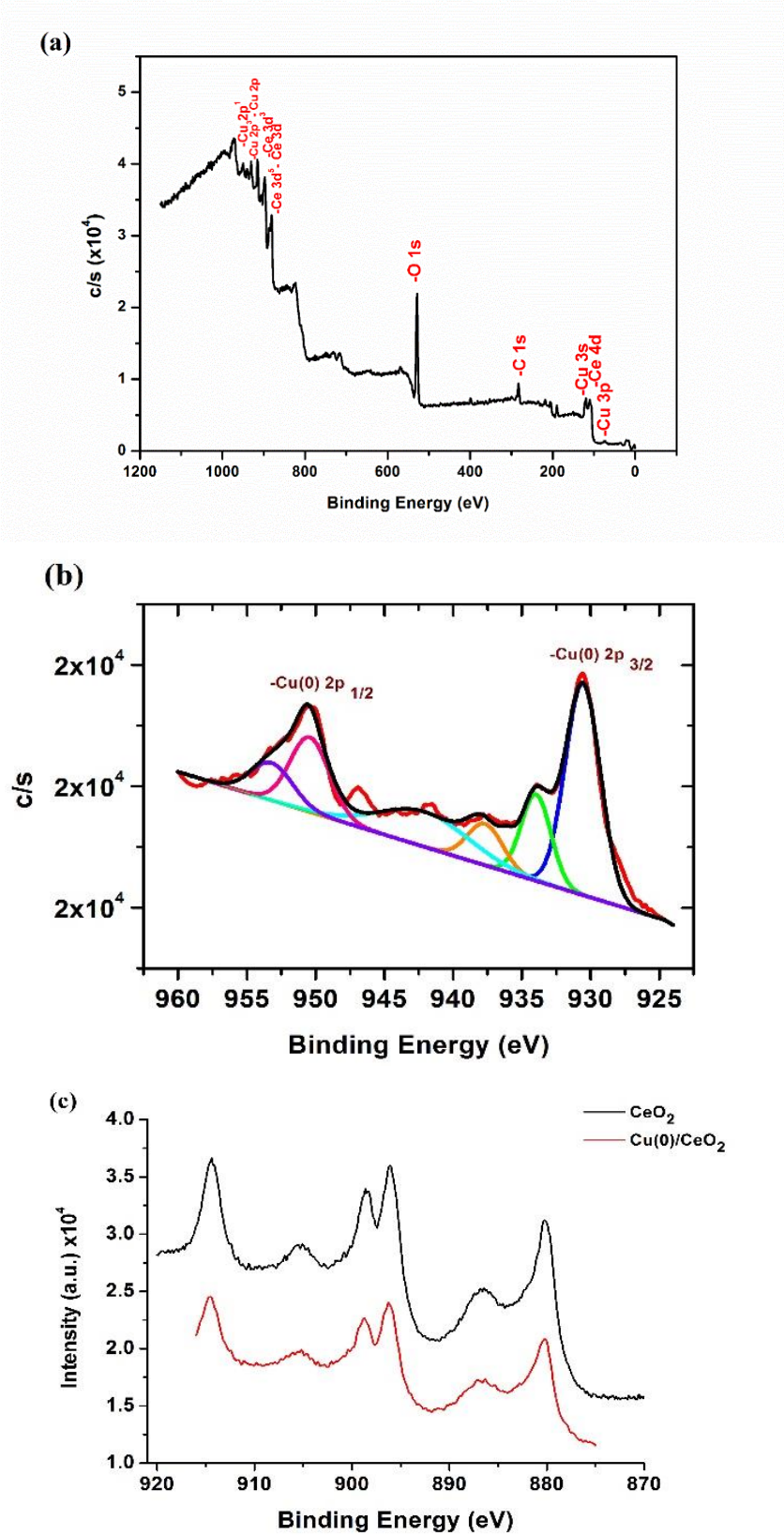

Figure 4.10. X-ray photoelectron (XPS) spectra of Cu(0)/CeO_2 sample with copper loading of 4.0% wt. Cu. (a) The survey scan. (b) The high resolution scan and deconvolution of Cu 2p bands. (c) The high resolution scan of Ce 3d bands.

4.1.3 Catalytic Activity of $Cu(0)/CeO_2$ in dehydrogenation of DMAB

In order to test the catalytic activity of nanoceria in dehydrogenation of DMAB, a control experiment was started with 1.0 mmol $(CH_3)_2NHBH_3$ and 100 mg powder of CeO_2 in 10 mL of toluene solution at 60.0 ± 0.5 ºC. No hydrogen evolution was observed over 2 h indicating that nanoceria support is catalytically inactive for the dehydrogenation of DMAB. The same experiment was performed starting with $Cu(0)/CeO_2$ samples having different loading of copper in the range 1-6% wt. Cu and the same amount of ceria support (100 mg CeO_2) in 10 mL toluene at 60.0 ± 0.5 ºC. The copper(0) nanoparticles supported on ceria nanopowders were found to be highly active catalyst in the dehydrogenation of DMAB. Note that all the experiments for measuring the catalytic activity of $Cu(0)/CeO_2$ samples were performed at least three times to estimate the percent error in the results of each experiment. Figure 4.11 indicates the plots of mol H_2 evolved per mole of DMAB versus time for the experiments performed starting with $Cu(0)/CeO_2$ samples of different copper loading in the range 2-6% wt. in the dehydrogenation of 100 mM $(CH_3)_2NHBH_3$ to determine the effect of copper loading on the activity of ceria supported copper(0) nanoparticles catalyst in dehydrogenation of DMAB.

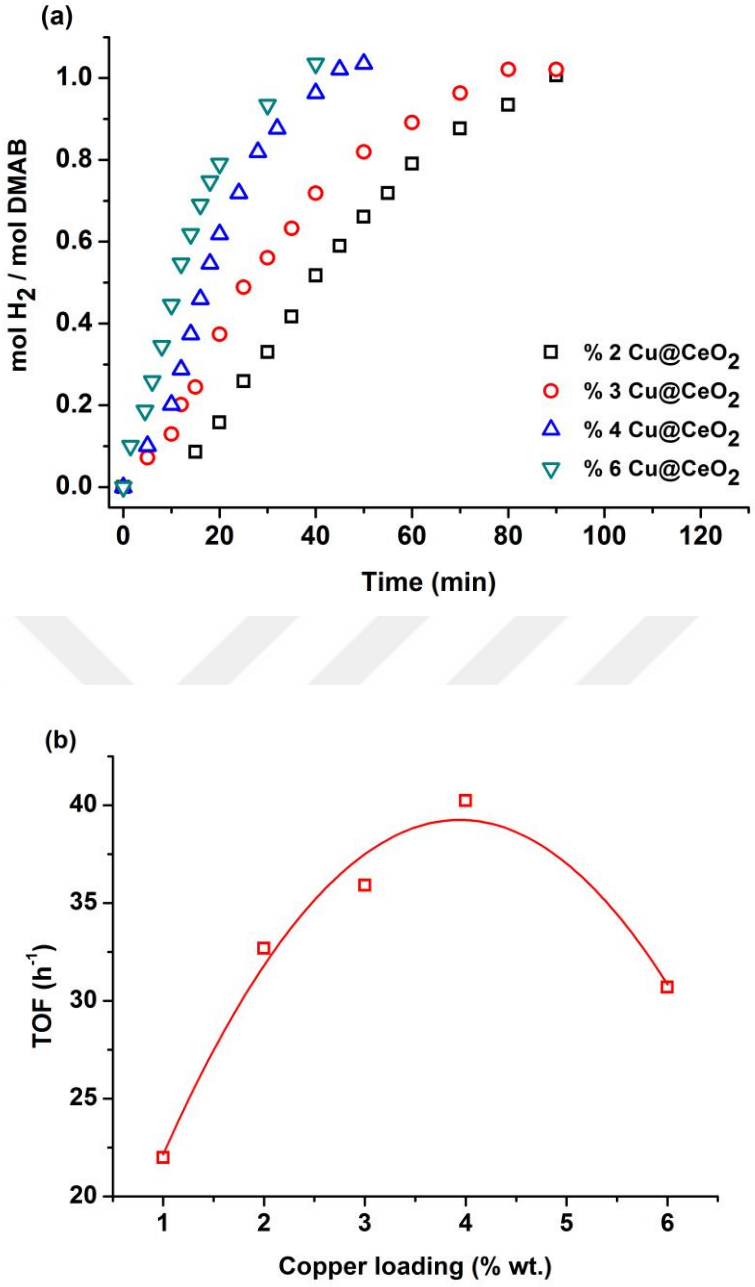

Figure 4.11. (a) mol H_2/ mol $(CH_3)_2NHBH_3$ versus time graph depending on the different copper loading in Cu(0)/CeO_2 for the dehydrogenation of DMAB (100 mM) at 60.0 ± 0.5 °C. (b) TOF values of the catalyst at different Cu loadings.

The turnover frequency (TOF) values in the catalytic dehydrogenation reactions of DMAB were calculated from the slope of each plot in linear portion and found to be 33, 35, 40, and 25 h^{-1} for Cu(0)/CeO_2 samples containing 2.0, 3.0, 4.0, and 6.0% wt. Cu, respectively. Plotting the TOF versus copper loading gives a volcano shape variation for the catalytic activity of copper(0) nanoparticles supported on ceria nanopowders in the dehydrogenation of DMAB at 60.0 ± 0.5 °C (Figure 4.11b). The

highest catalytic activity (TOF = 40 h^{-1}) was achieved by using the 4.0% wt. copper loaded ceria sample. The catalytic activity of $Cu(0)/CeO_2$ nanoparticles decreases with increasing of copper loading, most probably due to the agglomeration of metal nanoparticles. So, it leads to decrement in the accessibility of active sites and surface area. Therefore, $Cu(0)/CeO_2$ samples with copper loading 4.0 wt in percent were used for all experiments in this study. The apparent TOF value of 40 h^{-1} is comparable with that of the prior best heterogeneous catalyst (ruthenium nanoparticles, TOF = 137 h^{-1}) (Duman and Özkar, 2013), but much higher than those of the other heterogeneous and homogeneous catalysts, with one exception of homogeneous titanocene catalyst (Pun et al., 2007) reported for the dehydrogenation of DMAB up to now (Table 1).

Table 1. Heterogeneous catalysts used in the dehydrogenation of $(CH_3)_2NHBH_3$ obtained from SciFinder literature search.

Entry	Precatalyst /catalyst	Solvent	Temp. (°C)	Time (h)	Equivalent H_2	TOF(h^{-1})	Ea ($kmol^1$)	Ref
1	$[Rh(1,5\text{-cod})(\mu\text{-Cl})]_2$	Toluene	25	8	1.0	12.4	ND	Jaska et al., 2003
2	$[Ir(1,5\text{-cod})(\mu\text{-Cl})]_2$	Toluene	25	136	0.95	0.7	ND	Jaska et al., 2003
3	Rh(0)/$[Oct_4]Cl$	THF	25	6	0.9	8.2	ND	Jaska and Manners, 2004
4	Rh(0) Nanoclusters	Toluene	25	2.5	1.0	60	34± 2	Zahmakıran and Ozkar 2009
5	Pd(0)/MOF	Toluene	25	6	1.0	75	173.5± 2	Gulcan et al., 2014
6	Pt(0)NPs/AA	THF	25	0.6	1.0	15	64 ± 2	Sen et al., 2014
7	Pt(0)/TBA	THF	25	1	1.0	31	46.7± 2	Erken et al., 2016
8	Pt(0)/DPA@GO	THF	25	1	1.0	35	42± 2	Celik et al., 2016
9	OAm-stabilized Ru(0)NPs	Toluene	25	1.5	1.0	137	29 ± 2	Duman and Ozkar 2013
10	Ru(0)APTS	THF	25	2	1.0	55	61± 2	Zahmakiran et al, 2012
11	Cu(0) NPs	Toluene	60	1	1.0	40	76±2	This work

In order to investigate the effect of catalyst concentration on the catalytic activity in dehydrogenation of DMAB, a series of experiments were carried out by initiating with various amounts of ceria while adjusting the copper loading constant at 4.0 wt in percent.

Figure 4.12 indicates the plots of mol H_2 per mole of DMAB versus time throughout the catalytic dehydrogenation of 100 mM $(CH_3)_2NHBH_3$ solution in the presence of $Cu(0)/CeO_2$ nanoparticles in various copper concentrations (1.64, 3.27, 4.92 and 6.56 mM) at 60.0 ± 0.5 °C. To determine the hydrogen formation rate, the linear portion of the each plot was used. The linear line with a slope of 1.16 indicates that the dehydrogenation reaction is first order in respect of the catalyst concentration (Figure

4.12). The catalytic dehydrogenation of DMAB was also performed at different temperatures in the range of (45-60 ^{o}C) starting with Cu^{2+}/CeO_2, copper loading 4.0% wt. Cu, copper concentration [Cu] = 6.56 mM and substrate concentration [DMAB] = 100 mM. As expected, the rate of hydrogen generation from dehydrogenation of DMAB is directly proportional with the temperature.

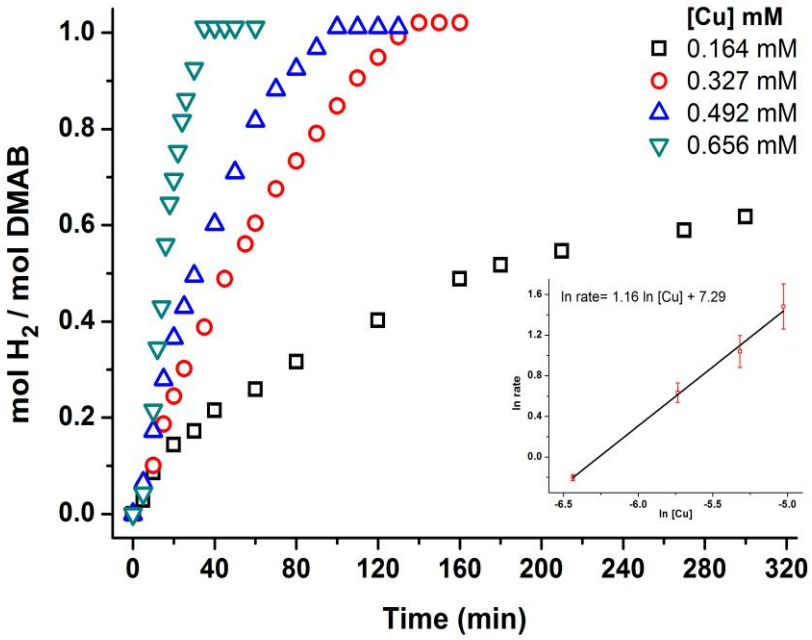

Figure 4.12. (a) mol H_2/ mol DMAB versus time graph depending on the copper concentration in $Cu(0)/CeO_2$ for the dehydrogenation of DMAB (100 mM) at 60.0 ± 0.5 ^{o}C. Inset: plot of H_2 generation rate versus concentration of copper (both in logarithmic scale)

The rate constants for the dehydrogenation of DMAB at various temperatures were determined by using the slope in linear part of each plot shown in Figure 4.13a and used for the construction of Arrhenius (Laidler, 1987) and Eyring (Eyring, 1935) plots given in Figure 4.13b and 4.13c, respectively, yielding the activation energy E_a = 76 ± 2 kJ/mol, activation enthalpy $\Delta H^{\#}$ = 80 ± 2 kJ/mol.

After the completion of dehydrogenation performed starting with 6.56 mM Cu/CeO_2 plus 100 mM $(CH_3)_2NHBH_3$ in 10 mL toluene at 60.0 ± 0.5 °C, the suspension was filtered and both the isolated solid and the filtrate solution were tested for their catalytic activity in the dehydrogenation of DMAB under the same reaction conditions by adding a new batch of $(CH_3)_2NHBH_3$ (100 mM). As shown in Figure 4.14, the filtrate

solution is silent in the dehydrogenation of DMAB indicating that there is no leaching of copper into the solution during the dehydrogenation reaction. The filtrate solution was also analyzed by ICP-OES for its copper content and found to have 0.005 mM copper. Compared to the initial concentration of 6.56 mM Cu, this small value indicates that the copper leaching into the solution is negligible.

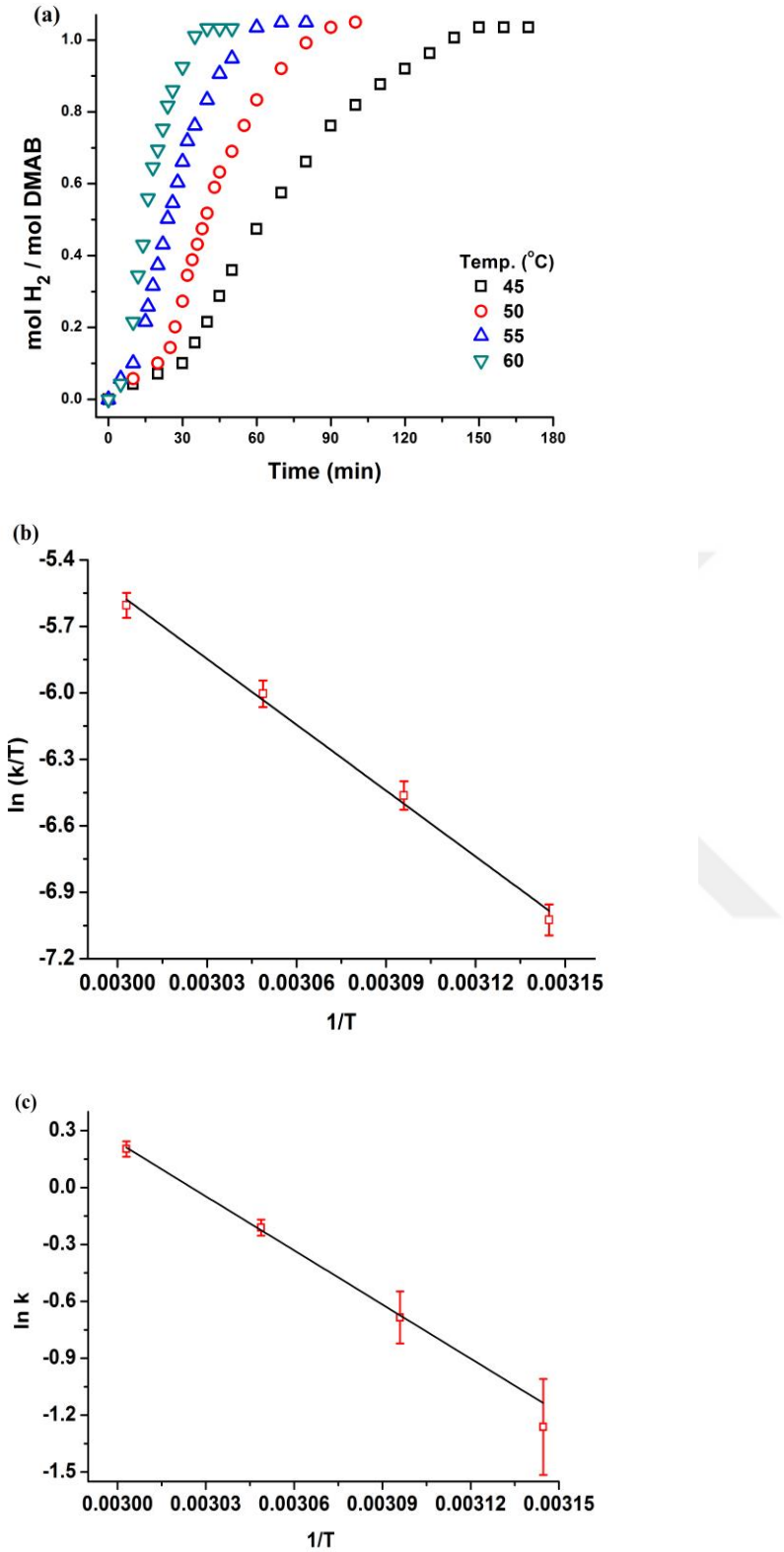

Figure 4.13. a) mole H_2 evolved per mole of $(CH_3)_2NHBH_3$ versus time plot for the catalytic dehydrogenation of dimethylamine borane at various temperatures in the range of 45-60 ^oC keeping the concentration of substrate at [DMAB]=100 mM and copper at [Cu]= 6.56 mM (4.0% wt. Cu) b) Arrhenius Plot c) Eyring Plot.

On the other hand, the isolated solid materials show catalytic activity when dispersed in 10 mL DMAB solution (100 mM). Compared to the initial catalytic activity (TOF = 40 h^{-1}) one observes a decrease in catalytic activity (TOF = 20 h^{-1}) of the solid materials. This decrease in catalytic activity may be arising from agglomeration of copper(0) NPs to the large particles or losing materials during the isolation of nanoparticles. Nevertheless, these two observations indicate that ceria supported copper(0) nanoparticles are adept competent catalyst in the dehydrogenation of DMAB.

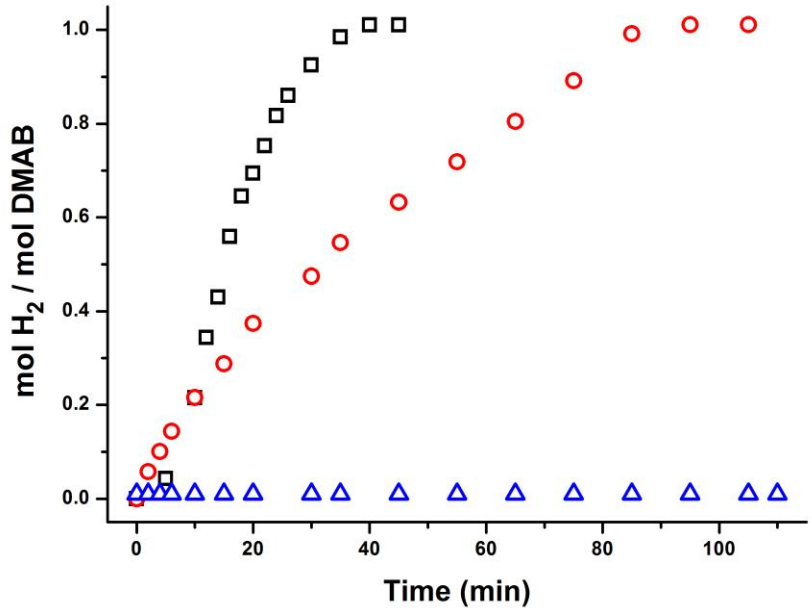

Figure 4.14. The evolution of equivalent hydrogen per mole of DMAB versus time plot for the dehydrogenation of DMAB (100mM) starting with Cu^{2+}/CeO_2 (square, □), $Cu(0)/CeO_2$ solid sample after first run (circle, o), the catalytic activity of filtrate solution obtained by filtration of active catalyst after reaction (triangle, Δ) at 60.0 ± 0.5 ºC.

The mechanism of catalytic dehydrogenation of DMAB over the transition metal center has been well established by identifying the intermediates (Douglas, 2009). Dimethylamine borane binds to the copper center through BH_2 group forming an inner sphere intermediate which undergoes first H-transfer and then β-hydrogen elimination from N-H bond yielding the metastable $Me_2N{=}BH_2$. The latter intermediate is not stable and converted to the stable cyclic dimer. At the end of the catalytic reaction the ^{11}B-NMR spectrum was taken from the reaction solution for a complementary experiment. The spectrum show that $Me_2NH_3BH_3$ (δ=-14 ppm, q) is completely turned to the cyclic dimer $[Me_2NBH_2]_2$ (δ= 5 ppm, t) after the catalytic reaction of DMAB.

In a control experiment, after the completion of hydrogen generation from the dehydrogenation of DMAB starting with 6.56 mM Cu(0)/CeO_2 plus 100 mM $(CH_3)_2NHBH_3$ in 10 mL toluene solution at 60.0 ± 0.5 °C, a second batch of DMAB was added to the solution without removing anything from the reaction flask and the hydrogen release from the DMAB was monitored as before. The complete release of hydrogen is achieved in both of the catalytic reactions of DMAB catalyzed by ceria supported copper(0) nanoparticles. A significantly decrement of catalytic activity was observed in the second run of dehydrogenation of DMAB added directly into the solution. However, the complete release of 1 equivalent H_2 is achieved in the second run as well (Figure 4.15a). The decrease in catalytic activity in the second run of dehydrogenation is due to agglomeration of copper(0 nanoparticles. Indeed, one observes an increase in average particle size of copper(0) nanoparticles supported on ceria as seen from the TEM image (Figure 4.15b) and corresponding histogram (Figure 4.15c) of the sample harvested after the second run of dehydrogenation of DMAB.

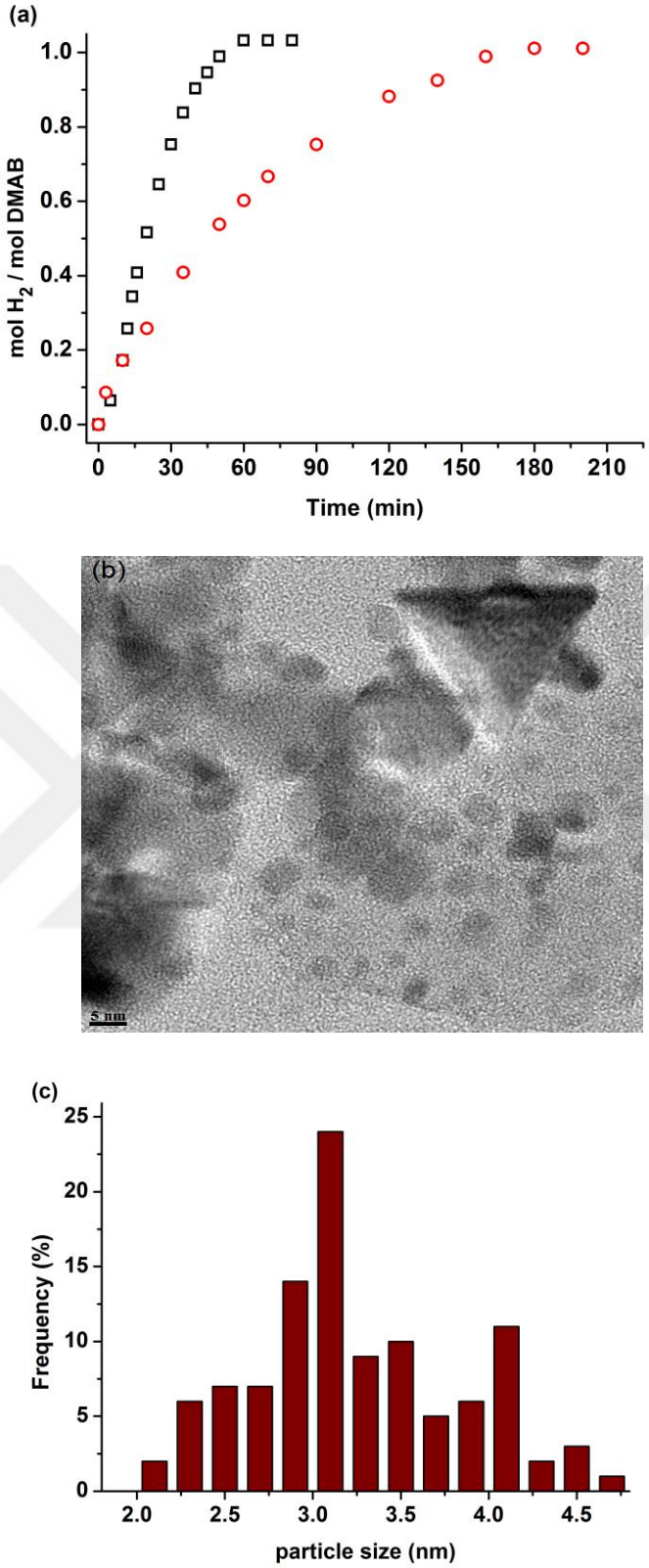

Figure 4.15. a) Plot of H_2 evolved per mole of $(CH_3)_2NHBH_3$ versus time for dehydrogenation of 100 mM DMAB starting with 6.56 mM (Cu^{2+}/CeO_2, 4.0% wt. Cu)(square, □), catalytic activity of the solution after the addition of a second batch of DMAB (100mM)(circle, o), b) TEM image of $Cu(0)/CeO_2$ NPs after the second run of the reaction, c) the corresponding histogram for the particle size distribution.

Measurement of TTO number was utilized to determine the catalytic lifetime of $Cu(0)/CeO_2$ catalyst in the dehydrogenation of DMAB. A lifetime experiment was performed by beginning with 6.56 mM Cu (copper loading on ceria is 4.0% wt. Cu) in 10 mL solution of DMAB at 60.0 ± 0.5 °C. Figure 4.16 gives the variations in total turnover number (TTO) and turnover frequency (TOF) versus time during the dehydrogenation of DMAB by $Cu(0)/CeO_2$ at 60.0 ± 0.5 °C. Ceria supported copper(0) nanoparticles provide 225 total turnovers in the dehydrogenation of DMAB at 60.0 ± 0.5 °C before deactivation. The observation of a decrease in the TOF value during the reaction indicates that the deactivation of the catalyst is due to the aggregation of metal nanoparticles.

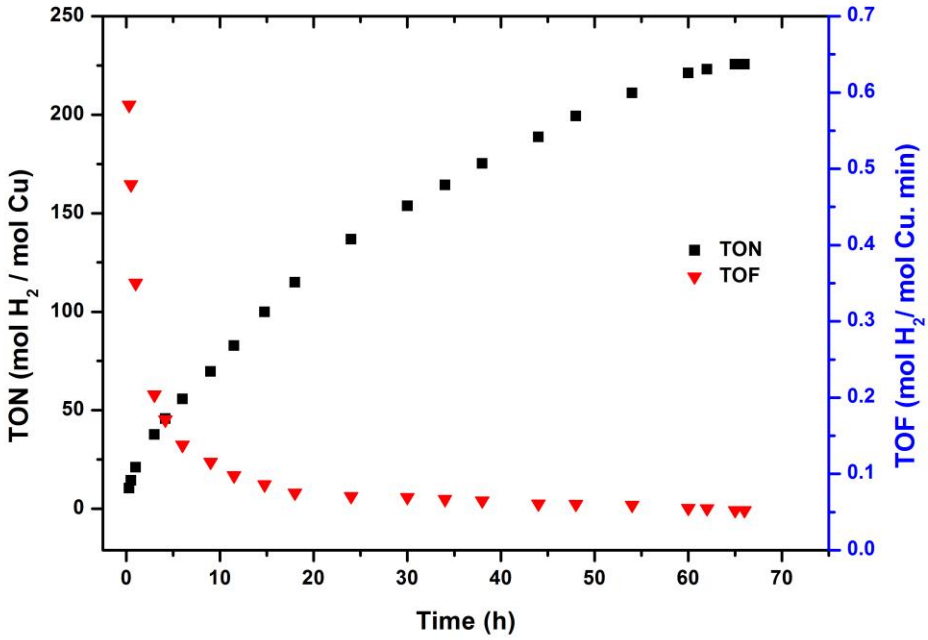

Figure 4.16. Plot of total turnover number (TTO) or turnover frequency versus time for the dehydrogenation of DMAB in 10.0 mL toluene solution containing Cu^{2+}/CeO_2 with (copper loading of 4.0% wt. Cu, 6.56 mM Cu), 250 mM $(CH_3)_2NHBH_3$ (for each run) at 60.0 ± 0.5 °C.

The heterogeneity of $Cu(0)/CeO_2$ catalyst was tested by poisoning experiment. The access of the substrate to the active site is locked by poison due to the binding of poison to the metal center (Hornstein et al., 2002; Vargaftik, 1989). In our poisoning experiment, carbon disulfide was used as poison and 0.2 equivalent CS_2 per mole of catalyst was injected into the solution throughout the dehydrogenation of DMAB. In a

typical poisoning test, 0.2 equivalent CS_2 per mole of catalyst was added to the reaction medium at 60.0 ± 0.5 °C after the release of 40% hydrogen from dehydrogenation of DMAB (100 mM) catalyzed by 6.56 mM Cu (4.0% wt. Cu) in 10 mL toluene solution. Figure 4.17 exhibits the plot of mole H_2 evolved per mole of DMAB vs time for the catalytic dehydrogenation of DMAB before and after addition of CS_2 poison.

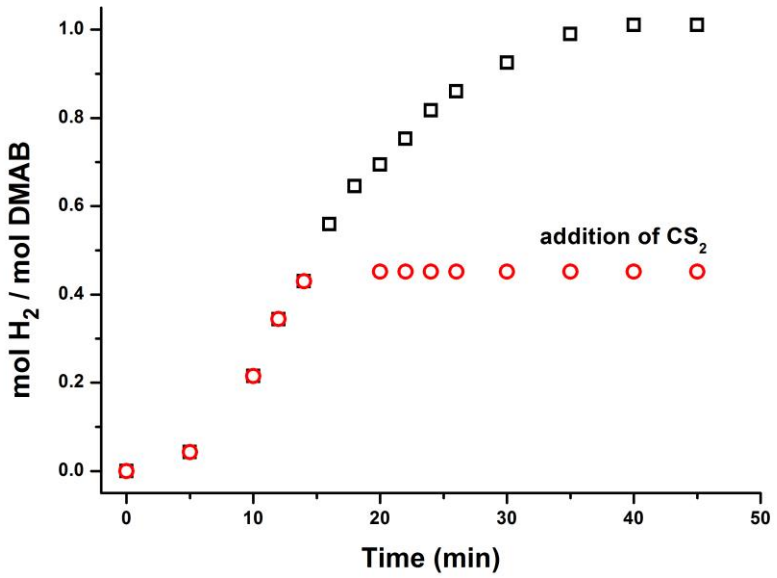

Figure 4.17. Plots of mole H_2 evolved per mole of dimethylamine borane versus time for the dehydrogenation reaction of 100 mM $(CH_3)_2NHBH_3$ catalyzed by Cu(0) NPs supported on ceria (copper loading of 4.0% wt., 6.56 mM Cu) with and without addition of 0.2 equiv. CS_2 at 60.0 ± 0.5 ºC.

It is clearly seen that the reaction is entirely ceased upon addition of 0.2 equivalents of CS_2 per mole of Cu catalyst in a very short time which indicates that the dehydrogenation of DMAB catalyzed by ceria supported copper(0) nanoparticles is indeed heterogeneous catalysis.

4.2 Rhodium(0)/Titania Nanoparticles

4.2.1 In situ generation of Rh(0) nanoparticles from the reduction of Rh(II) octanoate during the dehydrogenation of DMAB

Rhodium(II) hexanoate has been used as precursor leading to the formation of rhodium(0) nanoparticles which are catalytically active in the dehydrogenation of DMAB but not very stable (Zahmakıran and Ozkar, 2009). We tested the catalytic activity and stability of rhodium(0) nanoparticles formed from the reduction of rhodium(II) octanoate, with a 2-carbon longer carboxylate, in dehydrogenation of DMAB under the same conditions. Figure 4.18a shows the plots of mol H_2 evolved per mole of DMAB versus time for the catalytic dehydrogenation of 100 mM DMAB performed starting with rhodium(II) octanoate in different rhodium concentration (1.0, 2.0, 3.0 mM Rh) in 10 mL toluene at 25.0 ± 0.5 ^oC. The average turnover frequency is TOF = 44 h^{-1}, which is comparable to the value of 60 h^{-1} obtained by starting with rhodium(II) hexanoate at 25.0 ± 0.5 ^oC (Zahmakıran and Ozkar, 2009). The recyclability tests (Figure 4.18b) show that both the catalytic activity and conversion decrease in successive runs. In other words, less than 1 equivalent H_2 is evolved in the subsequent runs: Only 40% of H_2 can be obtained in the 5^{th} run of dehydrogenation of DMAB at 25.0 ± 0.5 ^oC. In order to test the temperature dependence of catalytic activity and stability of the rhodium(0) nanoparticles, the formation of rhodium(0) nanoparticles and concomitant dehydrogenation of DMAB were performed starting with 100 mM $(CH_3)_2NHBH_3$ and 1.0 mM rhodium(II) octanoate in 10 mL toluene solution at various temperature in the range of 25-60 ^oC (Figure 4.18c). In all experiments, the hydrogen evolution starts immediately and continues almost linearly until the complete conversion of DMAB present in the solution releasing 1.0 equivalent H_2 per mole of $(CH_3)_2NHBH_3$. Evaluation of the temperature dependent kinetic data by using the Arrhenius equation (Laidler, 1987) yields an activation energy of E_a = 43 ± 2 kJ/mol, which is comparable to the value obtained starting with rhodium(II) hexanoate (E_a = 34 ± 2 kJ/mol) (Zahmakıran and Ozkar, 2009).

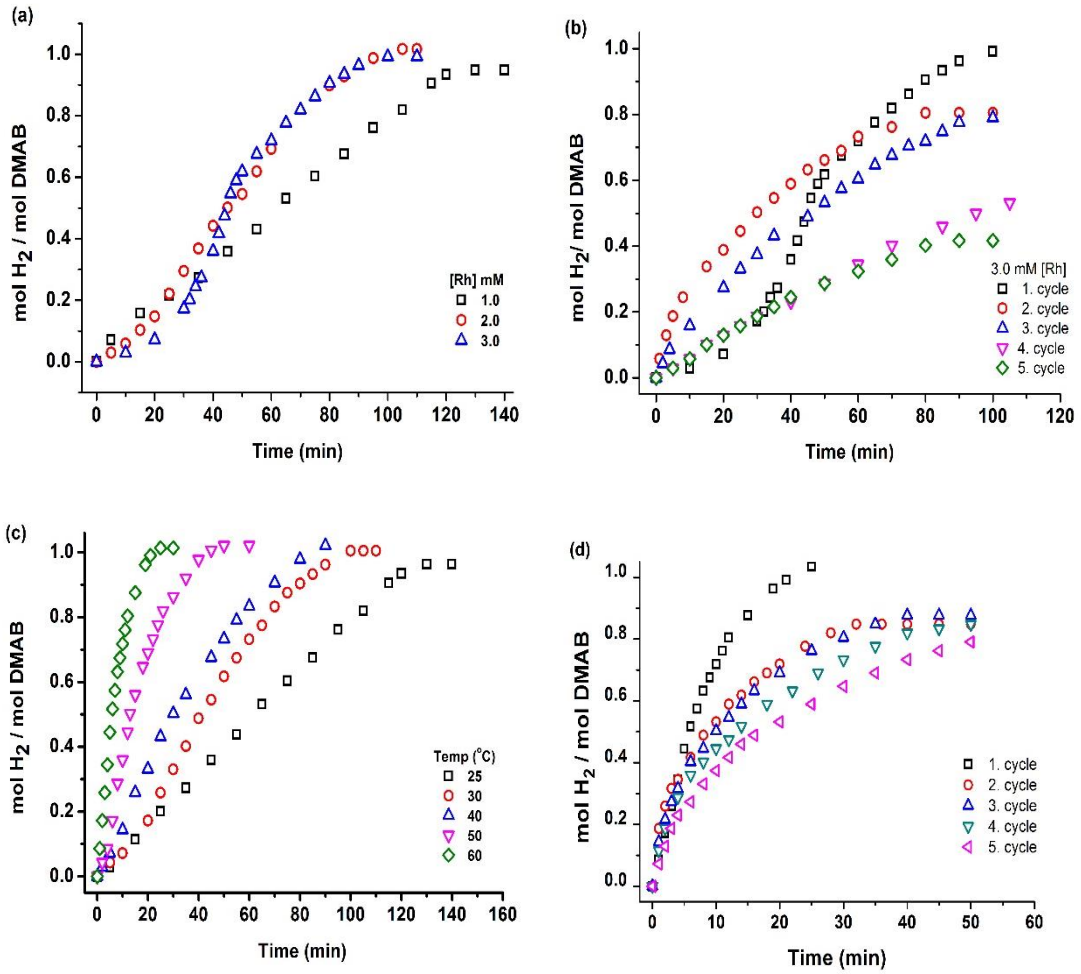

Figure 4.18. The evolution of equivalent H_2 per mole of $(CH_3)_2NHBH_3$ versus time for (a) the catalytic dehydrogenation of 100 mM $(CH_3)_2NHBH_3$ starting with rhodium(II) octanoate in different concentrations (1.0, 2.0, 3.0 mM Rh) in 10 mL toluene at 25.0 ± 0.5 °C, (b) the recyclability of the Rh(0) nanoparticles starting with 100 mM $(CH_3)_2NHBH_3$ and 3.0 mM Rh(octanoate)$_2$ at 25.0 ± 0.5 °C, (c) the catalytic dehydrogenation of DMAB at various temperatures in the range of 25-60 °C starting with 100 mM $(CH_3)_2NHBH_3$ and 1.0 mM Rh(octanoate)$_2$ in 10 mL toluene solution, (d) the recyclability of Rh(0) nanoparticles starting with 100 mM $(CH_3)_2NHBH_3$ and 1.0 mM Rh(octanoate)$_2$ in 10 mL toluene at 60.0 ± 0.5 °C.

When DMAB solution is added to the solution of rhodium(II) octanoate in toluene at 60.0 ± 0.5 °C one observes a color change from green to red and ultimately to dark brown. This color change indicates that reduction of the precursor rhodium(II) compound to rhodium(0) can be followed by UV-vis electronic absorption spectroscopy (Figure 4.19). The starting solution of $[Rh(CH_3(CH_2)_6CO_2)_2]_2$ in toluene exhibits a sharp absorption band at 286 nm, and two broad bands at 438 and 594 nm in the spectrum which can readily be attributed to the ligand to metal charge transfer

and d-d transition, (Stranger et al., 1996) respectively. UV-vis spectrum of the dark brown solution taken from after the catalytic reaction of DMAB indicates an absorption continuum for Rh(0) NPs because of the surface plasmon resonance. (Creighton and Eadon, 1991).

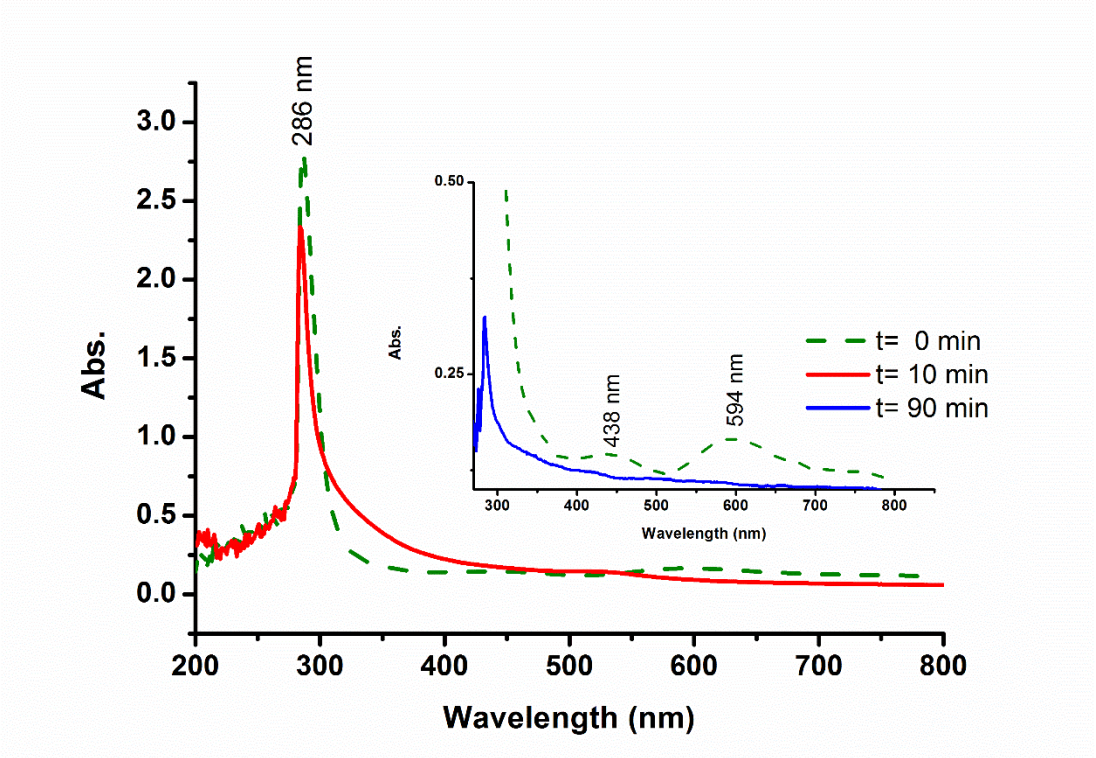

Figure 4.19. UV-vis spectra of solutions containing 1.0 mM ruthenium(II) octanoate in toluene before and after the injection of 100 mM $(CH_3)_2NHBH_3$ at 60.0 ± 0.5 °C.

In summary, the reduction of rhodium(II) octanoate during the dehydrogenation of DMAB leads to the formation of rhodium(0) nanosized particles which have catalytic activity and stability similar to that of the ones obtained by rhodium(II) hexanoate (Zahmakıran and Ozkar, 2009). The instability of rhodium(0) nanosized particles is not unexpected as the only stabilizer present in the toluene solution is the octanoate ion released from the reduction of precursor, which obviously doesn't provide enough stabilization for rhodium(0) nanoparticles (Özkar and Finke, 2002). From the short survey experiments performed starting with sole rhodium(II) octanoate, one can conclude that the rhodium(0) nanoparticles are not sufficiently stable in solution and need to be stabilized against the agglomeration. Titania nanopowders were used as support for the stabilization of rhodium(0) nanoparticles formed from the reduction of rhodium(II) octanoate during the dehydrogenation of DMAB.

The addition of DMAB solution to the flask containing a suspension of Rh(II)/nanoTiO$_2$ precatalyst causes reduction of rhodium(II) octanoate to rhodium(0) and hence dehydrogenation of dimethylamine borane. Figure 4.20 exhibits the graphs of mol H_2 per mole of DMAB *versus* time for the catalytic dehydrogenation of 100 mM DMAB in the presence of 50 mg Rh(II)/nanoTiO$_2$ with different rhodium loading of 0.1, 0.2, 0.3, 0.4, 0.5, 1.0, 2.0, 3.0% wt. Rh corresponding to [Rh] = 0.049, 0.097, 0.15, 0.20, 0.24, 0.49, 0.97, and 1.5 mM, respectively, at 60.0 ± 0.5 ^{o}C. The complete conversion of DMAB was seen for all experiments. The use of nanotitania support appears to provide enough stabilization for the rhodium(0) NPs formed from the reduction of rhodium(II) octanoate (*vide infra*).

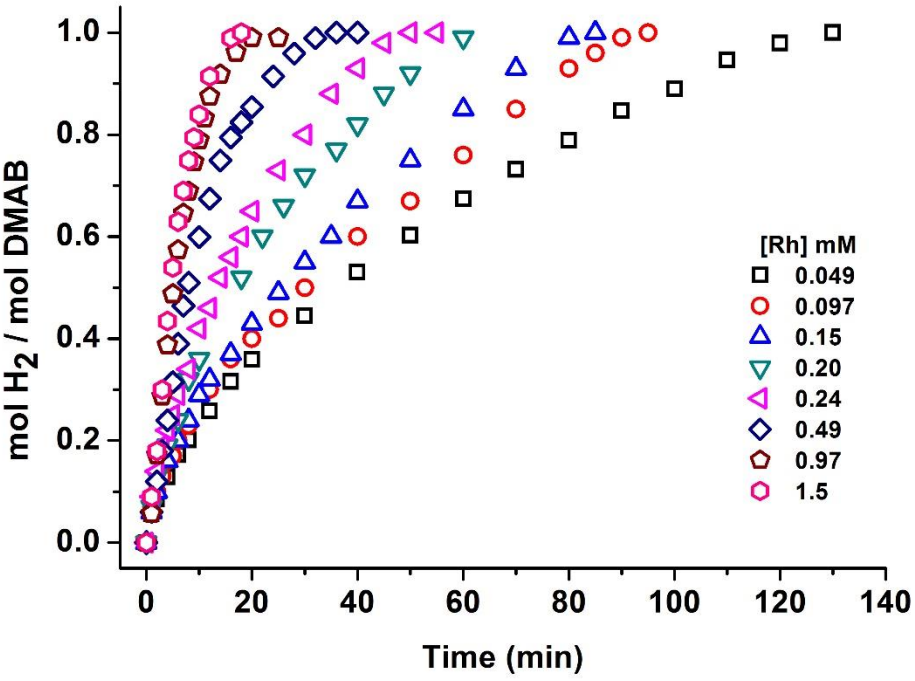

Figure 4.20. Plots of mole H_2 evolved per mole of DMAB versus time for dehydrogenation of dimethylamine borane performed starting with 100 mM DMAB and 50 mg Rh(II)/nanoTiO$_2$ with different rhodium loading of 0.1, 0.2, 0.3, 0.4, 0.5, 1.0, 2.0, 3.0% wt. Rh corresponding to [Rh] = 0.049, 0.097, 0.15, 0.20, 0.24, 0.49, 0.97, and 1.5 mM, respectively, at 60 ± 0.5 ^{o}C.

The ^{11}B-NMR spectra (Figure 4.21) taken at the beginning and the end of reaction show the complete conversion of dimethylamine borane (quartet, -15.0 ppm) to the cyclic dimeric product $(Me_2NBH_2)_2$ (triplet, 5.0 ppm). Taking all the results together, one is able to establish Equation 1 for the catalytic dehydrogenation of DMAB.

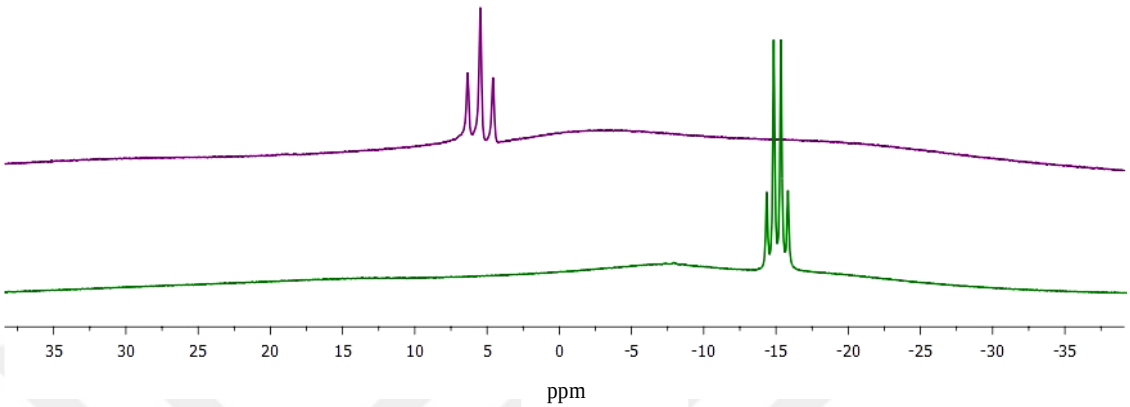

Figure 4.21. ^{11}B-NMR spectra taken from the reaction solution at the beginning (green line) and at the end of (purple line) dehydrogenation of 100 mM DMAB catalyzed by rhodium (0) NPs at 60 ± 0.5 ºC.

Nanotitania-supported rhodium(0) NPs, formed from the reduction of Rh(II)/nanoTiO_2 precursor during the dehydrogenation of DMAB at 60.0 ± 0.5 ºC, were isolated from the reaction solution and characterized by using a several analytical techniques. XRD patterns of nanoTiO_2 and Rh(0)/nanoTiO_2 (0.5% wt. Rh) in Figure 4.22 show the characteristic diffraction peaks of nanotitania at 25.2º, 36.9º, 37.8º, 38.5º, 48.4º, 53.8º, 55.0º, 62.1º, 62.6º, 68.7º, 70.3º, 75.0º, 76.0º and 83.1º assigned to the (101), (103), (004), (112), (200), (105), (211), (213), (204), (116), (220), (215), (301) and (312) reflections of anatase TiO_2, respectively (JCPDS Card 21-1272). This indicates that nanotitania maintains its crystallinity after the preparation of Rh(II)/nanoTiO_2 and the reduction of rhodium(II) to rhodium(0) during the dehydrogenation of DMAB. The powder XRD pattern of Rh(0)/nanoTiO_2 (0.5 wt % Rh) shows no additional diffraction peaks which would be attributable to rhodium(0) nanoparticles, most likely due to the low metal loading of nanotitania.

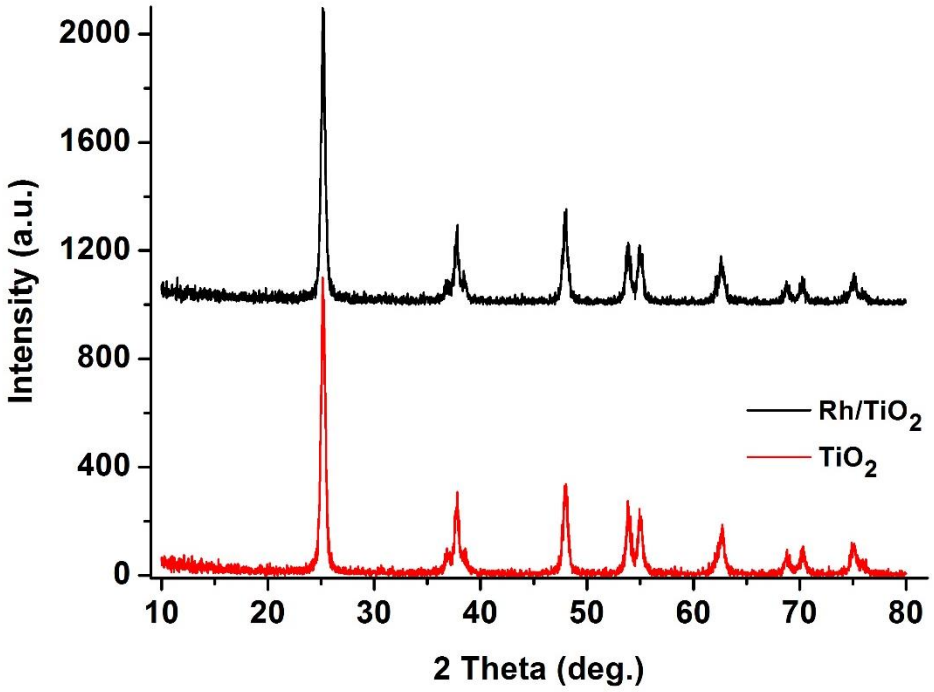

Figure 4.22. X-ray diffraction (XRD) patterns of nanoTiO_2 and Rh(0)/nanoTiO_2 with rhodium loading of 0.5% wt. Rh.

The crystallite size of titania nanopowders in two samples was calculated from (101) peak at 25.2^o using Debye Scherrer equation to be 19.5 and 20.9 nm for nanoTiO_2 and Rh(0)/nanoTiO_2 with a 0.5% wt. Rh, respectively. The slight increase in the crystallite size might be attributed to the formation of rhodium(0) nanoparticles.

The SEM images and SEM-EDX spectrum of Rh(0)/nanoTiO_2 with a 0.5% wt. Rh in Figures 4.23 and 4.24, respectively, indicate (i) no defects in the structure of titania caused by the preparation of titania supported rhodium(0) nanoparticles, in agreements with XRD results, (ii) no bulk rhodium metal formation, and (iii) Rh element exist in the sample in addition to framework elements Ti and O of titania (Jones, 1992).

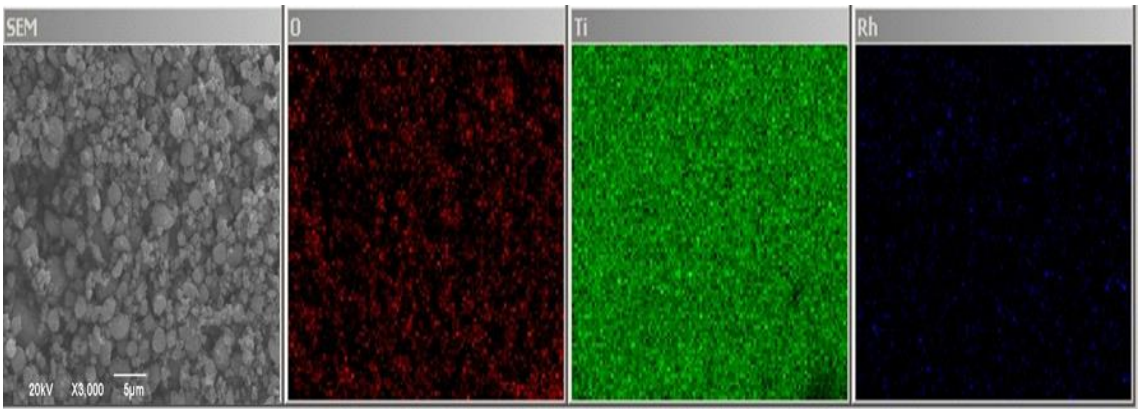

Figure 4.23. The micrographs of specimen surfaces obtained from the secondary electron image mode at 3000-X magnification with the aid of SEM measurements are used to investigate the morphological structure of Rh(0)/TiO_2 with a 0.5 wt. Rh.

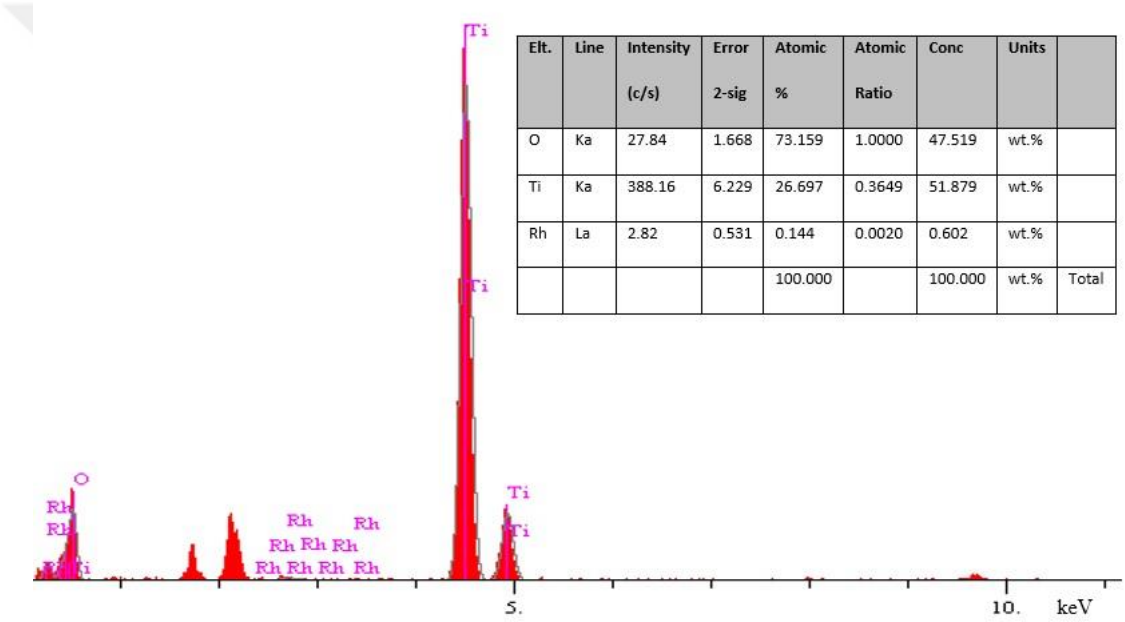

Elt.	Line	Intensity (c/s)	Error 2-sig	Atomic %	Atomic Ratio	Conc	Units	
O	Ka	27.84	1.668	73.159	1.0000	47.519	wt.%	
Ti	Ka	388.16	6.229	26.697	0.3649	51.879	wt.%	
Rh	La	2.82	0.531	0.144	0.0020	0.602	wt.%	
				100.000		100.000	wt.%	Total

Figure 4.24. SEM-EDX spectrum of the titania supported rhodium(0) nanoparticles with a rhodium loading of 0.5% wt.

The oxidation state of rhodium and surface compostion of the resultant Rh(0)/nanoTiO_2 was illumunated using XPS. The survey scan XPS of Rh(0)/nanoTiO_2 (0.5% wt. Rh) in Figure 4.25a indicates the existence of Rh with the framework elements of titania (Ti and O) in agreement with the SEM-EDX results.

In high resolution Rh 3d XPS spectrum of the same sample indicated in Figure 4.25b, two prominent peaks appear at 311.79 and 304.79 eV being readily assigned to Rh(0) $3d_{3/2}$ and Rh(0) $3d_{5/2}$, respectively (Mevellec et al., 2006; Baer, 1970).

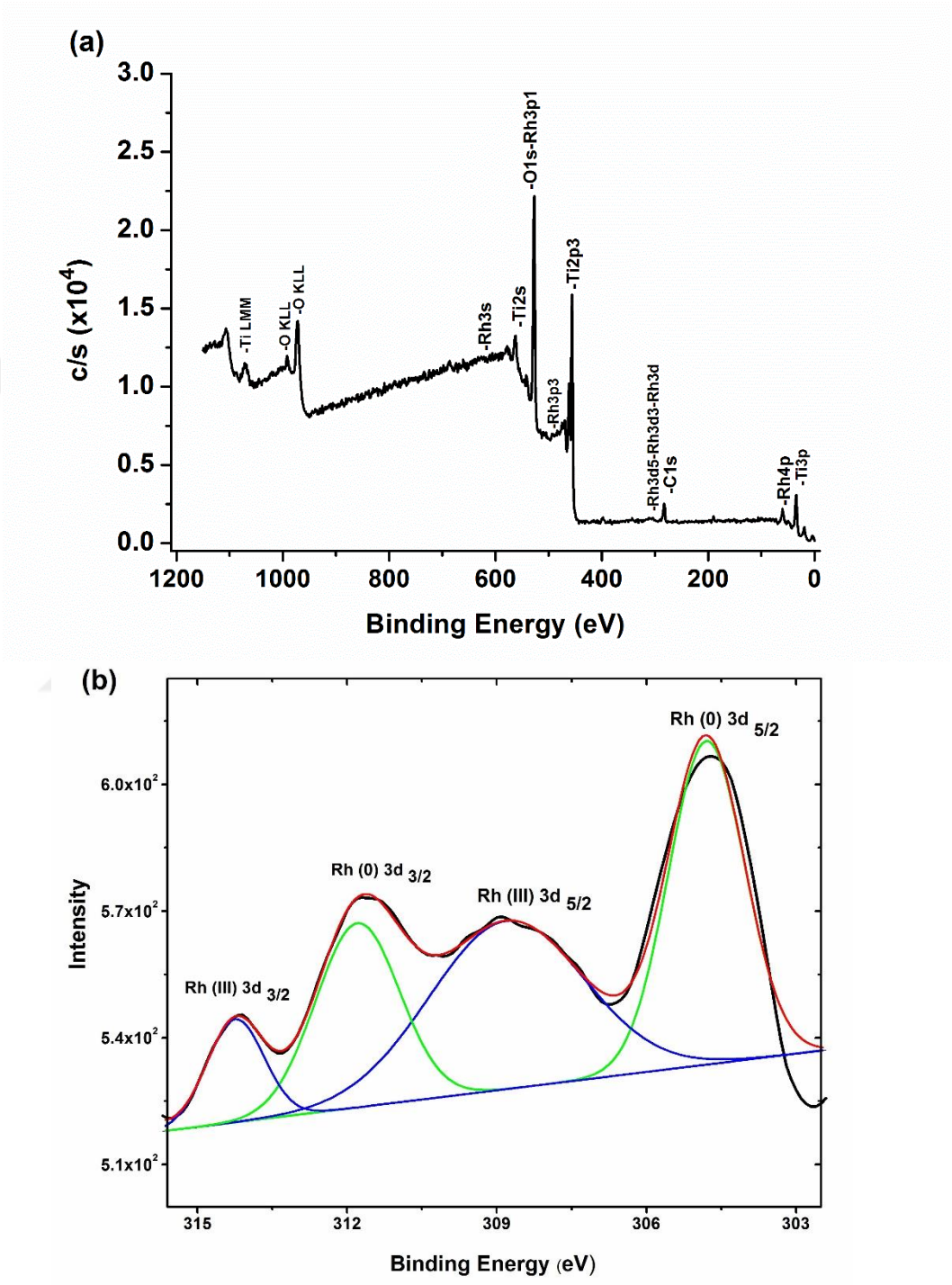

Figure 4.25. Survey scan XPS spectrum of Rh(0)/nanoTiO_2 (0.5% wt. Rh) after the dehydrogenation of dimethylamine borane. Inset shows high resolution XPS Rh 3d spectrum with deconvolution.

Two additional low intensity bands observed at 308.80 eV and 314.24 eV are attributed to the Rh(III) $3d_{5/2}$ and Rh(III) $3d_{3/2}$ which might be formed by partial oxidation of Rh(0) NPs when kept in air for a few minutes during the XPS sampling (Peuckert, 1984; Barr, 1978).

The particle size and morphology of rhodium nanoparticles supported on nanotitania were investigated by TEM and TEM- EDX analyses. Figure 4.26 displays the TEM images of samples of titania supported rhodium(0) nanoparticles with various rhodium loadings (0.1, 0.2, 0.3, 0.4, and 0.5 % wt. Rh) harvested at the last of catalytic dehydrogenation reaction along with particle size distribution of rhodium(0) nanoparticles for all of the samples. As the rhodium loading of Rh(0)/nanoTiO2 increases, the mean particle size of rhodium(0) nanoparticles increases as seen in Table 2.

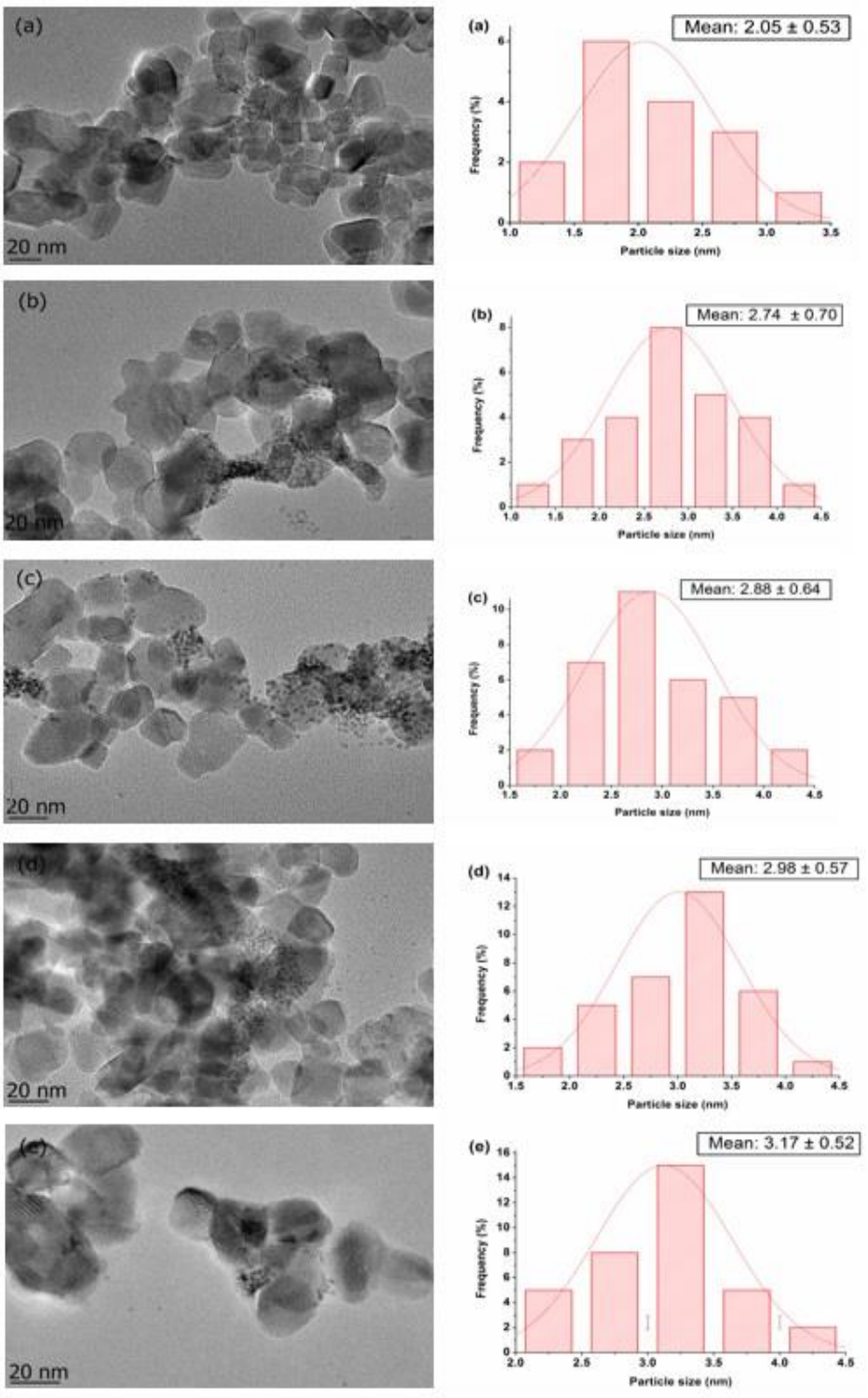

Figure 4.26. TEM images of Rh(0)/nanoTiO$_2$ with different loading (a) 0.1, (b) 0.2, (c) 0.3, (d) 0.4 and (e) 0.5% wt. Rh after catalytic dehydrogenation reaction performed starting with 100 mM $(CH_3)_2NHBH_3$ at 60.0 ± 0.5 ^oC. The particle size histograms are given at the right to the corresponding TEM image.

Table 2. The rhodium contents, catalytic activity and mean particle size of Rh(0) NPs supported on nanotitania in dehydrogenation of DMAB at 60.0 ± 0.5 ºC.

Rh loading (wt.%)	[Rh] (mM)	Particle size (nm)	TOF (h^{-1})
0.1	**0.049**	**2.05 ± 0.53**	**2900**
0.2	**0.097**	**2.74 ± 0.70**	**1626**
0.3	**0.15**	**2.88 ± 0.64**	**1203**
0.4	**0.20**	**2.98 ± 0.57**	**1104**
0.5	**0.24**	**3.17 ± 0.52**	**1081**
1.0	**0.49**	**-**	**789**
2.0	**0.97**	**-**	**639**
3.0	**1.5**	**-**	**422**

4.2.2 Catalytic activity of Rh(0)/nanoTiO_2 nanoparticles in the dehydrogenation of DMAB

The control experiment was performed to test the catalytic activity of nanotitania in dehydrogenation of DMAB under the same reaction conditions. The control experiment performed starting with 1.00 mmol $(CH_3)_2NHBH_3$ and 50.0 mg TiO_2 in 10 mL toluene at 60.0 ± 0.5 ºC shows no hydrogen evolution in 1 h indicating inactivity of titania in the dehydrogenation of DMAB under the conditions where rhodium catalysts will be tested. However, Rh(0)/nanoTiO_2 samples were found to be highly active catalyst in the dehydrogenation of DMAB. Figure 4.20 shows the plots of equivalent H_2 evolved per mole of DMAB versus time during the catalytic dehydrogenation reaction performed starting with 100 mM $(CH_3)_2NHBH_3$ and Rh(II)/nanoTiO_2 with various rhodium loading, thus in various rhodium concentration, at 60.0 ± 0.5 ºC. The linear portion of each plot was used to determine the hydrogen generation rate and plotted versus the initial concentration of rhodium, both axis in logarithmic scale in Figure 4.27a. The slope of straight line was found as 0.97 indicating that Rh(0)/nanoTiO_2 catalyzed dehydrogenation of DMAB is first order with respect to the rhodium concentration.

Turnover frequency (TOF) values were found by using the hydrogen formation rate in the linear part of each plot in Figure 4.20 for the dehydrogenation of 100 mM DMAB at 60.0 ± 0.5 °C and listed in Table 1 along with the mean diameter of rhodium(0) nanoparticles determined from the TEM images in Figure 4.26. Rh(0)/nanoTiO_2 with 0.1 wt. % Rh ([Rh] = 0.049 mM) provides the biggest activity with an initial TOF value of 2900 h^{-1} in H_2 generation from the dehydrogenation of DMAB at 60.0 ± 0.5 ^oC (Table 1). This is a record turnover frequency value ever reported for the dehydrogenation of DMAB. As the rhodium loading in the Rh(0)/nanoTiO_2 catalyst increases the TOF value decreases down to 422 h^{-1} for the Rh(0)/nanoTiO_2 with 3.0 wt. % Rh (Figure 4.27b). The inverse concentration dependence of TOF (Figure 4.27b) can be correlated to the increasing size of rhodium(0) nanoparticles (Figure 4.27c) as precedented in literature for various catalytic reactions (Özhava and Özkar, 2016; Shmidt et al., 2005; Steinhoff et al., 2002; Sanchez-Delgado et al., 1987; . Doll and Finke, 2004).

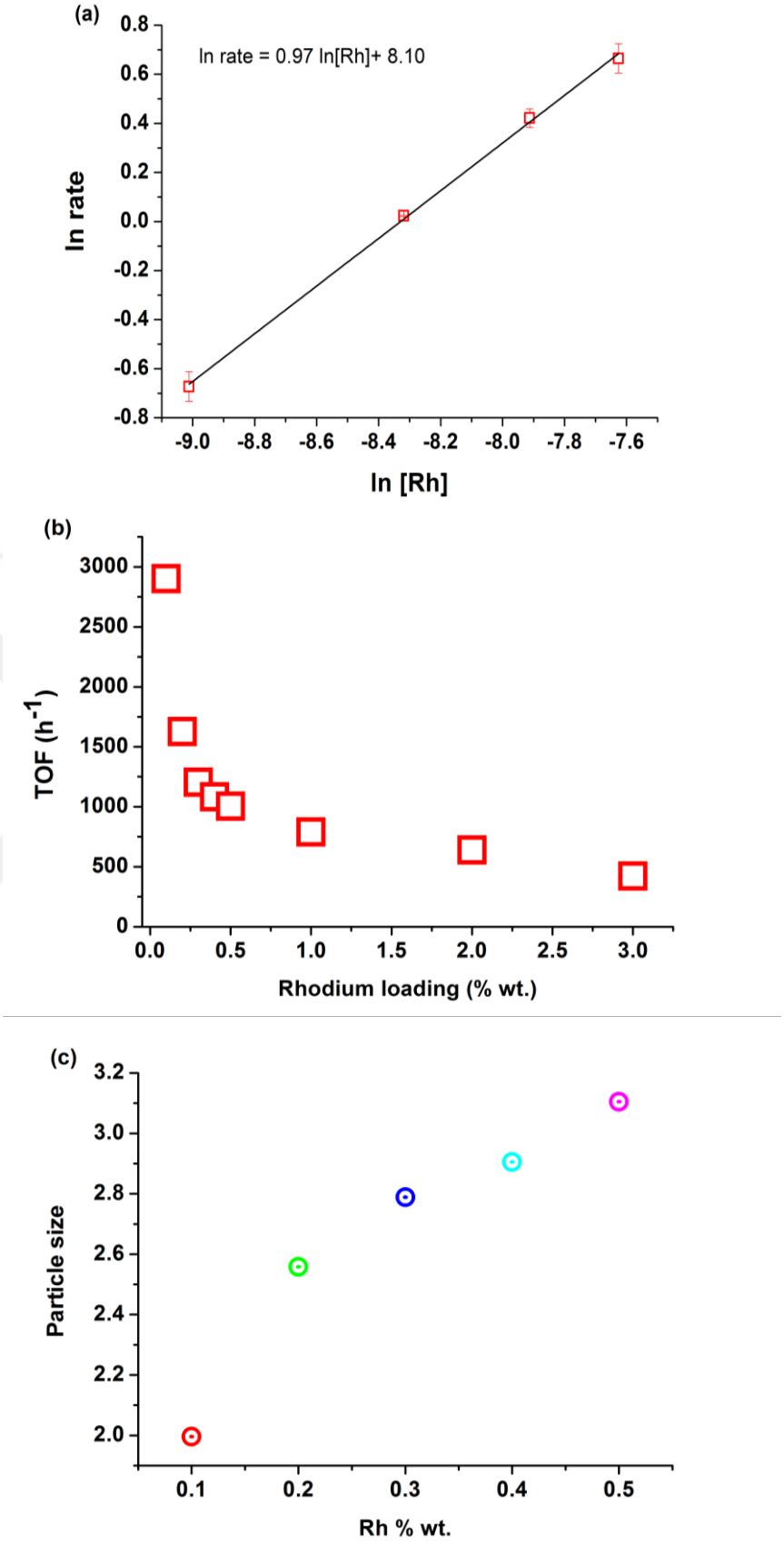

Figure 4.27. (a) Plot of hydrogen generation rate versus the concentration of rhodium (both in logaritmic scale.). (b) TOF versus rhodium loading (% wt.). (c) Particle size versus rhodium loading (% wt.).

However, only our previous four reports have provided the experimental evidence showing that the increasing particle size with the increasing catalyst concentration is the reason of the decrease in catalytic activity (Özhava and Özkar, 2016; Akbayrak and Özkar, 2016; Akbayrak et al., 2016). In the work, we also demonstrate that the catalytic activity of Rh(0)/nanoTiO$_2$ in H_2 generation from DMAB decreases as the particle size of the nanoparticles increases with the increasing loading of Rh. (Figures 4.27b and 4.27c) (Steinhoff et al., 2002; Doll and Finke, 2004).

The catalytic dehydrogenation of DMAB was also performed starting with 100 mM $(CH_3)_2NHBH_3$ and 50 mg Rh(0)/nanoTiO$_2$ catalyst with (0.24 mM Rh) at various temperature in the range of 40-60 ^oC (Figure 4.28).

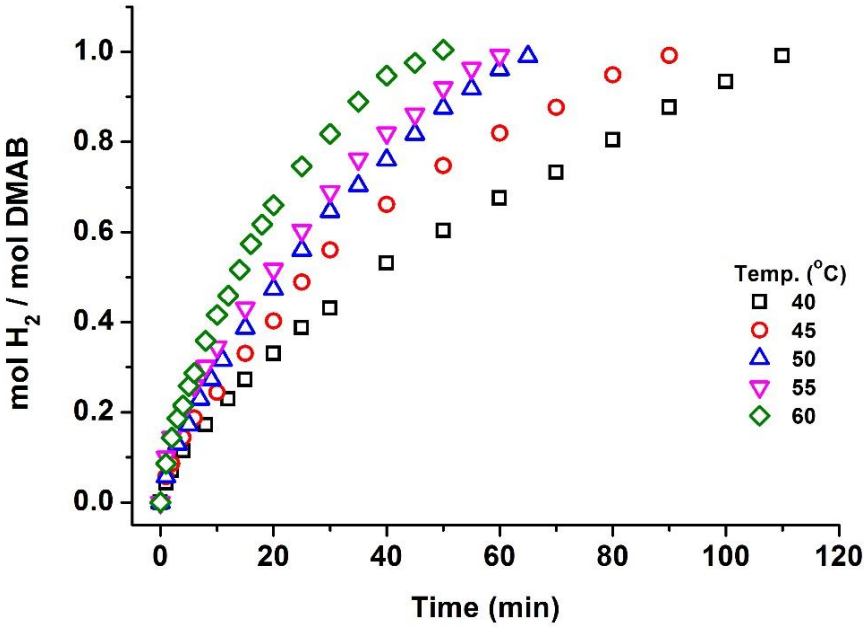

Figure 4.28. Plots of mole H_2 evolved per mole of DMAB versus time for the catalytic dehydrogenation of DMAB at various temperatures in the range of 40-60 oC starting with 100 mM DMAB and 50 mg Rh(II)/nanoTiO2 (0.5 wt. % Rh, [Rh]= 0.24 mM) in 10 mL toluene solution.

The activation parameters for the dehydrogenation of DMAB in the presence of Rh(0)/nanoTiO$_2$ catalyst were calculated by using the Arrhenius (Laidler, 1987) and Eyring (Eyring, 1935) equations: The activation energy E_a = 37 ± 2 kJ/mol; the enthalpy of activation $\Delta H^{\#}$ = 34 ± 2 kJ/mol; the entropy of activation $\Delta S^{\#}$ = -144 ± 7 J/mol K. It can be concluded that the reaction follows an associative mechanism in the

transition state during the catalytic dehydrogenation of DMAB due to the small value of the activation enthalpy and the large negative value of the activation entropy (Connors, 1990).

The catalytic activity and the activation energy values for all the catalyst reported for the dehydrogenation of DMAB were listed in Table 3 along with the other parameters. One can see that Rh(0)/nanoTiO_2 catalyst with a rhodium loading of 0.1% wt Rh provides the highest catalytic activity and quite low activation energy for the dehydrogenation of DMAB.

Table 3. Catalytic activity (Turnover frequency TOF h^{-1}) and activation energy of various catalysts with other parameters in dehydrogenation of DMAB.

Entry	Precatalyst /catalyst	Solvent	Temp. (°C)	Time (h)	Equivalent H_2	TOF(h^{-1})	Ea ($kmol^{1}$)	Ref
1	$[Rh(1,5\text{-cod})(\mu\text{-Cl})]_2$	Toluene	25	8	1.0	12.4	ND	Jaska et al., 2003
2	$[Ir(1,5\text{-cod})(\mu\text{-Cl})]_2$	Toluene	25	136	0.95	0.7	ND	Jaska et al., 2003
3	Rh(0)/$[Noct_4]Cl$	THF	25	6	0.9	8.2	ND	Jaska and Manners, 2004
4	Rh(0) Nanoclusters	Toluene	25	2.5	1.0	60	34± 2	Zahmakıran and Ozkar 2009
5	Pd(0)/MOF	Toluene	25	6	1.0	75	173.5± 2	Gulcan et al., 2014
6	Pt(0)NPs/AA	THF	25	0.6	1.0	15	64 ± 2	Sen et al., 2014
7	Pt(0)/TBA	THF	25	1	1.0	31	46.7± 2	Erken et al., 2016
8	Pt(0)/DPA@GO	THF	25	1	1.0	35	42± 2	Celik et al., 2016
9	OAm-stabilized Ru(0)NPs	Toluene	25	1.5	1.0	137	29 ± 2	Duman and Ozkar 2013
10	Ru(0)APTS	THF	25	2	1.0	55	61± 2	Zahmakiran et al, 2012
11	Cu(0) NPs	Toluene	60	1	1.0	40	76±2	This work

4.2.3 The recyclability and catalytic lifetime of titania supported rhodium(0) nanoparticles in the dehydrogenation of DMAB

The recyclability test was performed on both rhodium nanoparticles catalysts, unsupported and supported on nanotitania in the dehydrogenation of DMAB at 60.0 ± 0.5 °C. First, a standard dehydrogenation of DMAB was carried out starting with either 1.00 mM rhodium(II) octanoate or Rh(II)/nanoTiO_2 with 0.5% wt. Rh ([Rh] = 0.24 mM) plus 100 mM $(CH_3)_2NHBH_3$ in 10 mL toluene solution. After the complete dehydrogenation, having released 1.0 equiv. H_2 per mole of DMAB, a new batch of 100 mM DMAB was transferred to the flask and a new run of dehydrogenation was started. This hydrogen generation process was repeated 4 times in the same way for

the both set of experiments at 60.0 ± 0.5 ^{o}C. The results of recyclability tests for both of the catalysts are given in Figure 4.29.

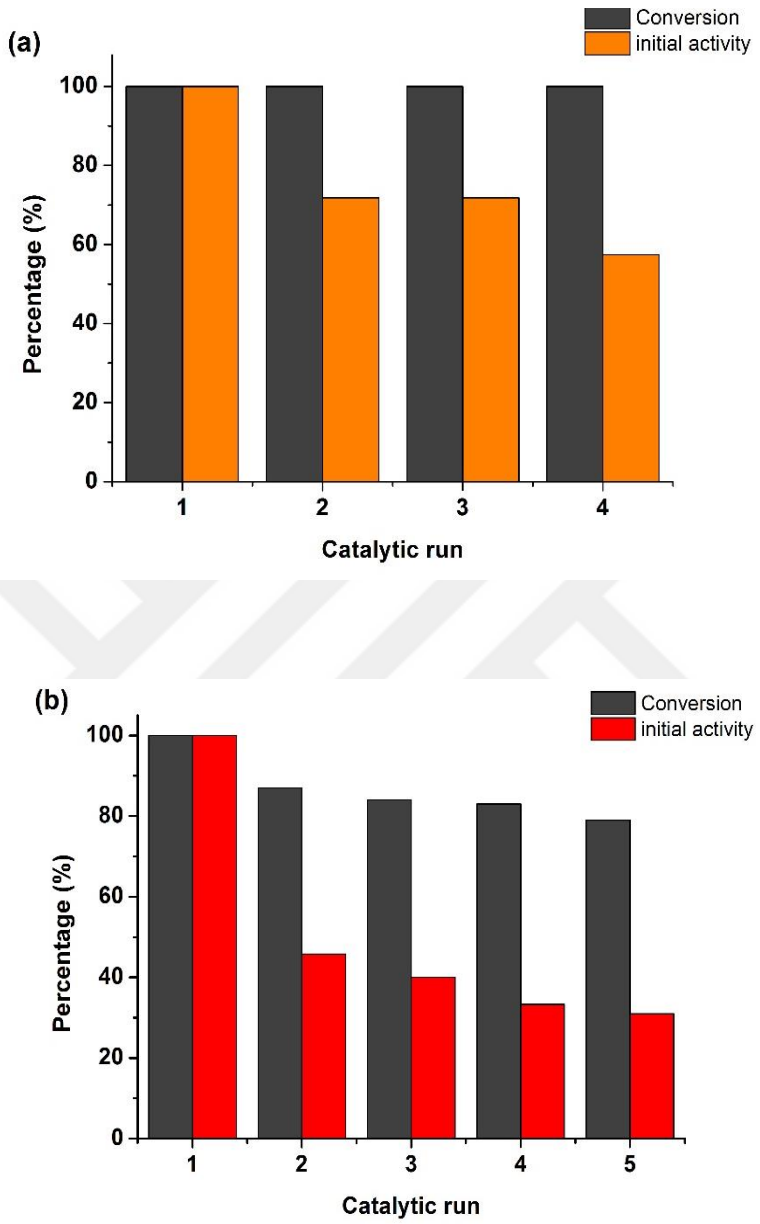

Figure 4.29. Percentage of initial activity vs number of cycle for (a) Rh(0)/nanoTiO_2 (0.5 wt. % Rh, [Rh] = 0.24 mM), (b) 1.00 mM Rh(II) octanoate in the subsequent dehydrogenation of 100 mM $(CH_3)_2NHBH_3$ at 60 ± 0.5 ^{o}C.

Although both rhodium(0) nanoparticles catalysts, unsupported and supported on nanotitania have similar initial catalytic activity in the first run of dehydrogenation, the catalytic activity of the unsupported rhodium(0) nanoparticles decreases in the subsequent runs. More importantly, for Rh(octanoate)$_2$ the conversion of DMAB decreases as well, i.e. less than 1 equiv. H_2 per mole of $(CH_3)_2NHBH_3$ is produced in subsequent runs (Figure 4.29b), while Rh(0)/nanoTiO_2 provides 100% conversion (Figure 4.29a) even in the fourth cycle. After the fourth run of dehydrogenation of DMAB, Rh(0)/nanoTiO_2 maintains 57% of the initial catalytic activity possessing still a high TOF value of 576 min^{-1}. The decrease in catalytic activity of Rh(0)/nanoTiO_2 in further runs is most likely due to the agglomeration of NPs on the surface of titania nanopowders. Indeed, TEM image (Figure 4.30) of the Rh(0)/nanoTiO_2 catalyst sample harvested after the last run of dehydrogenation shows slight agglomeration of Rh(0) NPs. The mean particle size of rhodium(0) nanoparticles increases from 3.17 ± 0.52 nm for the first run to 3.46 ± 0.49 for the last run.

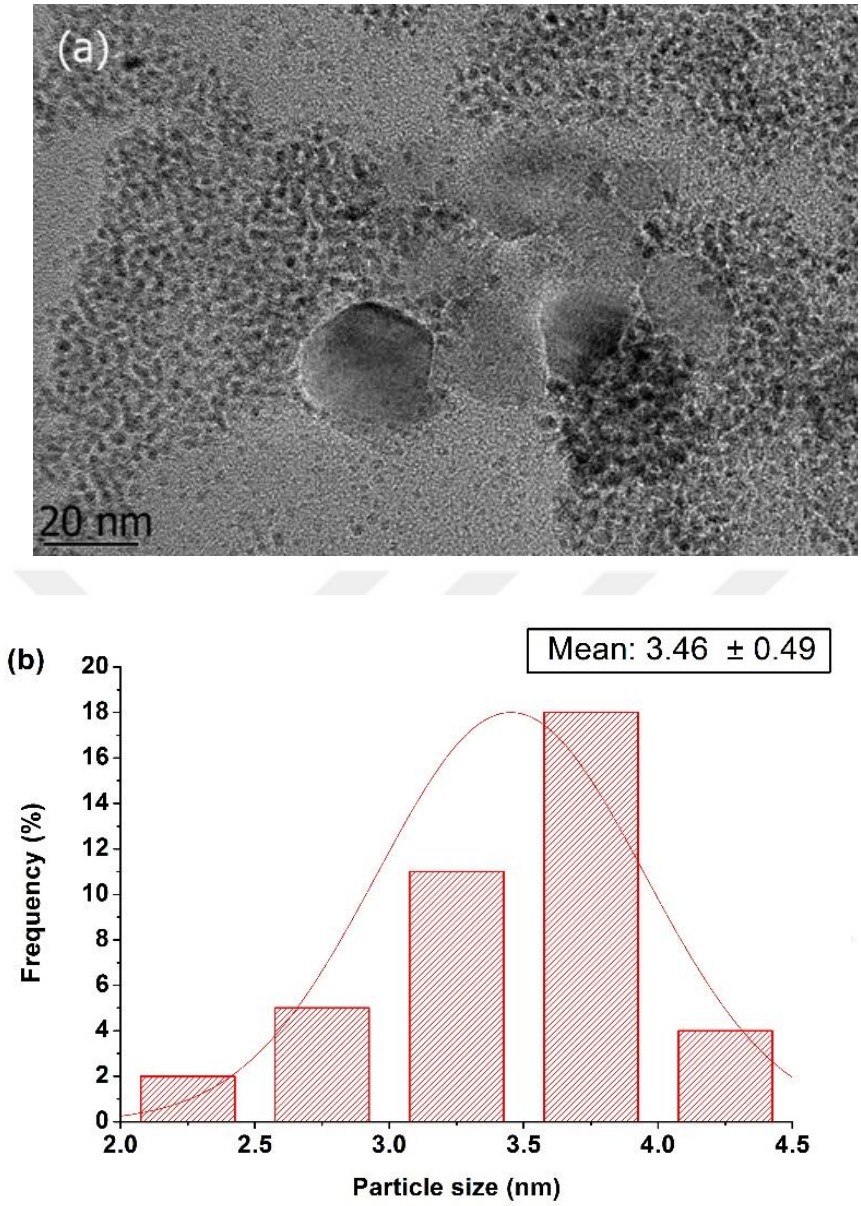

Figure 4.30. (a) TEM image of Rh(0)/nanoTiO_2 after 4th cycle in dehydrogenation reaction of DMAB, (b) corresponding particle size histogram of Rh(0) nanoparticles.

The catalytic lifetime of Rh(0)/nanoTiO_2 was measured by determining the total turnover number in hydrogen generation from the dehydrogenation of DMAB. Such a lifetime experiment was performed starting with 10 mL solution containing 0.24 mM rhodium(II) octanoate impregnated on nanotitania and 100 mM $(CH_3)_2NHBH_3$ at 60.0 ± 0.5 °C. When all the DMAB present in solution was completely dehydrogenated, a new batch of DMAB was added and the reaction was continued in this way until no hydrogen gas evolution was observed. Rh(0)/nanoTiO_2 with 0.5% wt. Rh ([Rh] = 0.24 mM) provide 9700 turnovers over 27 h in the dehydrogenation of DMAB at 60.0 ± 0.5 °C before deactivation (Figure 4.31).

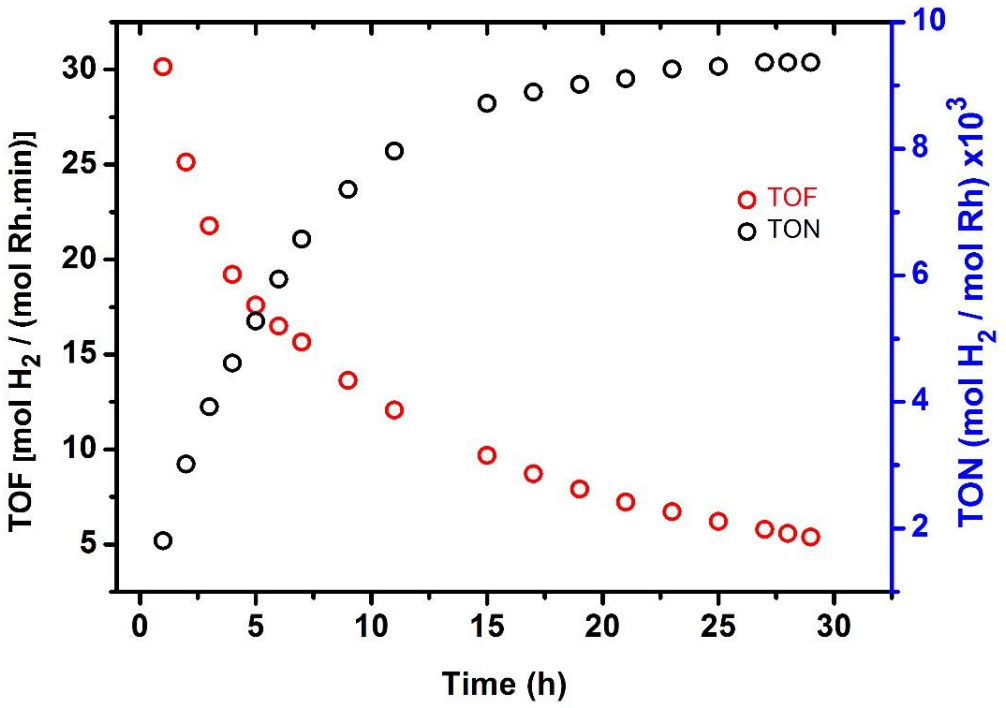

Figure 4.31. Plot of total turnover number (TTO) or turnover frequency versus time for the dehydrogenation of DMAB in 10.0 mL toluene solution containing Rh(II)/nanoTiO2 (0.5% wt. Rh, 0.24 mM Rh), with 100 mM DMAB (for each run) at 60.0 ±0.5 °C.

4.2.4 Poisoning experiment (CS_2) for Rh(0)/TiO_2 in the dehydrogenation of DMAB.

The heterogeneity of Rh(0)/nanoTiO_2 nanoparticles was performed by CS_2 poisioning experiment. The access of the substrate to the active site is blocked by poison due to the strong binding of poison to the metal center (Hornstein et al., 2002; Vargaftik et al., 1989). A typical dehydrogenation of 100 mM $(CH_3)_2NHBH_3$ in the presence of 0.24 mM Rh catalyst was started in 10 mL toluene at 60.0 ± 0.5 °C. When 0.20 equivalent CS_2 was injected into the reaction medium after the liberation of 30% hydrogen from dehydrogenation of DMAB, hydrogen evolution stopped immediately due to the inhibition of activity of nanotitania stabilized rhodium(0) nanoparticles (Figure 4.32). This provides a compelling evidence for the heterogeneity of the dehydrogenation of DMAB catalyzed by Rh(0)/nanoTiO_2 nanoparticles.

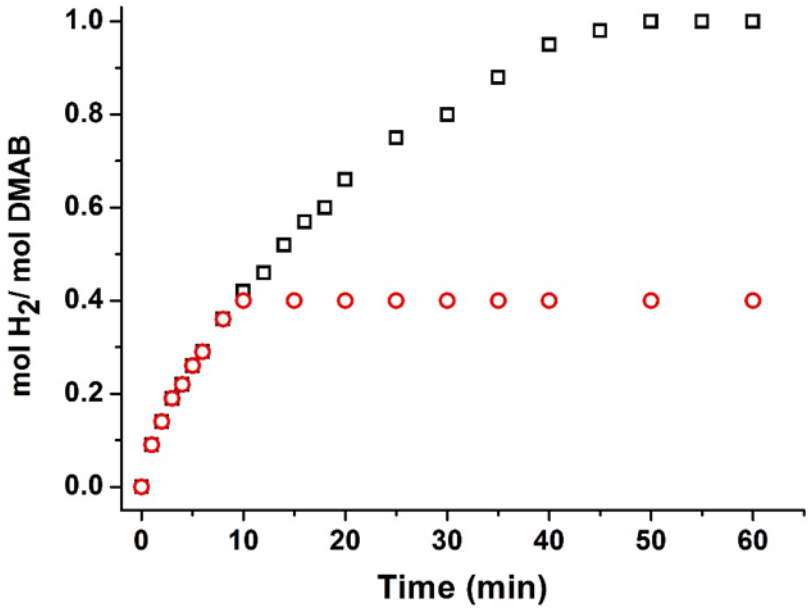

Figure 4.32. Plots of mol H_2 evolved per mole of DMAB versus time for the dehydrogenation of 100 mM $(CH_3)_2NHBH_3$ catalyzed by Rh(0) nanoparticles supported on nanotitania (0.5% wt. Rh, [Rh] = 0.24 mM) with and without addition of 0.2 equiv. CS_2 at 60.0 ± 0.5 °C.

4.2.5 Leaching test for Rh(0)/nanoTiO$_2$

The catalytic activity of the filtrated solution at the end of the catalytic reaction in the dehydrogenation of $(CH_3)_2NHBH_3$ (100 mM) was tested to check whether any rhodium is leaching from the solid Rh(0)/nanoTiO$_2$ to the solution. Figure 4.33 depicts the plots of mol H_2 evolved per mole of DMAB versus time during the dehydrogenation of 100 mM DMAB at 60.0 ± 05 ^oC starting with (a) 0.24 mM Rh (0.5% wt. Rh, Rh(II)/nanoTiO$_2$) (black squares), (b) solid sample obtained by filtration after the first run in (a) (red circles), and (c) filtrate solution obtained by filtration after the first run in (a) (blue triangles). The catalytic activity of the isolated solid Rh(0)/nanoTiO$_2$ sample decreases due to the materials loss during the isolation and redispersing processes. The filtrate solution is catalytically silent in the dehydrogenation of DMAB. The filtrate solution obtained by filtration from the reaction medium after the first run of dehydrogenation was also analyzed by ICP technique. Rhodium concentration of the filtrated solution was determined as 0.6 ppm in solution, which was negligible compared to the initial Rh concentration in the reaction solution in the mM level. The results of the ICP analysis and leaching test confirms the retaining of Rh(0) on the surface of nanoTiO$_2$ during the catalytic reaction. Hence, we can conclude that nanotitania supported rodium(0) nanoparticles are adept competent catalyst in the dehydrogenation of DMAB.

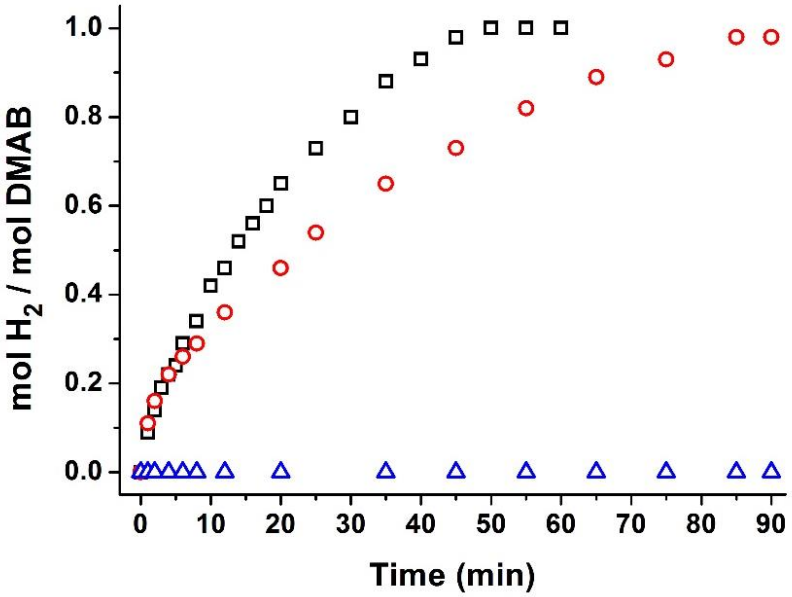

Figure 4.33. The evolution of equivalent H_2 per mole of DMAB verus time plot for the dehydrogenation of 100 mM $(CH_3)_2NHBH_3$ at 60.0 ± 0.5 ^oC starting with Rh(II)/nanoTiO_2 (black squares, □), Rh(0)/nanoTiO_2 solid sample obtained by filtration after the first run (red circles, o), filtrate solution obtained by filtration after the reaction (blue triangles, Δ).

5. CONCLUSIONS

In summary, the preparation and characterization of ceria supoorted copper(0) nanoparticles and titania supported rhodium(0) nanoparticles as catalysts for dehydrogenation of DMAB has led to the following conclusions;

Part I. Preparation and Characterization of Ceria supported Copper(0) Nanoparticles

a) Cu(0) NPs are formed from the reduction of copper(II) 2-ethylhexanoate throughout the dehydrogenation of DMAB at 60 ± 0.5 ^{o}C and initially active catalysts in hydrogen generation. However, they are not stable and undergo aggregation to the bulk metal.
b) Stable copper(0) nanoparticles can be obtained when the reduction of copper(II) to copper(0) is performed on the surface of ceria nanopowders. The resulting nanoparticles are active catalyst providing a release of 1.0 equivalent of H_2 per mole of DMAB.
c) The results of characterization reveal the formation of highly dispersed copper(0) nanoparticles with an average particle size of 3.1 ± 0.8 nm on the ceria surface.
d) Ceria supported copper(0) nanoparticles with a loading of 4.0% wt. Cu provide the highest activity with turnover frequency of 40 h^{-1} in hydrogen generation from DMAB at 60.0 ± 0.5 ^{o}C.
e) Ceria supported copper(0) nanoparticles can provide only 225 turnovers in generation of H_2 from the dehydrogenation of DMAB at 60.0 ± 0.5 ^{o}C before they are deactivated. Thus, the catalytic lifetime of Cu(0/CeO_2 nanoparticles (225 TTO) is significantly lower than the ones reported for the precious metal catalysts. Nevertheless, Cu(0/CeO_2 nanoparticles can be considered as cost-effective catalyst compared to the precious metals such as Ru and Rh based catalyst system in the dehydrogenation of DMAB.
f) Ceria supported copper(0) nanoparticles are shown to be heterogeneous and kinetically adept catalysts in dehydrogenation of DMAB.
g) Low cost, easy preparation, relatively high stability, and high catalytic activity of nanoceria supported Cu(0) NPs make them promising candidate to be exploited as catalyst in hydrogen generation from DMAB.

Part II. Preparation and Characterization of Titania supported Rhodium(0) Nanoparticles

a) Rh(0) nanosized particles can be formed from the reduction of rhodium(II) octanoate in toluene solution during the catalytic dehydrogenation of DMAB. These Rh(0) nanoparticles have initially high catalytic activity in the dehydrogenation of DMAB, however they are not very stable losing their catalytic activity in time. When the same nanoparticle formation and concomitant dehydrogenation of DMAB performed in the presence of titania nanopowders one obtains nanotitania supported rhodium(0) nanoparticles, which are not only highly active catalyst in dehydrogenation of DMAB, but also stable, so that they can be isolated as solid materials from the reaction medium, stored under inert atmosphere, and redispersed in toluene for the further reuse as catalyst.
b) Supported on the surface of titania nanopowders, one obtains highly dispersed rhodium(0) NPs with average particle size depending on the rhodium loading of Rh(0)/nanoTiO_2, in the range 2.0-3.2 nm. Inversely with the size, the catalytic activity of Rh(0)/nanoTiO_2 decreases with the increasing loading of nanotitania.
c) The highest initial turnover frequency of 2900 h^{-1} is obtained by using Rh(0)/nanoTiO_2 with rhodium loading of 0.1% wt. Rh in the dehydrogenation of DMAB at 60.0 ± 0.5 ^oC. This is a record TOF value ever reported for the same reaction up to now.
d) The recyclability tests show that Rh(0)/nanoTiO_2 retains 57% of its initial catalytic activity even after the fourth run of dehydrogenation reaction releasing 1.0 equivalent H_2 per mole of DMAB.
e) Also, Rh(0)/nanoTiO_2 is long-lived catalyst providing 9700 turnovers for hydrogen generation from the dehydrogenation of DMAB at 60.0 ± 0.5 ^oC.
f) The results of carbon disulfide poisoning and leaching tests reveal that nanotitania supported rhodium(0) NPs are adept competent catalyst and the dehydrogenation of DMAB is heterogeneous catalysis.
g) Easy preparation, high activity, recyclability, and long lifetime of the nanotitania supported rhodium(0) NPs make them promising candidate for developing highly

efficient catalysts in dehydrogenation/dehydrocoupling reactions of dimethylamine borane.

REFERENCES

Aiken JD and Finke RG (1999) “A review of modern transition-metal nanoclusters: their synthesis, characterization, and applications in catalysis”, Journal of Molecular Catalysis A-Chemical, 145: 1-44.

Akbayrak S and Ozkar S (2016) “Inverse relation between the catalytic activity and catalyst concentration for the ruthenium(0) nanoparticles supported on xonotlite nanowire in hydrogen generation from the hydrolysis of sodium borohydride”, Journal of Molecular Catalysis A-Chemical, 424: 254-260.

Akbayrak S, Tonbul Y and Özkar S (2016a) “Ceria-supported ruthenium nanoparticles as highly active and long-lived catalysts in hydrogen generation from the hydrolysis of ammonia borane”, Dalton Transaction, 45: 10969-10978.

Akbayrak S, Tonbul Y and Özkar S, (2016b) “Ceria supported rhodium nanoparticles: Superb catalytic activity in hydrogen generation from the hydrolysis of ammonia borane”, Applied Catalysis B-Environmental, 198: 162.

Alcaraz G, Vendier E, Clot S and Olasagasti SE (2010) “Ruthenium Bis(sigma-B-H) Aminoborane Complexes from Dehydrogenation of Amine-Boranes: Trapping of H_2B-NH_2 ”, Angewandte Chemie-International Edition, 49: 918-920.

Alves HJ, Bley Junior C, Niklevicz RR, Frigo EP, Frigo MS and Coimbra-Araújo CH (2013) “Overview of hydrogen production technologies from biogas and the applications in fuel cells”, International Journal of Hydrogen Energy, 38: 5215.

Amendola SC, Janjua JM, Spencer NC, Kelly MT, Petillo PJ, Sharp-Goldman SL and Binder M (2000) “A safe, portable, hydrogen gas generator using aqueous borohydride solution and Ru catalyst”, International Journal of Hydrogen Energy, 25: 969.

Amiens C, Decaro D, Chaudret B, Bradley JS, Mazel R and Roucau C (1993) “Selective Synthesis, Characterization and Spectroscopic Studies on a Novel Class of Reduced Platinum and Palladium Particles Stabilized by Carbonyl and Phosphine-Ligands”, Journal of the American Chemical Society, 115: 11638-11639.

Arcadi A (2008) “Alternative synthetic methods through new development in catalsysis by gold”, Chemical Reviews, 108: 3266.

Astruc D (2008) Nanoparticles and Catalysis (ed. D. Astruc), Wiley-VCH, Weinheim, Germany.

Baer Y, Heden PF, Hedman J, Klasson M, Nordling C and Siegban K (1970) “Band structure of transition metals studied by ESCA”, Physica Scripta, 1: 55-65.

Bagheri S, Julkapli NM and Hamid SBA (2014) “Recent Advances in Heterogeneous Photocatalytic Decolorization of Synthetic Dyes”, The Scientific World Journal, 692307: 25.

Balanta A, Godard C and Claver C (2011) “Pd nanoparticles for C-C coupling reactions”, Chemistry Society Reviews, 40: 4973.

Bamwenda GR, Tsubota S, Nakamura T and Haruta M (1997) “The influence of the preparation methods on the catalytic activity of platinum and gold supported on TiO_2 for CO oxidation”, Catalysis Letters, 44: 83.

Bard AJ and Faulkner LR (1980) Electrochemical Methods: Fundamentals and Applications, Wiley, New York.

Barr TL (1978) “Esca Study of Termination of Passivation of Elemental Metals”, Journal of Physical Chemistry, 82: 1801-1810.

Bêche E, Charvin P, Perarnau D, Abanades S and Flamant G (2008) “Ce 3d XPS investigation of cerium oxides and mixed cerium oxide (CexTiyOz)”, Surface and Interface Analysis, 40: 264-267.

Berg V, Annemieke WC and Arean CO (2008) “Materials for hydrogen storage: current research trends and perspectives”, Chemistry Communication, 6: 668.

Berhault G, Bisson L, Thomazeau C, Verdon C and Uzio D (2007) “Preparation of nanostructured Pd particles using a seeding synthesis approach -application to the selective hydrogenation of buta-1,3-diene”, Applied Catalysis A, 327: 32.

Bluhm ME., Bradley MG, Butterick R, Kusari U and Sneddon LG (2006) “Amineborane-based chemical hydrogen storage: Enhanced ammonia borane dehydrogenation in ionic liquids”, Journal of the American Chemical Society, 128: 7748.

Campelo JM, Lee AF, Luque R, Luna D, Marinas JM and Romero AA (2008) “Preparation of highly active and dispersed platinum nanoparticles on mesoporous Al-MCM-48 and their activity in the hydroisomerisation of n-octane”, Chemistry-A European Journal, 14: 5988-5995.

Castillejos E, Debouttire PJ, Roiban L, Solhy A, Martinez V, Kihn Y, Ersen O, Philippot K, Chaudret B and Serp P (2009) “An Efficient Strategy to Drive Nanoparticles into Carbon Nanotubes and the Remarkable Effect of

Confinement on Their Catalytic Performance", Angewandte Chemie International Edition, 48: 2529.

Celik B, Baskaya G, Sert H, Karatepe O, Erken E and Sen F (2016) "Monodisperse Pt(0)/DPA@GO nanoparticles as highly active catalysts for alcohol oxidation and dehydrogenation of DMAB", International Journal of Hydrogen Energy, 41: 5661-5669.

Chawla SK, Sankarraman N and Payer JH (1992) "Dianostic Spectra for XPS Analysis of Cu-O-S-H Compounds", Journal of Electron Spectroscopy and Related Phenomena, 61: 1-18.

Chen CL and Mou CY (2004) "Mesoporous materials as catalyst supports", Nanotechnology in Catalysis, 1: 313-327.

Chen ZJ, Guan ZH, Li MR, Yang QH and Li C (2011) "Enhancement of the performance of a platinum nanocatalyst confined within carbon nanotubes for asymmetric hydrogenation", Angewandte Chemie-International Edition, 50: 4913.

Choi H, Al-Abed SR, Agarwal S and Dionysiou DD (2008) "Synthesis of reactive nano-Fe/Pd bimetallic system-impregnated activated carbon for the simultaneous adsorption and dechlorination of PCBs", Chemistry of Materials, 20: 3649-3655.

Chusuei CC, Brookshier MA and Googman DW (1999) "Correlation of relative X-ray photoelectron spectroscopy shake-up intensity with CuO particle size ", Langmuir, 15: 2806-2808.

Clark JT, Lee K and Manners I (2006) "Transition-metal-catalyzed dehydrocoupling: a convenient route to bonds between main-group elements", Chemistry – A European Journal, 12: 8634.

Claus P (2005) "Heterogeneously catalysed hydrogenation using gold catalysts", Applied Catalysis A, 291: 222.

Cole-Hamilton D (2003) "Homogeneous catalysis – new approaches to catalyst separation, recovery, and recycling", Science, 299 (5613): 1702.

Connors KA (1990) Theory of Chemical Kinetics, First Edition, VCH, New York.

Corma A, and Garcia H (2008) "Supported gold nanoparticles as catalysts for organic reactions", Chemistry Society Reviews, 37: 2096.

Creighton JA, and Eadon DG (1991) “Ultraviolet–visible absorption spectra of the colloidal metallic elements”, Journal of the Chemical Society Faraday Transations, 87: 3881-3891.

Dai Q, Bai S, Wang X and Lu G (2013) “Catalytic combustion of chlorobenzene over Ru-doped ceria catalysts: Mechanism study”, Applied Catalysis B-Environmental 129: 580.

Dasog M and Scott RWJ (2007) “Understanding the oxidative stability of gold monolayer-protected clusters in the presence of halide ions under ambient conditions”, Langmuir, 23: 3381-3387.

De Vries AHM, Mulders JMCA, Mommers JHM, Henderickx HJW, and de Vries JG (2003) “Homeopathic ligand-free palladium as a catalyst in the Heck reaction. A comparison with a palladacycle”, Organic Letters, 5: 3285-328.

Deacon GB and Phillips RJ (1980) “Relationships Between The Carbon-Oxygen Stretching Frequencies of Carboxylato Complexes and The Type of Carboxylate Coordination”, Coordination Chemisty Reviews, 33: 227-250.

Della Pina C, Falletta E, Prati L and Rossi M (2008) “Selective oxidation using gold”, Chemistry Society Reviews, 37: 2077.

Della Pina C, Falletta E and Rossi M (2012) “Update on selective oxidation using gold”, Chemistry Society Reviews, 41: 350.

Denney MC, Pons V, Hebden TJ, Heinekey DM and Goldberg KI (2006) “Efficient catalysis of ammonia borane dehydrogenation”, Journal of the American Chemical Society, 128: 12048.

Duman S and Ozkar S (2013) “Oleylamine-stabilized ruthenium(0) nanoparticles catalyst in dehydrogenation of dimethylamine-borane”, International Journal of Hydrogen Energy, 38: 10000-10011.

Doll KM and Finke RG (2004) “Adenosylcobinamide plus exogenous, sterically hindered, putative axial bases: A reinvestigation into the cause of record levels of Co-C heterolysis”, Inorganic Chemistry, 43: 2611-2623.

Douglas TM, Chaplin AB, Weller AS, Yang X and Hall MB (2009) “Monomeric and Oligomeric Amine-Borane sigma-Complexes of Rhodium. Intermediates in the Catalytic Dehydrogenation of Amine-Boranes”, Journal of the American Chemical Society, 131: 15440-1545.

Duman S and Ozkar S (2013) “Oleylamine-stabilized ruthenium(0) nanoparticles catalyst in dehydrogenation of dimethylamine-borane”, International Journal of Hydrogen Energy, 38: 10000-10011.

Duteil A, Schid G and Meyer-Zaika W (1995) “Ligand stabilized nickel colloids”, Chemistry Communication, 1: 31-32.

Ehrenreich H and Philipp HR (1962) “Optical Properties of Ag and Cu”, Physical Review, 128: 1622-1629.

El-Shall MS, Abdelsayed V, Khder AERS, Hassan HMA, El-Kaderi HM, Reich TE (2009) “Metallic and bimetallic nanocatalysts incorporated into highly porous coordination polymer MIL-101”, Journal of Materials Chemistry, 19: 7625.

Erdogan H, Metin Ö, and Özkar S (2009) “In situ-generated PVP-stabilized palladium(0) nanocluster catalyst in hydrogen generation from the methanolysis of ammonia-borane”, Physical Chemistry Chemical Physics, 11: 10519-10525.

Erken E, Pamuk H, Karatepe O, Baskaya G, Sert H, Kalfa OM and Sen F (2016) “New Pt(0) Nanoparticles as Highly Active and Reusable Catalysts in the C1-C3 Alcohol Oxidation and the Room Temperature Dehydrocoupling of Dimethylamine-Borane (DMAB) ”, Journal of Cluster Science, 27: 9-23.

Ertl G, Knozinger H and Weitkamp J (1997) Handbook of Heterogeneous Catalysis, Wiley/VCH, New York.

Eyring H (1935) “The Activated Complex and The Absolute Rate of Chemical Reactions”, Journal of Chemica Physics, 3: 107-115.

Fahlman BD (2011) What is Materials Chemistry?, Springer, New York, DOI: 10.1007/978-94-007-0693-4.

Feng X, Ding XS and Jiang DL (2012) “Covalent organic frameworks”, Chemical Society Reviews, 41: 6010.

Fernandes R, Patel N and Miotello A (2009) “Hydrogen generation by hydrolysis of alkaline NaBH4 solution with Cr-promoted Co-B amorphous catalyst”, Applied Catalysis B: Enviromental, 92: 68.

Fihri A, Bouhrara M, Nekoueishahraki B, Basset JM and Polshettiwar V (2011) “Nanocatalysts for szuzuki cross-coupling reactions”, Chemistry Society Reviews, 40: 5181.

Flipponi L and Sutherland D (2010) Introduction to Nanoscience and Nanotechnologies, Interdisciplinary Nanoscience Center, Denmark.

Fu X, Wang Y, Wu N, Gui L and Tang Y (2002) "Shape-selective preparation and properties of oxalate-stabilized Pt colloid", Langmuir, 18(12): 4619.

Fulton JL, Linehan JC, Autrey T, Balasubramanian M, Chen Y and Szymczak NK (2007) "When is a nanoparticle a cluster? An operando EXAFS study of amine borane dehydrocoupling by Rh4-6 clusters", Journal of the American Chemical Society, 129: 11936-11949.

Furukawa H and Yaghi OM (2009) "Storage of Hydrogen, Methane, and Carbon Dioxide in Highly Porous Covalent Organic Frameworks for Clean Energy Applications", Journal of the American Chemical Society, 131: 8875.

Gary JH and Handwerk GE (2001) Petroleum Refining: Technology and Economics, Fourth Edition, CRC Press, Boca Raton.

Ghijsen J, Tjeng LH, van Elp J, Eskes H, Westerink J and Sawatzky GA (1988) "Electronic-Structure of CuO_2 and CuO", Physical Review B, 38: 11322-11330.

Graeser M, Pippel E, Greiner A and Wendorff JH (2007) "Polymer core-shell fibers with metal nanoparticles as nanoreactor for catalysis", Macromolecules, 40: 6032.

Granovskii M, Dincer I and Rosen MA (2007) "Exergetic life cycle assessment of hydrogen production from renewables", Journal of Power Sources, 167: 461.

Grochala W and Edwards PP (2004) "Thermal decomposition of the non-interstitial hydrides for the storage and production of hydrogen", Chemical Reviews, 104: 1283.

Gude K and Narayanan R (2011) "Colloidal supported metal nanoparticles (CSMNs) as effective nanocatalysts for liquid-phase suzuki cross-coupling reactions", Journal of Physical Chemistry C, 115: 12716.

Gutowska A, Li L, Shin Y, Wang CM, Li XS, Linehan JC, Smith RS, Kay BD, Schmid B, Shaw W, Gutowski M and Autrey T (2005) Angewandte Chemie-International Edition, 44: 3578.

Gülcan M, Zahmakiran M and Ozkar S (2014) "Palladium(0) nanoparticles supported on metal organic framework as highly active and reusable nanocatalyst in dehydrogenation of dimethylamine-borane", Applied Catalysis B-Environmental, 147: 394-401.

Hagen J (2006) Industrial Catalysis: A Practical Approach, Wiley-VCH, Mannheim, Germany.

Hamilton CW, Baker RT, Staubitz A, Manners I (2009) "B–N compounds for chemical hydrogen storage", Chemical Society Reviews, 38: 279.

Haruta M (1997) "Size- and support-dependency in the catalysis of gold", Catalysis Today, 36: 153.

Haruta M, Kobayashi T, Sano H, Yamada N (1987) "Novel gold catalysts for the oxidation of carbon-monoxide at a temperature far below 0-degrees-C", Chemistry Letters, 2: 405.

Hashmi ASK, Hutchings GJ (2006) "Gold catalysis", Angewandte Chemie-International Edition, 45: 7896.

Hirtzel CS and Rajagopalan R (1985) Colloidal Phenomena: Advanced Topics, Noyes Publications, Park Ridge.

Holladay JD, Hu J, King DL, Wang Y (2009) "An overview of hydrogen production Technologies", Catalysis Today, 139: 244.

Hornstein BJ, Aiken JD and Finke RG (2002) "Nanoclusters in catalysis: A comparison of CS_2 catalyst poisoning of polyoxoanion- and tetrabutylammonium-stabilized 40 +/- 6 angstrom Rh(0) nanoclusters to 5% Rh/Al2O3, including an analysis of the literature related to the CS_2 to metal stoichiometry issue ", Inorganic Chemistry, 41: 1625-1638.

Hou WB, Dasog M and Scott RWJ (2009) "Probing the Relative Stability of Thiolate- and Dithiolate-Protected Au Monolayer-Protected Clusters", Langmuir, 25: 12954-12961.

Hunter RJ (1986) Foundations of Colloid Science, First Edition, Oxford University Press, New York.

Hunter RJ (1987) Foundations of Colloid Science, Oxford University Press, New York.

Hutchings GJ (1985) "Vapor-phase hydrochlorination of acetylene -correlation of catalytic activity of supported metal chloride catalysts", Journal of Catalysis, 96:292.

International Energy Outlook 2013 with Projections to 2040, www.eia.gov/ieo/ , 6th February 2015.

Jacquemin D, Lambert C and Perpete EA (2004) "Structures and properties of polyphosphinoborane: an oligomeric theoretical study", Macromolecules, 37: 1009.

Jaska CA and Manners I (2004) "Ambient temperature, tandem catalytic dehydrocoupling hydrogenation reactions using Rh colloids and Me_2NH center

dot BH_3 as a stoichiometric H-2 source", Journal of the American Chemical Society, 126: 2698.

Jaska CA and Manners I (2004) "Heterogeneous or homogeneous catalysis? Mechanistic studies of the rhodium-catalyzed dehydrocoupling of amine-borane and phosphine-borane adducts", Journal of the American Chemical Society, 126: 9776-9785.

Jaska CA, Temple K, Lough AJ and Manners I (2001) "Rhodium-catalyzed formation of boron-nitrogen bonds: a mild route to cyclic aminoboranes and borazines", Chemistry Communication, 11: 962.

Jaska CA, Temple K, Lough AJ and Manners I (2003) "Transition metal-catalyzed formation of boron-nitrogen bonds: Catalytic dehydrocoupling of amine-borane adducts to form aminoboranes and borazines", Journal of the American Chemical Society, 125: 9424.

Jiang Y and Berke H (2007) "Dehydrocoupling of dimethylamine-borane catalysed by rhenium complexes and its application in olefin transfer-hydrogenations", Chemistry Communication, 34: 3571-3573.

Jones IP (1992) Microanalysis Using Electron Beams, First Edition, The Institute of Materials, London.

Jong-San C, Jin-Soo and Sang-Eon P (2003) "Preparation and application of nanocatalysts via surface functionalization of mesoporous materials", Research on Chemical Intermediates, 29: 921-938.

Ju-Nam Y and Lead JR (2008) "Manufactured Nanoparticles: An overview of their chemistry, interactions and potential environmental implications", Science of the Total Environment, 400: 396-414.

Kato H, Minami T, Kanazawa T and Sasaki Y (2004) "Mesopores created by platinum nanoparticles in zeolite crystals",Angewandte Chemie International Edition, 43: 1251-1254.

Kalidindi SB and Jagirdar BR (2010) "Hydrogen generation from ammonia borane using nanocatalysts", Journal of the Indian Institute of Science, 90: 181-187.

Keaton RJ, Blacquiere JM and Baker RT (2007) "Base metal catalyzed dehydrogenation of ammonia-borane for chemical hydrogen storage", Journal of the American Chemical Society, 129: 1844.

Kozuch S and Martin JML (2012) "Turning Over" Definitions in Catalytic Cycles", American Chemical Society Catalysis, 2: 2787.

Kustov LM Tarasov AL, Sung J and Godovsky DY (2014) "Hydrogen storage materials", Mendeleev Communications, 24: 1.

Laidler KJ (1987) Chemical Kinetics, Third Edition, Harper-Row, New York.

Langmi HW and McGrady GS (2007) "Non-hydride systems of the main group elements as hydrogen storage materials", Coordination Chemistry Reviews, 251: 925.

Lee J, Kong KY, Jung CR, Cho E, Yoon SP, Han J, Lee TG and Nam SW (2007) "A structured Co-B catalyst for hydrogen extraction from $NaBH_4$ solution", Catalysis Today, 120: 305.

Lee Y, Choi J, Lee KJ, Stott E and Kim D (2008) "Large-scale synthesis of copper nanoparticles by chemically controlled reduction for applications of inkjet-printed electronics", Nanotechnology, 19: 415604-415611.

Lever ABP (1984) Inorganic Electronic Spectroscopy, Second Edition, Elsevier, New York.

Lin SJ, Hong TN, Tung JT and Chen JH (1997) "Molecular structures of Ge(tpp)(OAc)(2) and In(tpp)(OAc) and their implications", Inorganic Chemistry, 36: 3886-3891.

Lin Y and Finke RG (1994) "Novel Polyoxoanion-Stabilized and Bu(4)N(+)-Stabilized, Isolable and Redissolvable, 20-30-Angstrom Ir-Similar-to(300)-(900) Nanoclusters- The Kinetically Controlled Synthesis, Characterization and Mechanism of Formation of Organic Solvent-Soluble, Reproducible size and Reproducible Catalytic Activity Metal Nanoclusters", 116: 8335-8353.

Malin JM, Toma HE and Giesbrecht E (1977) "Undergraduate kinetics experiment demonstrating unusual behavior of kobs", Journal of Chemcal Education, 54: 385-386.

Manbeck KA, Musselwhite NE, Carl LM, Kauffman CA, Lyons OD, Navin JK and Marsh AL (2010) "Factors affecting activity and selectivity during cyclohexanone hydrogenation with colloidal platinum nanocatalysts", Applied Catalysis A, 384: 58.

Marder TB (2007) "Will we soon be fueling our automobiles with ammoniaborane?", Angewandte Chemie International Edition**,** 46: 8116.

McEwan L, Julius M, Roberts S and Fletcher JCQ (2010) "A review of the use of gold catalysts in selective hydrogenation reactions", Gold Bulletin, 43: 298.

Metin O, Ozkar S and Sun S (2010) "Monodisperse nickel nanoparticles supported on SiO_2 as an effective catalyst for the hydrolysis of ammonia-borane", Nano Research, 3: 676-684.

Mevellec V, Nowicki A, Roucoux A, Dujardin C, Granger P and Payer E (2006) "A simple and reproducible method for the synthesis of silica-supported rhodium nanoparticles and their investigation in the hydrogenation of aromatic compounds", New Journal of Chemistry, 30: 1214-1219.

Miller AC and Simmons GW (1993) “Copper by XPS”, Surface Science Spectra, 2:55-56.

Mingshu C and Wayne GD (2008) “Catalytically active gold on ordered titania supports”, Chemical Society Reviews, 37: 1860-1870.

Mohajeri N, T-Raissi A and Adebiyi O (2007) “Hydrolytic cleavage of ammonia-borane complex for hydrogen production”, Journal of Power Sources, 167: 482.

Munoz-Olasagasti M, Telleria A, Perez-Miqueo J, Garralda MA and Frexia ZA (2014) “A readily accessible ruthenium catalyst for the solvolytic dehydrogenation of amine-borane adducts”, Dalton Transactions, 43: 11404-1409.

Murray LJ, Dinca M and Long JR (2009) “Hydrogen storage in metal-organic frameworks”, Chemical Society Reviews, 38: 1294.

Nixon TD, Whittlesey MK, and Williams JMJ (2011) “Ruthenium-catalysed transfer hydrogenation reactions with dimethylamine borane”, Tetrahedron Letters, 52: 6652.

Nolan N, Pillai S and Seery M (2009) “Spectroscopic Investigation of the Anatase-to-Rutile Transformation of Sol-Gel-Synthesized TiO_2 Photocatalysts”, Journal of Physical Chemistry C, 113: 16151-16157.

Nouailhat A (2010) An Introduction to Nanoscience and Nanotechnology, Wiley, New York, DOI: 10.1002/9780470610954.

Ozhava S and Ozkar S (2016) “Rhodium(0) nanoparticles supported on nanosilica: Highly active and long lived catalyst in hydrogen generation from the methanolysis of ammonia borane”, Applied Catalysis B-Environmental, 181: 716-726.

Ozkar S and Finke RG (2002) “Nanocluster Formation and Stabilization Fundamental Studies: Ranking Commonly Employed Anionic Stabilizers via the Development, Then Application, of Five Comparative Criteria”, Journal of the American Chemical Society, 124: 5796.

Ozkar S and Finke RG (2002) “Nanocluster Formation and Stabilization Fundamental Studies. 2. Proton Sponge as an Effective H^+ Scavenger and Expansion of the Anion Stabilization Ability Series”, Langmuir, 18: 7653-7662.

Pachon LD (2008) Synthesis and Application of Nano-Structured Metal Catalysts, Dissertation, University of Amsterdam, Amsterdam.

Pachon LD and Rothenberg G (2008) “Transition-metal nanoparticles: synthesis, stability and the leaching issue”, Applied Organometallic Chemistry, 22: 288-299.

Patel N, Fernandes R, Guella G and Miotella A (2010) “Nanoparticle-assembled Co-B thin film for the hydrolysis of ammonia borane: A highly active catalyst for hydrogen production”, Applied Catalysis B-Enviromental, 95: 137.

Paul A and Musgrave CB (2007) “Catalyzed dehydrogenation of ammonia-borane by iridium dihydrogen pincer complex differs from ethane dehydrogenation”, Angewandte Chemie-International Edition, 46: 8153.

Peuckert MA (1984) “ A Comparison of Thermally and Electrochemically Prepared Oxidation Adlayers on Rhodium- Chemical Nature nand Thermally- Stability”, Surface Science, 141: 500-514.

Piccolo L, Valcarcel A, Bausach M, Thomazeau C, Uziob D and Berhault G (2008) “Tuning the shape of nanoparticles to control their catalytic properties: selective hydrogenation of 1,3-butadiene on Pd/Al(2)O(3)”, Physical Chemistry Chemical Physics, 10: 5504.

Pileni M (1997) “Nanosized particles made in colloidal assemblies”, Langmuir, 13(13): 3266.

Poizot P, Laurelle S, Grugeon S, Dupont L and Tarascon JM (2000) “Nano-sized transition-metaloxides as negative-electrode materials for lithium-ion batteries”, Nature, 407: 496.

Pun D, Lobkovsky E and Chirik PJ (2007) “Amineborane dehydrogenation promoted by isolable zirconium sandwich, titanium sandwich and N-2 complexes”, Chemistry Communication, 48: 3297.

Raimondi F, Scherer GG, Kötz R and Wokaun A (2005) “Nanoparticles in energy technology: Examples from electrochemistry and catalysis”, Angewandte Chemie-International Edition, 44: 2190.

Ramachandran PV and Gagare PD (2007) “Preparation of ammonia borane in high yield and purity, methanolysis, and regeneration”, Inorganic Chemistry, 46: 7810.

Rao CNR, Müller A and Cheetham A (2004) The Chemistry of Nanomaterials: Synthesis, Properties and Applications, Wiley-VCH, Weinheim.

Reetz MT, Breinbauer R and Wanninger K (1996) “Suzuki and Heck reactions catalyzed by preformed palladium clusters and palladium/nickel bimetallic clusters”, Tetrahedron Letters, 37: 4499-4502.

Reetz M and de Vries J (2004) “Ligand-free Heck reactions using low Pd-loading”, Chemical Communications, 14: 1559-1563.

Reetz MT, Helbig W, Quaiser SA, Stimming U, Breuer N and Vogel R (1995) “Visualization of surfactants on nanostructured palladium clusters by a combination of STM and high-resolution TEM”, Science, 267: 367-369.

Ren Y, Chia GH and Gao Z (2013) “Metal–organic frameworks in fuel cell Technologies”, Nano Today, 8: 577.

Rothenberg G (2008) Catalysis: Concepts and Green Applications, Wiley- VCH, Weinheim.

Sanchezdelgado RA, Andriollo A, Puga J and Martin G (1987) “Homogeneous Catalysis By Metal-Clusters. 2. Tetranuclear Osmium Complexes As Catalyst

Precursors in the Hydrogenation of Styrene", Inorganic Chemistry, 26: 1867-1870.

Sayle DC, Doig JA, Parker SC and Watson GW (2003) "Metal oxide encapsulated nanoparticles", Journal of Material Chemistry, 13: 2078-2089.

Schmid G (2004) Nanoparticles: From Theory to Application, Wiley-VCH, Weinheim.

Schlapbach L and Züttel A (2001) "Hydrogen-storage materials for mobile applications", Nature, 414: 353.

Sen F, Karatas Y, Gülcan M and Zahmakiran M (2014) "Amylamine stabilized platinum(0) nanoparticles: active and reusable nanocatalyst in the room temperature dehydrogenation of dimethylamine-borane", RSC Advances, 4: 1526-1531.

Sheldon RA and van Bekkum H (2001) Fine Chemicals Through Heterogeneous Catalysis, Wiley-VCH, Weinheim.

Shenhar R and Rotello VM (2003) "Nanoparticles: scaffolds and building blocks", Accounts of Chemical Research, 36: 549-561.

Shi L, Liu Y, Liu Q, Wei B and Zhang G (2012) "Sele Selective reduction of aldehydes and ketones to alcohols with ammonia borane in neat waterctive reduction of aldehydes and ketones to alcohols with ammonia borane in neat water", Green Chemistry, 14: 1372.

Shi F, Zhang Q, Ma Y, He Y and Deng Y (2005) "From CO oxidation to CO2 activation: An unexpected catalytic activity of polymer-supported nanogold", Journal of the American Chemical Society, 127: 4182.

Shmidt FK, Nindakova LO, Shainyanb BA, Saraev VV, Chipaninab NN and Umanetz VA (2005) "Hydrogenation catalysts formation in the system AlEt3-Co(acac)(2,3) ", Journal of Molecular Catalysis A-Chemical, 235: 161-172.

Sloan ME, Staubitz A, Clark TJ, Russell CA, Lloyd-Jones GC and Maners I (2010) "Homogeneous Catalytic Dehydrocoupling/Dehydrogenation of Amine-Borane Adducts by Early Transition Metal, Group 4 Metallocene Complexes", Journal of the American Chemical Society, 132: 3831-3841.

Sørensen B (2012) Hydrogen and Fuel Cells: Emerging Technologies and Applications, Second Edition, Elsevier, Denmark.

Steinhoff BA, Fix SR and Stahl SS (2002) "Mechanistic study of alcohol oxidation by the Pd(OAc)($_2$)/O-2/DMSO catalyst system and implications for the development of improved aerobic oxidation catalysts", Journal of the American Chemical Society, 124: 766-767.

Stephens FH, Pons V and Baker RT (2007) "Ammonia-borane: the hydrogen source par excellence?", Dalton Transaction, 25: 2613.

Stranger R, Medley AG, McGrady JE, Garrett JM and Appleton TG (1996) “Electronic structure of [Pt-2(mu-O2CCH3)(4)(H2O)(2)](2+) using the quasi-relativistic X alpha-SW method: Analysis of metal-metal bonding, assignment of electronic spectra, and comparison with $Rh\text{-}_2(mu\text{-}O_2CCH_3)_{(4)}(H_2O)_{(2)}$”, Inorganic Chemistry, 35: 2268-2275.

Sun C, Li H and Chen L (2012) “Nanostructured ceria-based materials: synthesis, properties, and applications”, Energy Environmental Science, 5: 8475.

Thomas JM (2010) The advantages of exploring the interface between heterogeneous and homogeneous catalysis. ChemCatChem, 2: 127.

Thomas KG and Kamat PV (2003) “Chromophore-functionalized gold nanoparticles”, Accounts of Chemical Research, 36: 888.

Tonbul Y, Akbayrak S and Özkar S (2016) “Palladium(0) nanoparticles supported on ceria: Highly active and reusable catalyst in hydrogen generation from the hydrolysis of ammonia borane”, International Journal of Hydrogen Energy, 41: 11154.

Tosheva L and Valtchev VP (2005) “Nanozeolites: Synthesis, crystallization mechanism, and applications”, Chemistry Materials, 17: 2494.

Twigg MV (1994) Mechanisms of Inorganic and Organometallic Reactions, First Edition, Plenum, New York.

Vargaftik MN, Zargorodnikov VP, Stolarov IP, Moiseev II, V. Kochubey A, Likholobov AL, Chuvilin AL and Zamaracv KI (1989) “Giant palladium clusters as catalysts of oxidative reactions of olefins and alcohols”, Journal of Molecular Catalysis, 53: 315-348.

van der Waals D, Pettmanb A and Williams JMJ (2014) “Copper-catalysed reductive amination of nitriles and organic-group reductions using dimethylamine borane”, Royal Society of Chemistry Advances, 4: 51845.

Watzky MA and Finke RG (1997) “Transition metal nanocluster formation kinetic and mechanistic studies. A new mechanism when hydrogen is the reductant: Slow, continuous nucleation and fast autocatalytic surface growth”, Journal of theAmerican Chemical Society, 119: 10382-10400.

Watzky MA and Finke RG (1997) “Nanocluster size-control and "magic number" investigations, experimental tests of the "living-metal polymer" concept and of mechanism-based size-control predictions leading to the syntheses of iridium(0) nanoclusters centering about four sequential magic numbers”, 9: 3083-3095.

Widegren JA, Bennett MA and Finke RG (2003) “Large-scale synthesis of copper nanoparticles by chemically controlled reduction for applications of inkjet-printed electronics”, Nanotechnology, 125: 10301-10310.

White RJ, Luque R, Budarin VL, Clark JH and Macquarrie DJ (2009) “Supported metal nanoparticles on porous materials. Methods and applications”, Chemical Society Reviews, 38: 481-494.

Yadav GD (2005) “Synergism of clay and heteropoly acids as nanocatalysts for development of green processes with potential industrial applications. C”, Catalysis Surveys from Asia, 9: 117–137.

Yan JM, Zhang XB, Han S, Shioyama H and Xu Q (2009) “Synthesis of longtime water/air-stable Ni nanoparticles and their high catalytic activity for hydrolysis of ammonia borane for hydrogen generation”, Inorganic Chemistry, 48: 7389.

Yeung KL and Han W (2014) “Zeolites and mesoporous materials in fuel cell applications”, Catalysis Today, 236: 182.

Zakmakiran M, Akbayrak S, Kodaira T and Ozkar S (2010) “Osmium(0) nanoclusters stabilized by zeolite framework; highly active catalyst in the aerobic oxidation of alcohols under mild conditions”, Dalton Transactions, 39: 7521-7527.

Zahmakiran, M and Özkar, S (2009) “Dimethylammonium Hexanoate Stabilized Rhodium(0) Nanoclusters Identified as True Heterogeneous Catalysts with the Highest Observed Activity in the Dehydrogenation of Dimethylamine-Borane”, Inorganic Chemistry, 48: 8955-8964.

Zahmakiran M, Philippot, Ozkar S and Chaudret B (2012) “Size-controllable APTS stabilized ruthenium(0) nanoparticles catalyst for the dehydrogenation of dimethylamine-borane at room temperature”, Dalton Transactions, 41: 590-598.

Zahmakran M, Tonbul Y and Ozkar S (2010) “Ruthenium(0) Nanoclusters Stabilized by a Nanozeolite Framework: Isolable, Reusable, and Green Catalyst for the Hydrogenation of Neat Aromatics under Mild Conditions with the Unprecedented Catalytic Activity and Lifetime”, Jurnal of the American Chemical Society, 132: 6541-6549.

Zahmakiran M, Tristany M, Philippot K, Fajerwerg K, Ozkar S and Chaudret B (2010) “Aminopropyltriethoxysilane stabilized ruthenium(0) nanoclusters as an isolable and reusable heterogeneous catalyst for the dehydrogenation of dimethylamine-borane”, Chemistry Communication, 46: 2938-2940.

Zhao M, Sun L and Crooks RM (1998) “Preparation of Cu nanoclusters within dendrimer templates”, Journal of the American Chemistry, 120: 4877-4878.

Züttel A (2003) “Materials for hydrogen storage”, Materials Today, 6: 24.

CURRICULUM VITAE

Name SURNAME **:** Seda TANYILDIZI KARABOĞA

Place and Date of Birth **:** ELAZIĞ- 22.12.1986

Universities

- Bachelor's Degree **:** Abant İzzet Baysal University

MSc Degree **:** Abant İzzet Baysal University

e-mail **:** tanyildizi_s@ibu.edu.tr

Address **:** AİBÜ-Department of Chemistry

List of International Publications

- Akbayrak S, **Tanyildizi S**, Morkan I and Özkar S (2014)"Ruthenium(0) nanoparticles supported on nanotitania as highly active and reusable catalyst in hydrogen generation from the hydrolysis of ammonia borane", International Jornal of Hydrogen Energy, 39: 9628-9637.
- **Tanyildizi S**, Morkan I and Özkar S (2017) "Ceria supported copper(0) nanoparticles as efficient and cost-effective catalyst for the dehydrogenation of dimethylamine borane", Molecular Catalysis, 434: 57-68.
- **Tanyildizi S**, Morkan I and Özkar S (2017) "Nanotitania-Supported Rhodium(0) Nanoparticles: Superb Catalyst in Dehydrogenation of Dimethylamine Borane", Chemistry Select, DOI: 10.1002/slct.201700872.

Awards

- The First Undergraduate Student of Department of Chemistry, Abant İzzet Baysal University, Bolu, Turkey, 2010.
- Award for the accepted A or A1 article by Izzet Baysal foundation in 2015.

International Symposiums

- **Tanyildizi S**, Morkan I and Ozkar S. "Ruthenium Catalyzed Dehydrogenation and Transfer Hydrogenation Reactions Using Dimethylamine Borane as a Hydrogen Storage", 250th American Chemical Society National Meet ing & Exposition, August 16-20, 2015, Boston, USA.
- **Tanyildizi S**, Morkan I and Ozkar S. " Titania Supported Rhodium(0) Nanoparticles As Highly Active Catalyst in Dehydrogenation of Dimethylamine Borane ", International Congress on Chemistry and Materials Science", October 5-7, 2017, Ankara, TURKEY.

National Symposiums

- **Tanyildizi S**, Morkan I. synthesis, structural investigations and dft calculations of metal-carbonyl-pyrımıdınethiol complexes, III. Ulusal Anorganik Kimya Kongresi, 19-22 Mayıs 2011, Çanakkale.
- **Tanyildizi S**, Morkan I, Morkan A, İlkin Ö. Investigation of pentacarbonyl(pyrimidinethiol)chromium(0) complex by XRD, IR and Thermal analysis, 25th National Chemistry Congress with International Participation, Erzurum, Türkiye, 2011, Erzurum.
- **Tanyildizi S**, Morkan I. Grup 6B Elementlerinin Metal-karbonil-2-mercaptopirimidin Totomerlerinin Yoğunluk Fonksiyon teorisi (DFT) ile yapısal analizi, 12-15 Temmuz 2012, Balıkesir.
- **Tanyildizi S**., Akbayrak S., Gençtürk S., Morkan İ, Özkar S., ‘’ Usage of Ruthenium(0)Nanoparticles catalyst for the hydrogen generation from ammonia borane hydrolysis’’ V. Ulusal Kataliz Kongresi 23-26 Nisan 2014 Adana.
- Gençtürk S., Akbayrak S., **Tanyildizi S**., Morkan İ, Özkar S., Usage of Rhodium (0)Nanoparticles catalyst for the hydrogen generation from ammonia borane hydrolysis’’ V. Ulusal Kataliz Kongresi 23-26 Nisan 2014 Adana.
- **Tanyildizi S**, Morkan I and Ozkar S. "Catalytic transfer hydrogenation of acetophenone using dimethylamine borane as hydrogen source in the presence of ruthenium(III) acetylacetonate", V. Ulusal Anorganik Kimya Kongresi, 22-25 Nisan 2015, Mersin, Sözlü Sunum.

- **Tanyildizi S**, Morkan I and Ozkar S. Ceria supported copper0) nanoparticles as efficient and cost-effective catalyst for the dehydrogenation of dimethylamine borane, VI. Ulusal Anorganik Kimya Kongresi, 18-21 Mayıs 2017, Burdur, Sözlü Sunum.